



UNIVERSITÀ
DEGLI STUDI
DI PADOVA

UNIVERSITA' DEGLI STUDI DI PADOVA

Dipartimento di Ingegneria Industriale DII

Corso di Laurea Magistrale in Ingegneria dell'Energia Elettrica

Optimization problem: grid with two passive filters and an active power filter

Relatore: Luigi Alberti, Dipartimento di Ingegneria Industriale- DII

Correlatore: Fernando Briz, Department of Electrical Engineering, Oviedo

Gurjot Singh 2052292

Anno Accademico 2023/2024

Optimization problem: grid with two passive filters and an active power filter

Gurjot Singh

March 3, 2024

Contents

1	Introduction	4
1.1	Introduction and motivation	4
1.2	Thesis' structure	4
2	Framework of the problem	5
2.1	Description of the system	5
2.2	Active power filter	7
2.2.1	Control of active power filter	12
2.3	The IEEE 519-2022 Standard	13
2.4	Non optimized quantities	14
2.4.1	Resistance of filters	14
2.4.2	Non-linear load	16
2.5	Summarizing table	18
3	Review of Iterative Optimizations Methods	22
3.1	Newton-Raphson method [7]	22
3.2	Newton's Method in optimization	23
3.3	Pros and cons of iterative methods	23
3.4	Quadratic Programming (QP) [19]	24
3.5	Sequential quadratic programming (SQP) [14]	25
3.6	Interior point method (IPM)	26
3.6.1	IPM with LP [18]	26
3.6.2	IPM with NLP [4]	27
3.7	Gradient descent [9]	28
3.8	Conclusions about iterative methods	29
4	Optimization of passive filters and APF	30
4.1	Absence of L_{f1} and L_{f2} in the list of unknowns	30
4.2	Optimization of active power filter	31
4.3	Formalization of the problem	31
4.4	Lower bound lb and upper bound ub of C_f	32
4.5	Selection of lower and upper bounds for L_{APF}	33
4.6	Lower bound and upper bound of I_{APF}	35
4.7	Summarize of upper and lower bounds	35
4.8	Cost Function	36
4.9	Initial value	37

5	Constraints of the optimization problem	38
5.1	IEEE 519-2022	38
5.2	Quality factor	38
5.2.1	Parallel resonance frequency	39
5.3	L_{APF} and voltage drop	41
5.4	Reactive current into the grid	41
5.5	Nominal current of active power filter	42
5.6	Summarize of constraints	42
6	Results of optimization	45
6.1	Setting of optimization problem	45
6.2	Introduction of analysis	45
6.3	Optimization results using SQP	46
6.4	Optimization results using IPM	47
6.4.1	Second stage of optimization with IPM	48
6.5	Comparison between SQP vs. IPM	49
7	Sensitivity analysis to grid impedance and firing angle	51
7.1	Sensitivity to Z_g variations	51
7.2	Sensitivity to α variations	53
7.2.1	Case with highest reactive current of non-linear load: $\alpha = 48^\circ$.	55
7.3	Conclusion of sensitivity	57
8	Conclusions and future works	60
8.1	Summary of each chapter	60
8.2	Conclusions	60
8.3	Future works	61
9	Riassunto esteso in italiano / Extended summary in Italian	63
9.1	Descrizione del sistema	63
9.2	Metodi iterativi per l'ottimizzazione	63
9.3	Variabili da ottimizzare e funzione costo	63
9.4	Vincoli del problema di ottimizzazione	64
9.5	Risultati dell'ottimizzazione	64
9.6	Sensibilità dell'impedenza di rete e dell'angolo di accensione	65
9.7	Conclusioni e progetti futuri	65
A	Code defining non-linear load	70
B	Code defining optimization problem	73
C	Code verifying the constraints	81

Abstract

In this Master thesis document, there is an analysis on how to find the optimal values for a hybrid filter consisting of both two passive filters (series of R, L and C components) and an active power filter (APF), and comply with the harmonic content in the grid, according to the standard IEEE 519-2022 and with other constraints arbitrarily chosen. The solution is found using the Matlab solver *fmincon*, with the optimization tool *MultiStart*. The solution given out respects all the standards and the constraints imposed if the algorithm used by the solver *fmincon* is the *sequential quadratic programming (SQP)*. The solutions are verified through analytical equations. In the end, a sensitivity analysis is conducted and the differences between the system without and with filters are shown. Overall, this thesis contributes to the understanding of hybrid filter optimization and its impact on grid harmonics.

1 Introduction

1.1 Introduction and motivation

The problem of harmonics is assuming importance in recent years due to the increasing number of power converters being installed. This increase can be justified by the loads supplied by power converters, which consume non-sinusoidal currents.

This work continues a research topic that was started in [20] where an optimization of two passive filters was carried on. In this master thesis, an active power filter (APF) is added to the previous system. The aim is to eliminate the harmonic pollution into the grid, keeping as clean as the standard IEEE 519-2022 has stated. Moreover, the reactive current into the grid is limited thanks to the APF. The numerical analysis is led using the function *fmincon* in Matlab, with an optimization tool called *MultiStart*. One of the objectives of this work is to determine if *fmincon* with *MultiStart* can attain a feasible solution.

For all these reasons, the study of harmonics is addressed below.

1.2 Thesis' structure

The thesis consists of nine chapters with the following contents:

1. A brief introduction to the problem and explanation of the motivation
2. Detailed description of the system that will be optimized
3. Literary review of some algorithms used in the optimization: Newton-Raphson, Sequential quadratic programming, Interior point method and Gradient descent
4. Presentation of the variables to optimize, with their upper and lower bounds; description of the variables of cost function
5. List of the constraints that the optimization problem has to comply
6. Discussion of the results of the optimization problem, with the base values of the firing angle α and the load resistance R_L
7. Analysis of sensitivity of the grid impedance Z_g and of firing angle α
8. Summary, conclusions and future works
9. Extended summary in Italian

2 Framework of the problem

2.1 Description of the system

A full representation of the system is given in figure 2.1. The system of study consists of the following components:

1. voltage source of grid
2. impedance of grid
3. passive filter #1
4. passive filter #2
5. active power filter
6. diode or thyristor rectifier
7. downstream of the rectifier there is a DC-link, comprising a capacitor and a resistor, which represents the real load

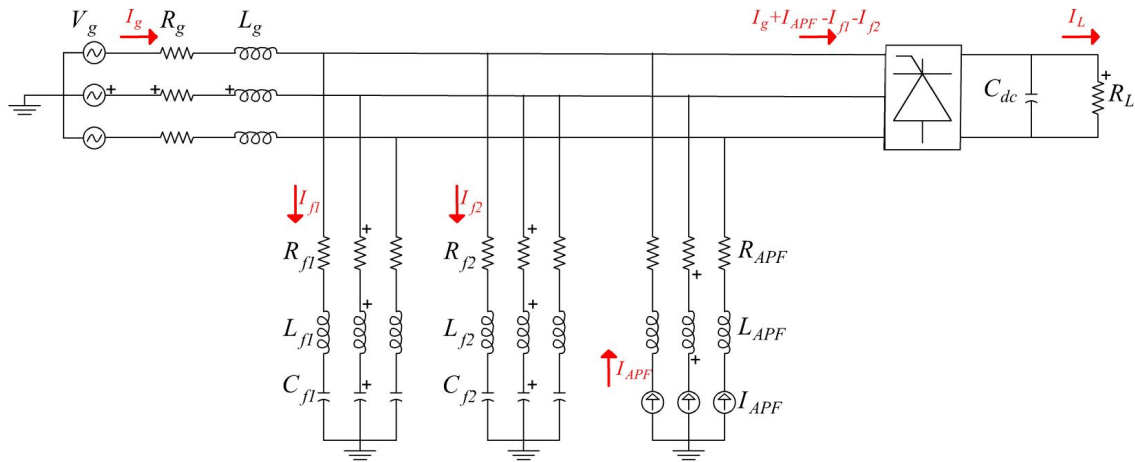


Figure 2.1: Three-phase model of the system.

The passive filters are represented as a series branch of a resistance, an inductance and a capacitance. The APF is modeled as a series of an impedance and a current source. The thyristor with capacitance and resistance ends the model.

The harmonic content of a diode or thyristor rectifier is given by (2.1), where $k \in \mathbb{N}$.

$$h = 6k \pm 1 \quad (2.1)$$

From (2.1), it is possible to substitute the thyristor, the capacitance of the DC-link and the load resistance by current sources injecting the current harmonics due to the non-linear load.

Instead of using a three-phase model, it's easier to use a single-phase equivalent model. Further, to avoid a mass figure, in figure 2.2 the current source of the APF and that of the non-linear load are depicted as a single current source; as a matter of fact, they are a parallel of current sources and each current source represent a specific harmonic. An important node of this circuit is the point of common coupling (PCC). This is the point at which the user is connected. All the standard specifications of IEEE are referred to at this point.

Glimpsing figure 2.2, is it possible to define the following quantities:

- f_g grid frequency
- V_g grid voltage

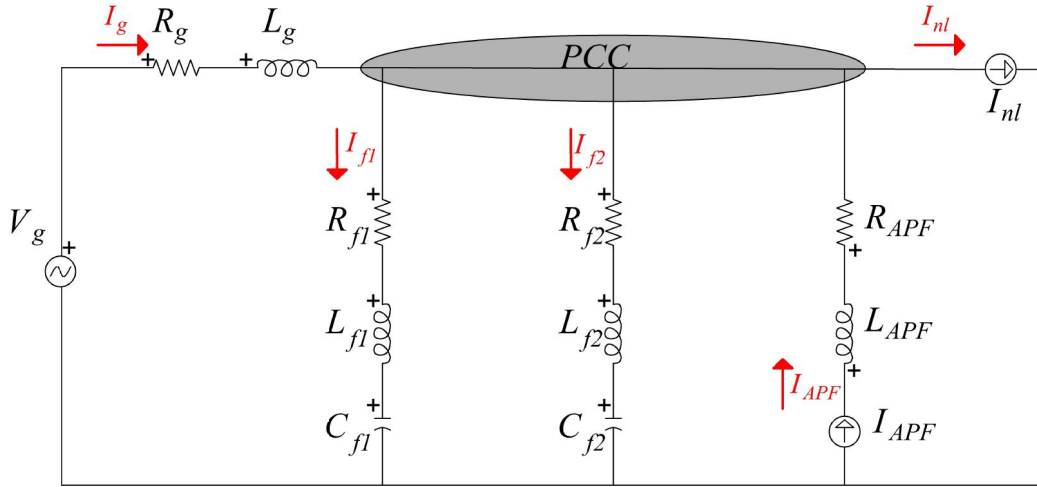


Figure 2.2: Single-phase equivalent circuit.

- $Z_g = R_g + j\omega L_g$ impedance of grid
- $Z_{f1} = R_{f1} + j\omega L_{f1} + \frac{1}{j\omega C_{f1}}$ impedance of passive filter #1
- $Z_{f2} = R_{f2} + j\omega L_{f2} + \frac{1}{j\omega C_{f2}}$ impedance of passive filter #2
- $Z_{APF} = R_{APF} + j\omega L_{APF}$ impedance of APF
- I_{APF} current of APF
- I_{nl} current of non-linear load

Solving the circuit using Kirchhoff current and voltage laws, the expressions of voltage at PCC and grid current are found:

$$V_{pcc} = \frac{V_g - Z_g I_{nl} + Z_g I_{APF}}{1 + \frac{Z_g}{Z_{f1}} + \frac{Z_g}{Z_{f2}}} \quad (2.2)$$

Eventually from (2.2)

$$I_g = \frac{V_g - V_{pcc}}{Z_g} = \frac{\frac{V_g}{Z_{f1}} + \frac{V_g}{Z_{f2}} - I_{APF} + I_{nl}}{1 + \frac{Z_g}{Z_{f1}} + \frac{Z_g}{Z_{f2}}} \quad (2.3)$$

It is helpful plotting the main quantities at 50 [Hz] without considering filtering action (i.e. there are neither passive filters nor the active one) and considering the compensation. The behaviour is depicted in figure 2.4. The grid voltage V_g has only the real part in both cases. I_{nl} does not change before and after compensation. When the filters are deactivated, $I_g = I_{nl}$, so the grid is polluted by the presence of the non-linear load: the vector I_{nl} is perfectly overlapped to I_g . If the filtering and compensation are looked upon, then I_g is lower in the active and reactive part than I_{nl} . The APF compensates for the non-linear load injecting a pure reactive current. The currents in the passive filters are negligible because they are tuned for a resonance frequency different from 50 [Hz]. At last, the voltage of the APF V_{APF} is slightly lower than V_{PCC} due to the voltage drop along the impedance of the APF.

The figure 2.3 represents the non-linear current of phase b, without considering any kind of compensation and setting a firing angle $\alpha = 10^\circ$ and a load resistance $R_L = 1$ [Ω]: it is quite different from a sinusoidal wave; however, the distortion can further be increased if α is increased.

The validity of equations (2.2) and (2.3) was confirmed from numerical simulation using Simulink results and Fourier analysis. They are very similar to each other. Figure 2.5 displays the grid current I_g for both methods:

- Analytical solution: $I_g = 403.5202404977312$ [A]

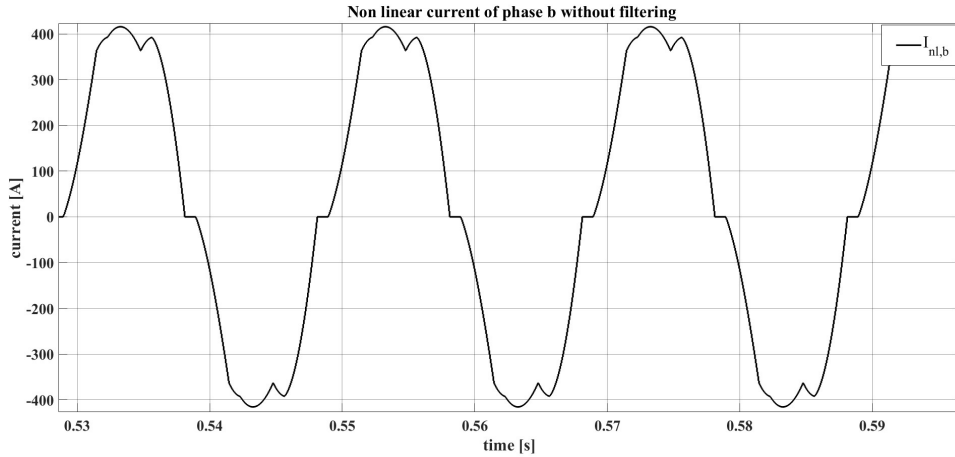


Figure 2.3: Current of phase b of non-linear load without compensation; $\alpha = 10^\circ$ and $R_L = 1 [\Omega]$.

- Numerical solution: $I_g = 403.5202479045316 [\text{A}]$

The two values are not exactly the same; a reasonable explanation is that the model implemented into Simulink is slightly different from that of figure 2.1 or figure 2.2: every time a current source is inserted into Simulink, it is necessary also to introduce a very huge resistance in parallel to it. If the value of this resistance were infinite, then the two solutions would be exactly the same. In the case presented in figure 2.5, the parallel resistance is $R_p = 10^8 [\Omega]$, viz. a big value but not infinite. Moreover, if $R_p > 10^{16}$ some numerical problems related to singularity of matrices occur.

Besides, the solutions resulting from the Simulink model depend on the step-size of the simulation: smaller is the step-size, more accurate is the result. In figure 2.5, the step-size selected is $T_{ss} = 10^{-6} [\text{s}]$.

Furthermore, both numerical and analytical results are attained in steady-state condition: in the Simulink analysis, the transient is neglected and only the last N samples are considered. The simulation time t lasts 1 [s] and the step-size, that is the sampling, happens every $T_{ss} = 10^{-6} [\text{s}]$. So a plausible value of N is $N = 40 \cdot 10^3$. The total number of samples is

$$N_t = \frac{t}{T_s} = 10^6 \quad (2.4)$$

The advantage of having an analytical equation is the time saved: a Simulink model requires more time to be run than the analytical equation. Using *tic-toc* command of Matlab is possible to quantify the time saved:

- analytical solution: 2.431138 [s]
- numerical solution: 80.834828 [s].

This huge time difference can be fathomed knowing that numerical solution has to proceed according to following steps: open the Simulink model, run a simulation lasting 1 [s], with a step size of $10^{-6} [\text{s}]$, importing data from Simulink to Matlab, eliminate the transients from the data, calculate the Fourier analysis and finally plot the results.

The solutions, both numerical and analytical, are produced by a system in which the non-linear load consists of 5^{th} and 7^{th} harmonic only and the two passive filters are not tuned to two specific frequencies.

The results found until now are valid for one value of frequency. If there are more than one frequency in the system, superposition can be applied.

2.2 Active power filter

One of the elements in figure 2.1 and figure 2.2 that deserves a detailed analysis is the APF. Its model is that of a current source, but in reality it functions as a voltage source inverter, as illustrated by figure 2.6. The aim of this device is to inject currents into the PCC to clean the grid from the pollution due to non-linear load. [1]

The APF has a DC-link voltage $V_{dc} = 600 [\text{V}]$. This value ensures an output line-to-line voltage higher than that of the grid, in fact $V_{grid,rms,l-l} = 230\sqrt{3} = 400 [\text{V}]$, which is a requirement to avoid uncontrolled operation

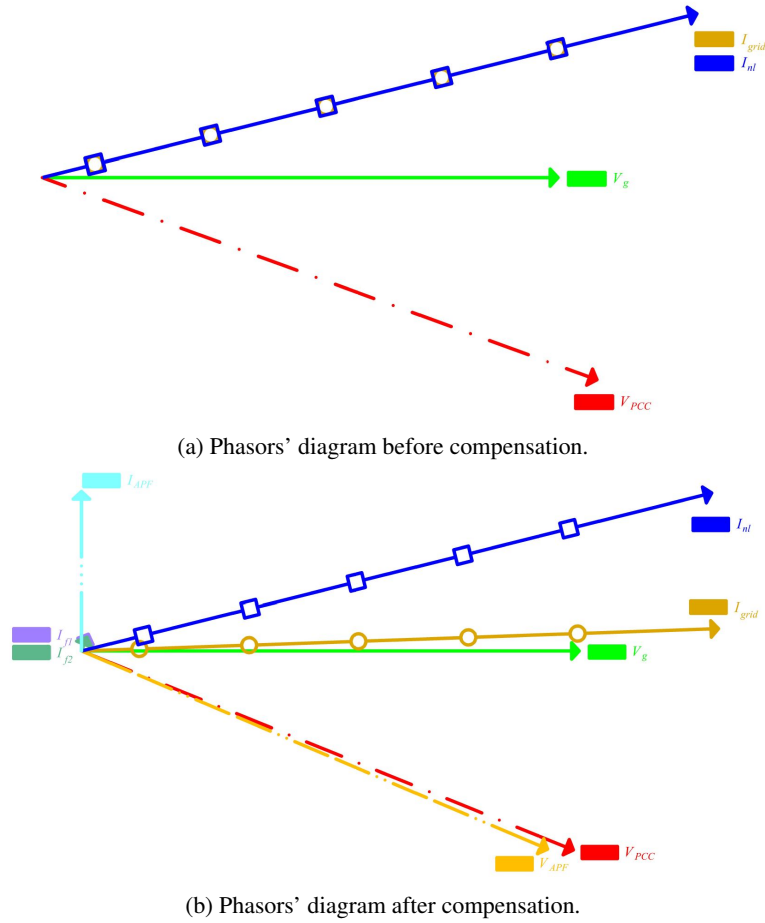


Figure 2.4: Phasors' diagram before and after compensation.

of the diodes. Using *space vector modulation* (SVM), the maximum phase voltage is $V_{dc}/\sqrt{3}$, so the line-to-line voltage of the inverter is reported in (2.5).

$$V_{inverter,rms,l-l} = \frac{V_{dc}}{\sqrt{3}} \cdot \frac{\sqrt{3}}{\sqrt{2}} = \frac{600}{\sqrt{2}} \approx 420 \text{ [V]} \quad (2.5)$$

DC-link consists of two capacitors $C_{dc} = 2 \cdot 10^{-3}$ [F] that allow the creation of a point O (see figure 2.6). The voltages of the inverter are referred to this middle point. If an APF has a battery connected to DC-link, then it has to deliver some net power to the grid: this situation is typically for converters connected to photovoltaic or wind plants or to some storage pack. A converter acting like this is an AC voltage source, and not an APF. In this thesis the APF does not inject a net active power into the grid, so net energy is not drawn by the DC side: the APF can be fed by the capacitors.

If the converter has to compensate for only the reactive power, then there is neither a flow of net energy towards the AC part: the voltage of the DC side is constant.

Differently, if the converter has to compensate for the harmonics, the DC-link capacitors are continuously charged and discharged (also in this case the net delivery of active energy is zero).

The capacitors are charged when modulation and control are disabled, through a pre-charge resistor.

In reality, the converter is not an ideal device, therefore during switching, losses are produced; these are compensated by the control system, keeping the voltage of DC-link to the reference value. The control system takes energy from the grid to compensate for the losses.

The main core of the inverter consists of six IGBTs, each one with a diode in antiparallel.

The inverter cannot be connected directly to the grid since, otherwise, two different voltage sources would be

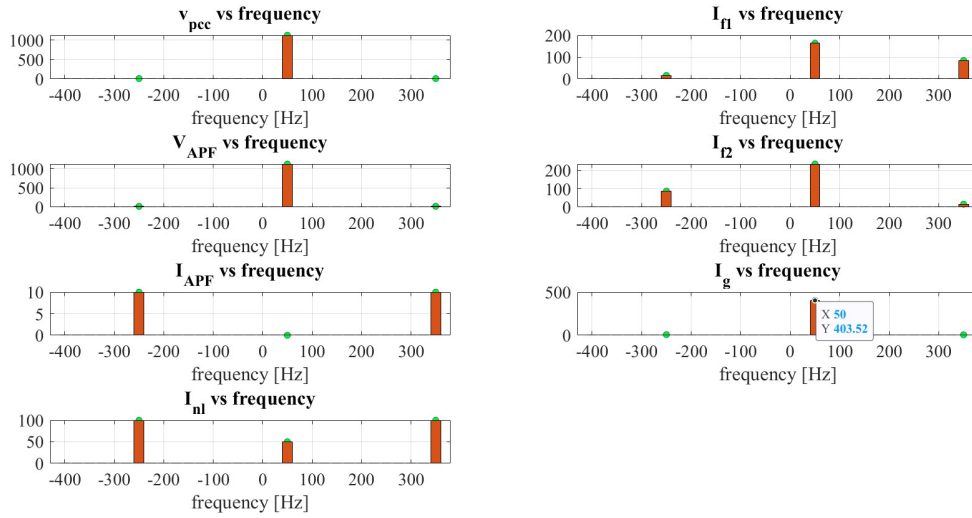


Figure 2.5: Red bars: numerical solution; green dots: analytical solution. Both solutions are in all plots very similar. For instance the grid currents are very similar (Analytical solution $I_{ganalytical}$ vs numerical solution $I_{gnumerical}$).

connected in parallel. To overcome this setback, series inductors are placed between the grid and the converter. The same result could be pursued, also using more complicated LCL filters as studied in [16]. The APF is connected to the grid through a boost inductor, which is the same emerging in figures 2.1 and 2.2. The point of connection is the PCC.

In this chapter, the APF is studied independently of other components such as passive filters and non-linear loads. This preliminary analysis aims to understand the control mechanisms governing the behavior of the APF.

The gate command of the IGBT is derived from the PWM block. The references are three sinusoidal waves like

$$v_{a,ref} = V_g \cdot \sin(2\pi f_g \cdot t) \quad (2.6)$$

$$v_{b,ref} = V_g \cdot \sin(2\pi f_g \cdot t - \frac{2}{3}\pi) \quad (2.7)$$

$$v_{c,ref} = V_g \cdot \sin(2\pi f_g \cdot t - \frac{4}{3}\pi) \quad (2.8)$$

It is valid that

$$v_{a,ref} + v_{b,ref} + v_{c,ref} = 0 \quad (2.9)$$

For a switching frequency $f_s = 10$ [kHz], the carrier is a triangular wave with a peak value of $V_{dc}/2$ at 0.05 [ms] and a minimum of $-V_{dc}/2$ at 0.1 [ms]. The AC/DC converter is able to compensate fast the arising of non-linearity because the switching period $T_s = 1/f_s = 1/10^3 = 100$ [μ s] is lower than the period of the grid quantities $T_g = 1/f_g = 1/50 = 20$ [ms]. [1]

To defined the average value of the output voltage, it is useful to introduce the modulation index

$$m_a = \frac{v_{ref,pk}}{v_{carrier,pk}} \quad (2.10)$$

In order to not lose linearity between the fundamental voltage at the output of the inverter and the modulation index, the voltage of the fundamental of the inverter is written in (2.11).

$$v_{inv,1} = m_a \frac{V_{dc}}{2} \quad (2.11)$$

It has been decided to not operate in overmodulation to avoid the associated harmonics. Consequently, the peaks of the references do not have to touch the limit voltages of the carriers.

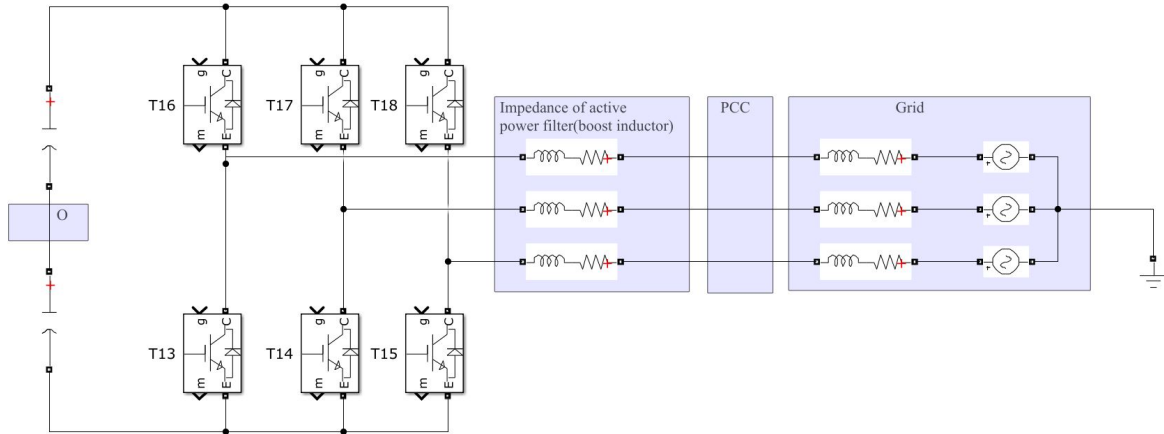


Figure 2.6: Active power filter: From left, there is a capacitance, six IGBT with diode, impedance of the APF and the grid.

Moreover, it has been thought to maintain the same difference of voltage between the positive maximum of the carrier and the maximum of the three sinusoidal references. The same is deliberated for the negative minimum of the carrier and the lowest of the three sinusoidal references. This target has to be accomplished each switching period $T_{ss} = 10^{-6}$ [s]. To achieve this result is it necessary to inject a homopolar component of voltage v_h at a triple frequency than the fundamental, i.e., at 150 [Hz]. Adding the same quantity of voltage for each phase, it can be demonstrated that the phase to neutral or phase to phase voltages are not changed. [2]

V_h , from a graphical point of view, can be figured out as that voltage that moves away the maximum reference from the maximum limit of the carrier and at the same time, v_h draws near the minimum value of the reference to the minimum limit of the carrier. The final objective is that the maximum and minimum references are equally spaced from maximum and minimum of the carrier.

So the homopolar voltage is written like:

$$v_h = \frac{v_+ - v_-}{2} \quad (2.12)$$

where

- $v_+ = \frac{V_{dc}}{2} - \max\{v_{a,ref}, v_{b,ref}, v_{c,ref}\}$
- $v_- = \frac{V_{dc}}{2} - |\min\{v_{a,ref}, v_{b,ref}, v_{c,ref}\}|$

So the new references are:

$$v_{ah,ref} = v_{a,ref} + v_h \quad (2.13)$$

$$v_{bh,ref} = v_{b,ref} + v_h \quad (2.14)$$

$$v_{ch,ref} = v_{c,ref} + v_h \quad (2.15)$$

and it is valid that

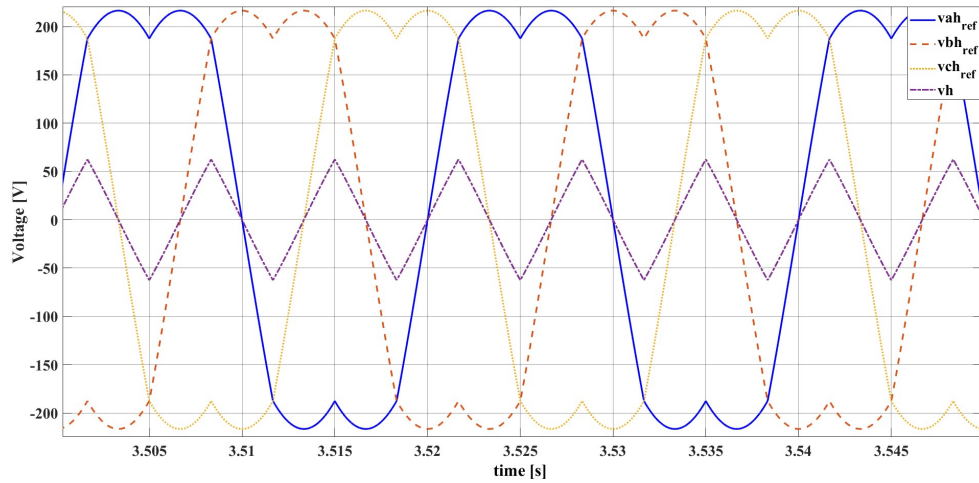
$$v_{ah,ref} + v_{bh,ref} + v_{ch,ref} = 3v_h \quad (2.16)$$

All these voltages are represented in figure 2.7.

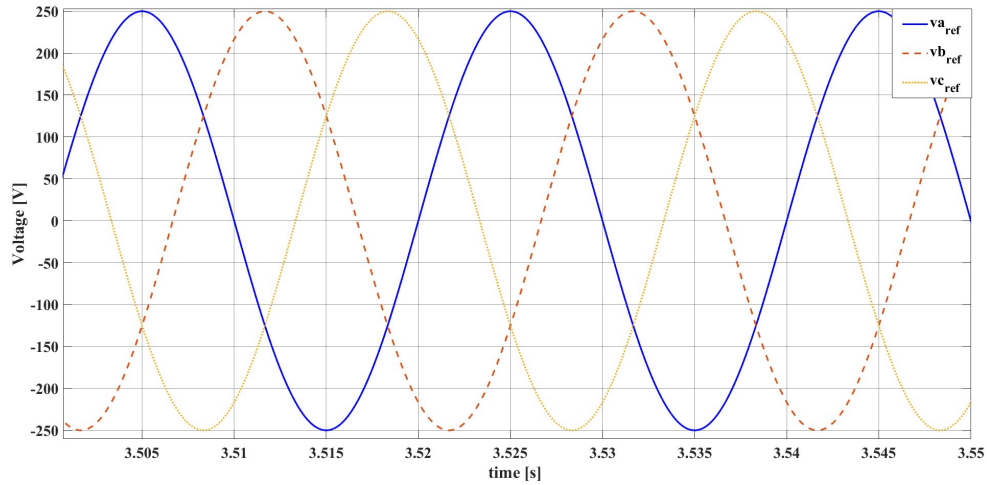
Following the analysis of reference-carrier behavior, a study of v_{pcc} , v_{inv} , v_{ref} , v_g , i_{inv} , and v_{href} at 50 [Hz] is conducted. They are analyzed using Simulink; then the data are imported into Matlab; here the transient is eliminated, so the considerations are valid only in steady state; once the data are at steady-state the three-phase quantities are turned into $\alpha\beta$ using

$$v_{\alpha\beta} = \frac{2}{3}(v_a + v_b \cdot e^{j\frac{2}{3}\pi} + v_c \cdot e^{j\frac{4}{3}\pi}) \quad (2.17)$$

with



(a) Voltage references with homopolar injection.



(b) Voltage references without homopolar injection.

Figure 2.7: Voltage references with and without homopolar injection.

- $v_\alpha = \text{Re}(v_{\alpha\beta})$
- $v_\beta = \text{Im}(v_{\alpha\beta})$

After that, the Fourier analysis is launched, using *fft* (*fast Fourier transform*) function of Matlab. Figure 2.8 reports the *fft* analysis.

The bars of figure 2.8 are so light because the x -axis spaces from -25 [kHz] to 25 [kHz]: there are a lot of frequencies on this axis. It is necessary to have a wide window of frequency because the switching frequency is $f_s = 10$ [kHz].

The plots of figure 2.8 are:

- the top left shows the V_{PCC} , so the voltage of the common coupling point and the ground. The waveform of V_{pcc} is very similar to that of a sine, so there is a main component at 50 [Hz]. There are also some harmonics at the same frequency of the voltage of the inverter: these harmonics are created because the APF is working. This voltage should be more distorted if non-linear loads would have been attached to PCC;
- the top right depicts the output voltage of the inverter, measured from the downstream inverter and the point O. The amplitude of the fundamental is calculate by (2.10) and (2.11), setting $v_{ref,pk} = 250$ [V] and

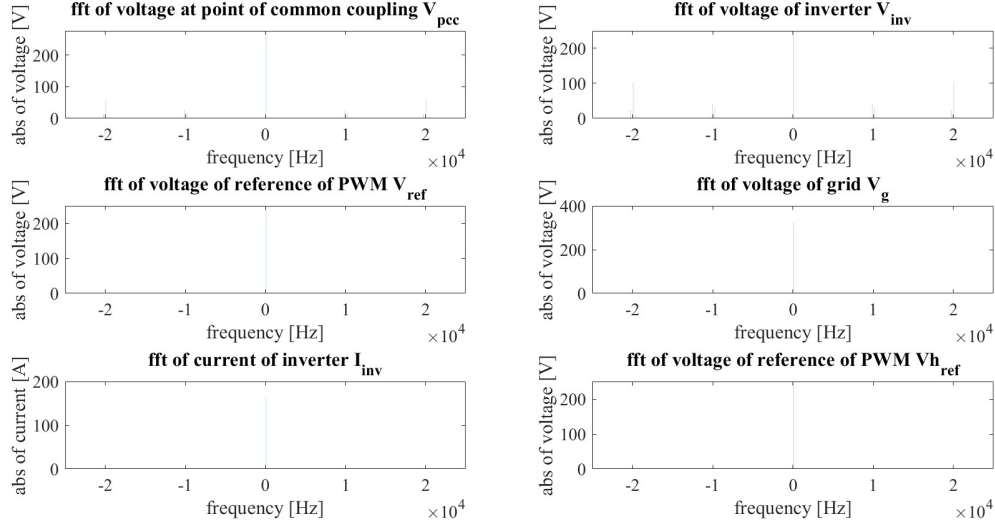


Figure 2.8: From top left to bottom right: V_{pcc} , V_{inv} , V_{ref} , V_g , I_{inv} , $V_{h,ref}$.

$v_{carrier,pk} = 300$ [V] so

$$v_{inv,1} = m_a \frac{V_{dc}}{2} = \frac{v_{ref,pk}}{v_{carrier,pk}} \frac{V_{dc}}{2} = \frac{250}{300} \cdot \frac{600}{2} = 250$$
 [V] (2.18)

The amplitude is that of the reference. The main harmonics are around the integer multiple of the f_s , so they are around 10, 20,..., [kHz]. Considering all the harmonics having positive sign, the order h of harmonics can be written as

$$h = p \cdot \frac{f_s}{f_1} \pm q$$
 (2.19)

where $p = 1, 2, 3, \dots$ and $q = 0, 2, 4, \dots$ if p is odd or $q = 1, 3, 5, \dots$ if p is even. Writing (2.19) as $h \cdot f_1 = p \cdot f_s \pm f_1 \cdot q$, it is more clear that the switching harmonics are around f_s and its multiples;

- the middle left displays the reference voltage. It is not measured. Only the fundamental is present because the references are three sinusoidal voltages at 50 [Hz];
- the middle right plot illustrates the grid voltage. It is measured between the PCC and the ground. Same consideration of references can be taken into account;
- the bottom left plot describes the behaviour of the output current of the inverter: only 50 [Hz] component is present;
- the bottom right plot portrays the $v_{h,ref}$, so the voltage of reference with injection of v_h . It is not measured. While the waveforms of V_{ref} and $V_{h,ref}$ differ, as illustrated in figure 2.7, their harmonic content remains the same.

2.2.1 Control of active power filter

The APF is an inverter: all the control techniques available for the inverters can be applied to the APF. In this work there is not a deep description of the control system because the main focus is reserved for the optimization stages. In reality, the APF works always in close loop as shown in figure 2.9; concerning the optimization, the APF is a parallel of current sources, as seen in figure 2.1 and 2.2. A current source can be obtained by a controlled voltage source. An inverter supplied by a DC voltage is considered as a controlled voltage source. To supply a certain current, a close loop-control scheme is to set up. The two main quantities to control are

- the grid current

Current distortion limits for systems rated 120 V through 69 kV						
Maximum harmonic current distortion in percent of I_L						
Individual harmonic order						
I_{sc}/I_L	$2 \leq h < 11$	$11 \leq h < 17$	$17 \leq h < 23$	$23 \leq h < 35$	$35 \leq h < 50$	TDD
< 20	4.0	2.0	1.5	0.6	0.3	5.0
20 < 50	7.0	3.5	2.5	1.0	0.5	8.0
50 < 100	10.0	4.5	4.0	1.5	0.7	12.0
100 < 1000	12.0	5.5	5.0	2.0	1.0	15.0
> 1000	15.0	7.0	6.0	2.5	1.4	20.0

Table 2.1: Current distortion limits admitted. [10]

Now it is the turn of I_L , i.e. the maximum demand load current at PCC under normal load operating conditions [10].

Considering a $R_{rated} = 1 [\Omega]$, the voltage measured at its terminal is $V_{load} = 400 [V]$; these values are obtained with $\alpha = 10^\circ$. The I_{load}

$$I_{load} = \frac{V_{load}}{R_{rated}} = 400 [A] \quad (2.21)$$

So equating the power in the DC-link and the power in the grid, $I_{L,rms}$ is calculated as

$$I_{L,rms} = \frac{V_{load} I_{load}}{3 \frac{V_g}{\sqrt{2}}} = 231.88 [A] \quad (2.22)$$

Therefore, the maximum demand load current is $I_L = I_{L,rms} \cdot \sqrt{2} = 327.93 [A]$. I_L is also called *rated current*.

Finally, the ratio of (2.20) and (2.22) is exactly the value appearing in the table 2.3 on the top left. This ratio is called *short circuit current ratio* (SCCR). This parameter is used to define if a PCC can be considered strong or weak. The higher is SCCR, the lower the grid senses the variation due to the presence of harmonics.

With the assumption made above, $SCCR = 3.149$, so the first row of table 2.3 has to be considered. The standard IEEE 519-2022 accounts for the harmonic until 50th order. In this work only the harmonic until 13th will be taken under examination. The harmonics of order greater than 13th are often neglected because, usually, they have small magnitude, and can be filtered by a low size LC filter [1].

The last column of table 2.3 is the TDD, i.e. total demand distortion. Its value is calculated using (2.23), where I_{gh} is the root-mean-square value of the current harmonic.

$$TDD = \frac{\sqrt{\sum_{h=2}^{50} I_{gh}^2}}{I_L} \quad (2.23)$$

2.4 Non optimized quantities

Not all the elements of the system of figure 2.1 have to be optimized because they can be parasitic elements or they belong to the non-linear load. These elements are known and are listed in this subsection.

2.4.1 Resistance of filters

As regards the resistance of the filters, it has been decided to not optimize their values because they are parasitic physical quantities and they depend on the value of capacitance and inductance chosen. As usual, the value of resistance of the filter has to be as small as possible in order to let the filter to act like short-circuit at cut-off frequency. However, a parasitic resistance is always present both in inductance and capacitor. Besides, a little bit of resistance is necessary to avoid undamped resonances. However, if the value of the resistance is too high, for instance it assumes values like 1 $[\Omega]$, at cut-off (or resonant) frequency, a part of the harmonic current will flow into the grid because it can have a value similar to that of the filter.

Considering the value of grid impedance aforementioned, and a cut-off frequency of 250 [Hz], the magnitude of grid impedance is around $|Z_g| = |22 \cdot 10^{-3} + j2\pi \cdot 250 \cdot 10^{-3}| = 1.57 [\Omega]$: this value is very similar to the resistance of the passive filter, assumed to be 1 [Ω].

In order to let the current to flow in the passive filter, a lower value for resistance is preferred since this resistance is a parasitic value: as low is this resistance, as better the response of the filter is close to the ideal one. The bigger the resistance, the bigger will be the deviations of the filter from the ideal response. It is noted, however, that the resistance will add damping to the LC circuit resonance, which is also desirable.

The resistance of the filter, at least, is the series of the parasitic resistance of capacitor and of inductor; to select properly these values, some datasheets have been examined; by [3], the capacitance in range [4.7, 100] [μF] is chosen. The manufacturer provides the equivalent series resistance (ESR), i.d. the parasitic resistance, of the capacitance as a function of frequency and temperature, as reported in figure 2.10.

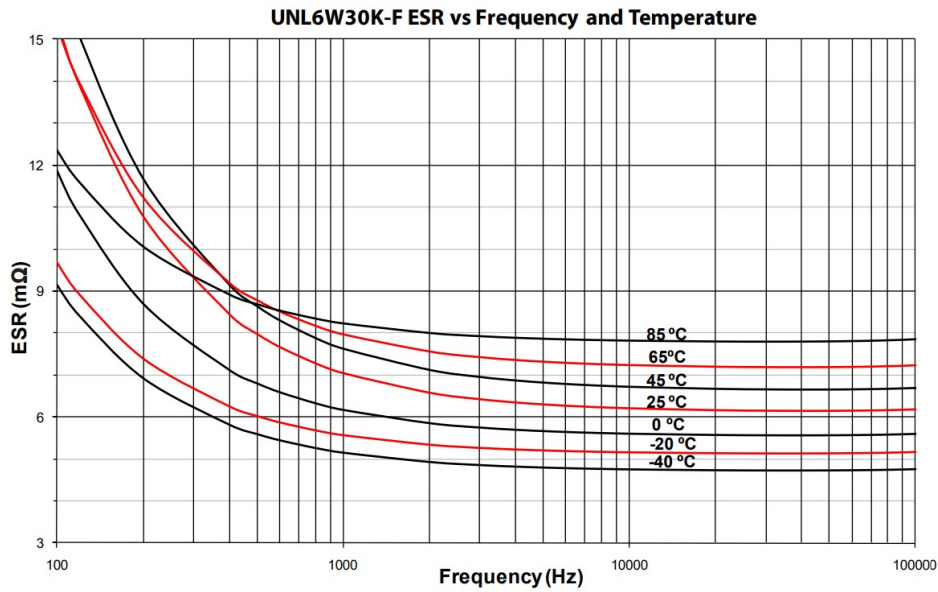


Figure 2.10: ESR of capacitance vs frequency and temperature. [3]

According to the main harmonics of the non-linear load, the operating frequency of the capacitors would be 250 [Hz] or 350 [Hz]. An average value of 45 [$^{\circ}C$] is considered. A reasonable value of ESR of capacitance is 8 [$m\Omega$].

In order to find the equivalent resistance of an inductor, [12] is taken into account. Although the filters are for converters connected to motors, they can be used to get orientative values for grid filters. It is noted that they are often designed ad hoc to fulfill the requirements from the customer, meaning that their values are not standardized. Figure 2.11 explains how to obtain the parasitic resistance of the inductance.

Unlike before, it is less trivial to find the resistance of the filter. By figure 2.11, it can be noticed that the current flowing through the filter has to be chosen. A value of 30 [A] is detected, considering the I_{nl} for 5th and 7th. Then, considering the $P_{loss} = 330$ [W] and the three-phase motor, the resistance of inductance is

$$R_{Lf} = \frac{P_{loss}}{3 \cdot I^2} = \frac{330}{3 \cdot 30^2} = 0.12 [\Omega] \quad (2.24)$$

In the end, the total resistance of the filter is the sum of the parasitic resistance of inductor and capacitor

$$R_f = R_{Cf} + R_{Lf} = 8 \cdot 10^{-3} + 0.12 = 0.13 [\Omega] \quad (2.25)$$

Nevertheless, the problem of having a very small or very high filter resistance is discussed in subsection 5.2.

The same procedure can be followed for the resistance of the APF: the value of current is $\frac{I_L}{2} = 164.0$ [A] (see

Seleccionar la intensidad del filtro conforme la potencia nominal del motor:

Potencia motor		Intensidad A	Ref. 50 Hz	Ref. 60 Hz	Dimensiones mm			Peso kg	Perdidas W	Placa condensadores	Tipo*
kW	CV				A	B	C				
4	5,5	9	SPFS004	SPFS004Z	210	205	410	14	165	-	I
5,5	7,5	12	SPFS005	SPFS005Z	210	210	410	16	180	-	I
7,5	10	16	SPFS007	SPFS007Z	210	230	410	20	215	-	I
11	15	23	SPFS011	SPFS011Z	260	245	495	25	335	-	I
15	20	30	SPFS015	SPFS015Z	260	250	495	30	330	-	I
18,5	25	37	SPFS018	SPFS018Z	260	265	495	38	375	-	I
22	30	43	SPFS022	SPFS022Z	260	280	495	44	460	-	I
30	40	58	SPFS030	SPFS030Z	320	325	555	59	540	-	I
37	50	72	SPFS037	SPFS037Z	320	330	555	65	610	-	I
45	60	86	SPFS045	SPFS045Z	320	345	555	77	650	-	I
55	75	104	SPFS055	SPFS055Z	320	355	555	87	690	-	I
75	100	140	SPFS075	SPFS075Z	380	345	940	105	925	-	II
90	125	168	SPFS090	SPFS090Z	380	360	940	120	1115	-	II

Figure 2.11: Inductance selection based on the current flowing through itself and the losses. [12]

paragraph 4.6). So the last row of figure 2.11 can be exploited:

$$R_{APF} = \frac{P_{loss}}{3 \cdot I^2} = \frac{1115}{3 \cdot 168^2} = 0.013 [\Omega] \quad (2.26)$$

2.4.2 Non-linear load

The load is a resistance connected to a DC-link in parallel with a capacitor (see figures 2.1 and 2.2). Upstream the DC-link there is a three-phase rectifier. To increase the generality of the problem, the rectifier is based on thyristor and not on diode. The diode rectifier is equivalent to a thyristor with firing angle $\alpha = 0^\circ$. As long as $\alpha < 90^\circ$, the device acts as a rectifier: however, to maintain a behaviour similar to diode rectifier, a low value of α is chosen, i.e. $\alpha = 10^\circ$. In the previous work, [20], a diode rectifier was used. Now it is important to have a thyristor rectifier in order to manage the reactive current. For the load, a resistance of 1 $[\Omega]$ is used. All these components are modelled as a current source at various harmonics. Current harmonics are pre-calculated for different loads and firing angles using numerical simulations in Simulink. The pre-calculated values are later inserted as harmonic current sources during the optimization process. It can be proved that increasing the firing angle, the reactive power into the grid increases and the voltage at the DC-link decreases; due to the latter, also the current at the upstream of the rectifier decreases. This is shown in figure 2.12, in which it is possible to see that increasing α , the ratio $\frac{P}{Q}$ decreases. By figure 2.13, it is shown the behaviour of P and Q when changing the load resistance: as load resistance increases P and Q decrease, keeping constant the voltage at DC-link. Note that when $\alpha = 90^\circ$, Q is greater than P; however this is an extreme case and it is not very common in practice because the variations of α around the base value are small.

Then, the model of current source of load resistance is obtained from a simulation in which the two parameters α and R_L are specified. Continuing with the harmonic study, the non-linear load is obtained from a Fourier analysis: it contains the first four harmonics and the fundamental. An example of current source of non-linear load is given in table 2.5. For the fundamental obtained from Fourier analysis, both real and imaginary parts are considered, as the account for the active and reactive power respectively. On the other hand, only the magnitude must be considered for harmonics. Harmonics not captured by the passive filters can be compensated, if necessary, by the APF. It is not always essential that APF compensate for harmonics not tuned with passive filters because these harmonics have a small magnitude and therefore they could comply with IEEE-519 without any intervention of APF. Only the fundamental of the non-linear load has the imaginary part due to the fact that the APF is able to control the amount of the reactive power into the grid only at 50 [Hz]. In figure 2.14 is also reported the magnitude of current as load resistance varies. As expected, the values of current decrease when the load resistance starts to increase. Looking upon the y axis it is clear that the amplitude of the fundamental is higher than the other harmonics: even if for low values of resistance the harmonics have peaks, the dominant behaviour is that of fundamental. The plot is marked for firing angle $\alpha = 10^\circ$ and a null value of the capacitance of the DC-link. As said before, the biggest harmonics are 5th and 7th.

Eventually, in figure 2.18 is reported the trend of active power P using the mesh function of Matlab. The plot shows that P has its maximum value when $\alpha = 0^\circ$ and $R_L = 0 [\Omega]$ (in plot the minimum value for R_L is 0.4 $[\Omega]$). When R_L and α start to increase, the active power P , decreases. If R_L augments, keeping constant the voltage at

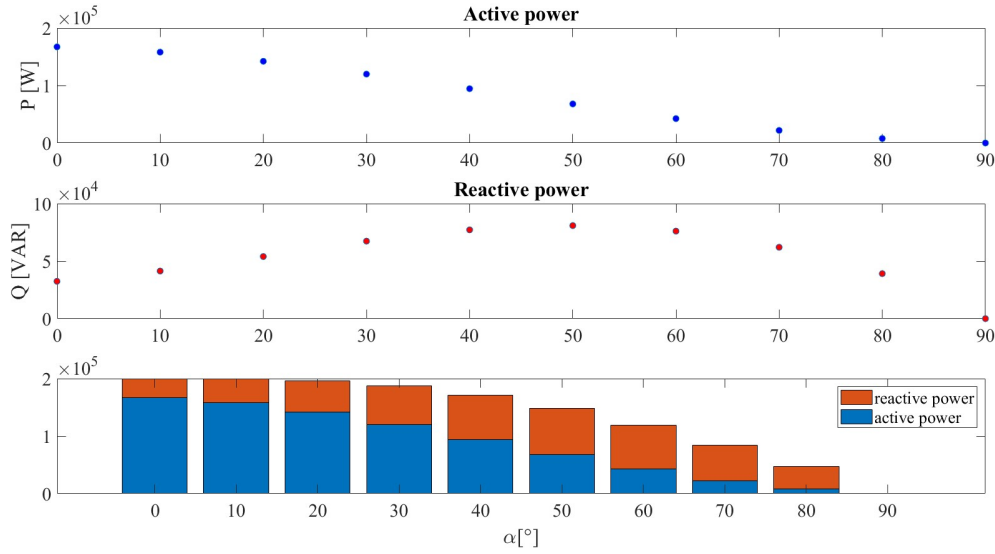


Figure 2.12: Active and reactive power vs. firing angle α with fixed load.

DC-link, the active current diminishes. As well, the active power P , proportional to the active current, diminishes. If α is enlarged, the displacement between phasor of current and voltage upstream the rectifier (that is V_{pcc}) is bigger, and as a consequence, there is a reduction in P because it is proportional to cosine of displacement.

Concerning the reactive power, figure 2.19 displays the results. The behaviour of the reactive power is stranger: from a theoretical point of view, when α augments, the reactive power increases as well because it is proportional to sin of the displacement between current and voltage. However, figure 2.19 shows that reactive power has a maximum when α is close to 50° . This trend is more evident when the load is minimum. While R_L increases, the reactive power decreases for the same reason as the active one.

In order to understand the shape of the reactive power, its equation has to be taken into account:

$$Q_t = 3 \cdot \frac{I}{\sqrt{2}} \frac{V_t}{\sqrt{2}} \sin(\theta_V - \theta_I) \quad (2.27)$$

where

- Q_t is the reactive power upstream the rectifier
- I is the phase current between grid and rectifier. This value comes from Fourier analysis, so it is a peak value.
- V_t (or V_{pcc}) is the phase voltage upstream the rectifier and downstream the grid impedance Z_g , that is the V_{pcc} . This value comes from Fourier analysis, so it is a peak value.
- θ_V is the phase of the voltage. It comes from Fourier analysis.
- θ_I is the phase of the current. It comes from Fourier analysis.

To realize figure 2.19, each element of (2.27) is analyzed:

- I : it is inversely proportional to R_L due to Ohm's law. It is also inversely proportional to firing angle α since as α increases the thyristors are conducting for less time, therefore the current decreases. The range of I is $0 < I < 760$ [A]. The behaviour is shown in figure 2.15.
- V_t : it is quite constant when R_L and α vary. It ranges from 325 to 180 [V], but the lowest value is hit just for low R_L and α . The trend is shown in figure 2.16.
- $\theta_V - \theta_I$: it does not change with R_L , although it varies with α . In particular as α increases the displacement between current and phase increases too. In the case of the problem, the range of variation of $\theta_V - \theta_I$ is

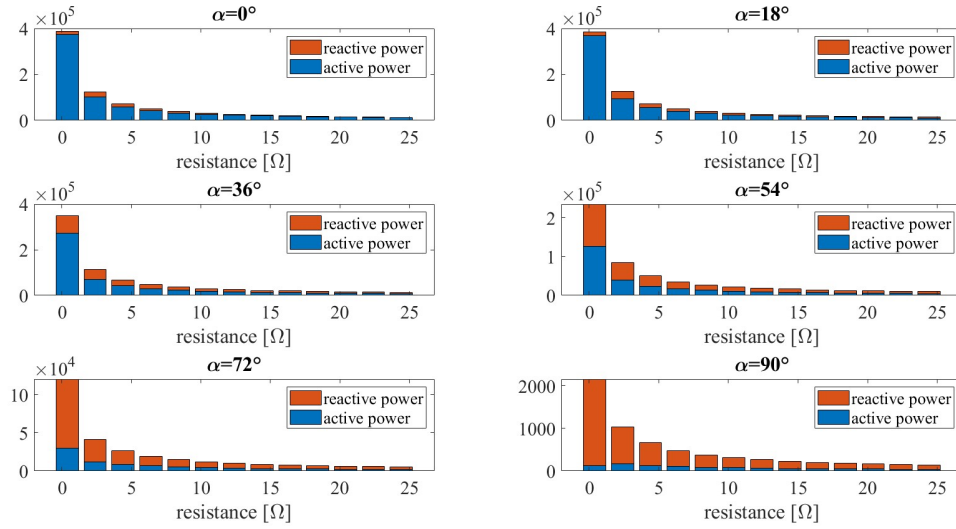


Figure 2.13: Active and reactive power vs. firing angle vs load resistance.

around $10^\circ < \theta_V - \theta_I < 70^\circ$. That said, the $\sin(\theta_V - \theta_I)$ is an increasing function. The trend is shown in figure 2.17.

In the end, considering that Q_t is a product of a decreasing element, i.e. I , an increasing element, i.e. $\sin(\theta_V - \theta_I)$ and a continuous element, i.e. V_t , it is reasonable that the trend of Q_t is that of figure 2.19.

2.5 Summarizing table

The table 2.2 summarize all the physical quantities already known, before the start of the optimization problem.

Physical quantity	Value	Unit of measure
f_g	50	Hz
V_g	$230\sqrt{2}$	V
R_g	$22 \cdot 10^{-3}$	Ω
L_g	10^{-3}	H
R_{f1}	0.13	Ω
R_{f2}	0.13	Ω
R_{APF}	0.013	Ω
I_{nl}^1	depend on α and R_L	A

Table 2.2: Table of assumptions.

-11 th harmonic	-5 th harmonic	1 st harmonic	7 th harmonic	13 th harmonic
9.2051	38.042	413.92+105.74i	21.306	6.3201

Table 2.3: Table of non-linear load with $\alpha = 10^\circ$ and $R_L = 1 [\Omega]$.

¹For $\alpha=10^\circ$ and $R_L=1 \Omega$, the vector of I_{nl} is in table 2.5

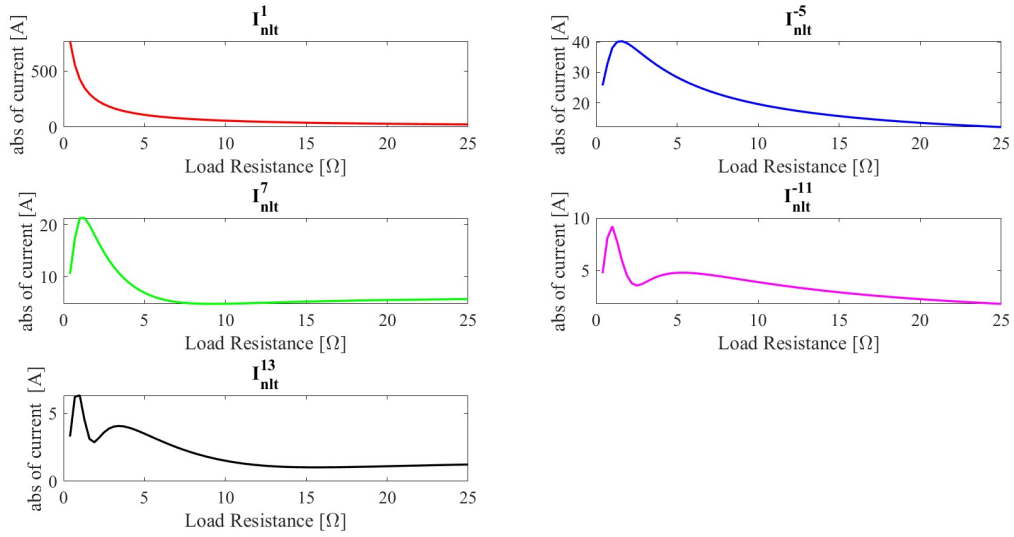


Figure 2.14: Absolute value of current upstream the rectifier, with firing angle $\alpha = 10^\circ$ and null capacitance of DC-link.

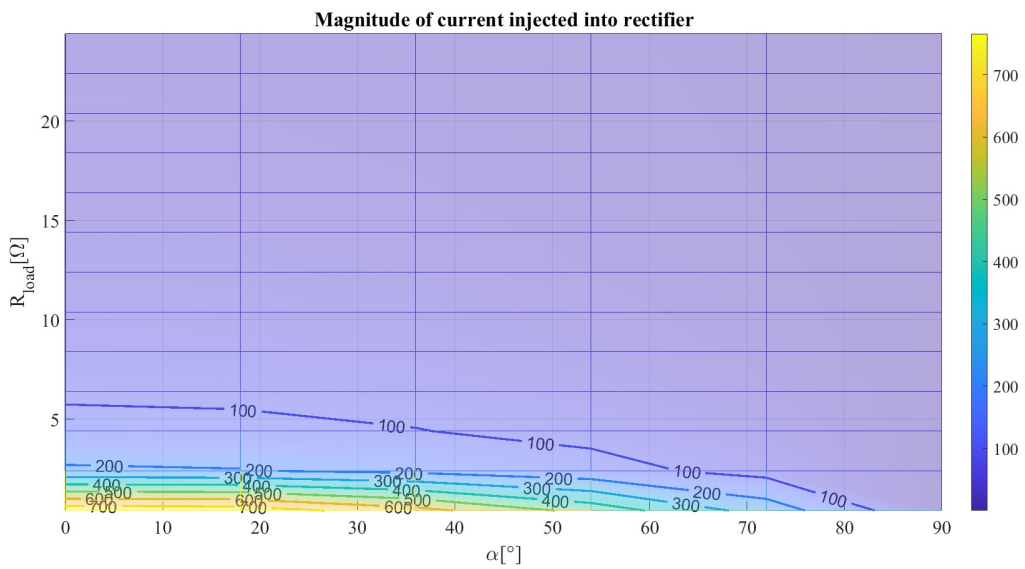


Figure 2.15: Magnitude of current. The colorbar illustrates the magnitude of the current in ampere [A]. The isocurves help to read the plot, without the exploitation of the colorbar.

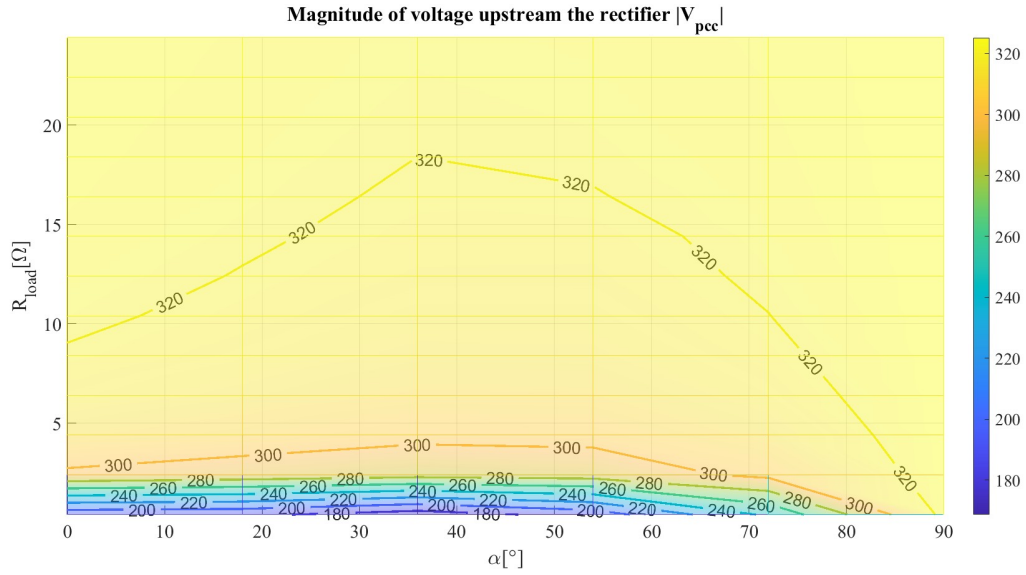


Figure 2.16: Magnitude of voltage at PCC. The colorbar displays the magnitude of V_{pcc} in volt [V].

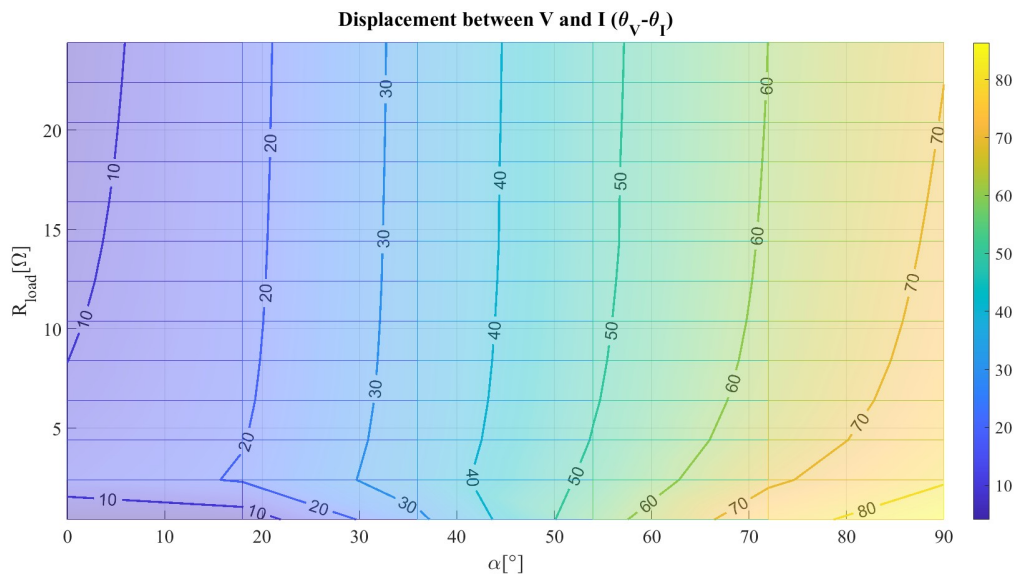


Figure 2.17: Displacement between V_t and I . The colorbar indicates the displacement in degree [°]. The isocurves help to read the plot, without the exploitation of the colorbar.

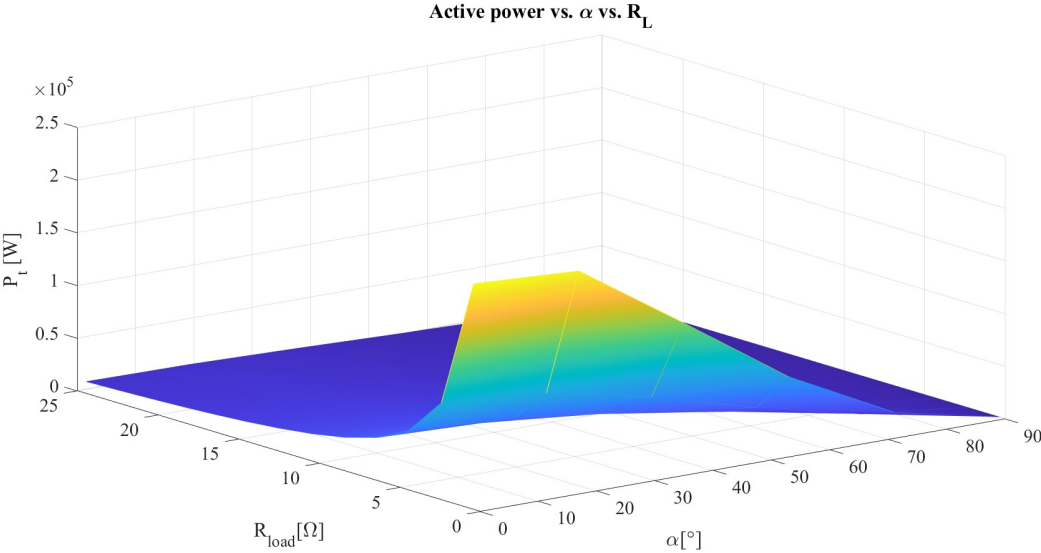


Figure 2.18: Active power vs. α vs. R_L .

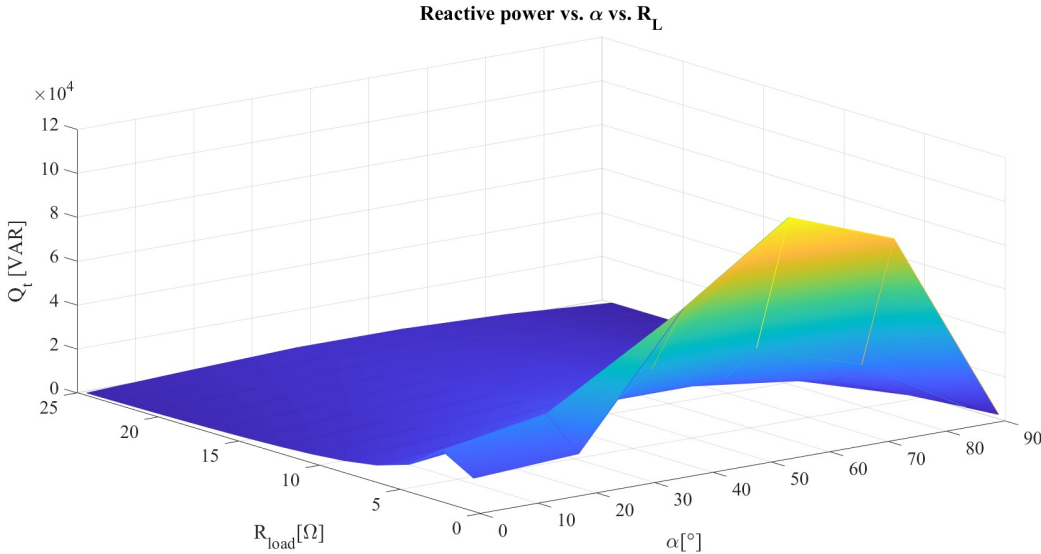


Figure 2.19: Reactive power vs. α vs. R_L .

3 Review of Iterative Optimizations Methods

The branch of mathematics studying optimization consists of many methods developed and improved during the last century, even if the main core was established by two English characters of the 17th century: Isaac Newton and Joseph Raphson.

In this section, it is presented a description of the general Newton-Raphson method and its application in optimization problems. Then other two algorithms, both available on the function `fmincon` of Matlab, are outlined: *sequential quadratic programming*² (SQP) and *interior-point method* (IPM). In addition, also a brief description of *gradient descent* method is provided, even if this method is not available in `fmincon`.

3.1 Newton-Raphson method [7]

This method is first described in one dimension and later generalized for n dimensions. Newton-Raphson is an iterative method that finds the zeros of a real function, under certain hypotheses. In order to start the iterative algorithm, an initial condition x_0 has to be known. Figure 3.1 shows immediately how the process works.

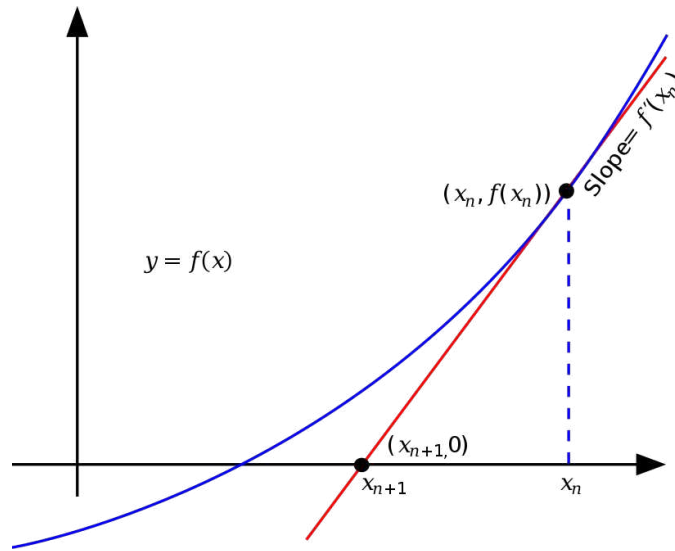


Figure 3.1: Graphical representation of Newton-Raphson method.

Figure 3.1 displays in blue the function of which is required to find the zero. Then, the starting point x_n (before is called x_0) intercepts the function in the point $(x_n, f(x_n))$. The red straight line is the tangent to the blue curve and intercepts on the x -axis the point $(x_{n+1}, 0)$, so the slope of the red straight line is given by

$$f'(x_n) = \frac{f(x_n) - 0}{x_n - x_{n+1}} \quad (3.1)$$

From (3.1), (3.2) is obtained

$$x_{n+1} = x_n - \frac{f(x_n)}{f'(x_n)} \quad (3.2)$$

That is the iterative method of Newton-Raphson, where n represents the number of the current iteration and $n + 1$ the next one.

²the term programming, in this context, is not referred to 'computer programming', but to finding procedures to solve mathematical problems. It can be a synonym of 'optimization'.

3.2 Newton's Method in optimization

In optimization focus is not on finding the zeros of a function, but the zeros of the first derivative of a function: these points, called 'critical points' can be maximums or minimums, according to the sign of the second order derivative. In one-dimension, given a twice differentiable³ function $f : \mathfrak{R} \rightarrow \mathfrak{R}$, the optimization problem is

$$\min_{x \in \mathfrak{R}} f(x) \tag{3.3}$$

This problem is solved, starting by an initial guess $x_0 \in \mathfrak{R}$, constructing an iterative sequence x_n , converging towards the minimizer x^* of f . The function f can be approximated using the 2^{nd} order Taylor expansion of f around each iteration x_n

$$f(x_n + t) \approx f(x_n) + f'(x_n) \cdot t + \frac{1}{2} f''(x_n) \cdot t^2 \tag{3.4}$$

where t is a small variation of x_n .

The next iteration x_{n+1} has to minimize (3.4) in t and setting $x_{n+1} = x_n + t$. If the second derivative is positive, (3.4) is a convex⁴ function of t and its minimum can be found setting the derivative to zero.

$$0 = \frac{d}{dt} [f(x_n) + f'(x_n) \cdot t + \frac{1}{2} f''(x_n) \cdot t^2] = f'(x_n) + f''(x_n) \cdot t \tag{3.5}$$

The minimum is achieved for $t = -\frac{f'(x_n)}{f''(x_n)}$. Finally, the iterative procedure for Newton's optimization is

$$x_{n+1} = x_n - \frac{f'(x_n)}{f''(x_n)} \tag{3.6}$$

Equation (3.6) is slightly different form (3.2) because it requires the evaluation of not only the first derivative, but also the second one.

Until now the function to minimize had only one variable, but the procedure can be generalized to more variables to optimize. Stating from (3.6), it is possible to replace the first derivative with the gradient and the reciprocal of the second derivative with the inverse of the Hessian matrix, resulting:

$$x_{n+1} = x_n - [f''(x_n)]^{-1} \cdot f'(x_n) \tag{3.7}$$

The Newton's method can be modified to assume the form:

$$x_{n+1} = x_n - \gamma \cdot [f''(x_n)]^{-1} \cdot f'(x_n) \tag{3.8}$$

If $0 < \gamma < 1$, the step-size of Newton's method is smaller, so the iterative process reaches the optimum with higher accuracy, but it requires longer time. If $\gamma > 1$, the step-size is larger, therefore the time spent on convergence towards the optimum is lower, but it could happen that the iteration 'jumps' over the minimum, skipping it. Newton's method with $\gamma > 1$ is also known as 'damped (or relaxed) Newton's method.

In some cases, it is preferred to avoid the calculation of the inverse of the Hessian. Thanks to the last definition Newton's method is stated in the following form:

$$x_{n+1} = x_n + \gamma \cdot d_n \tag{3.9}$$

where d_n is the search direction towards convergence. Figure 3.2 compares Newton's method using the Hessian and the gradient descent.

3.3 Pros and cons of iterative methods

The main drawback of Newton's optimization is that the inverse of Hessian matrix may not exist or its computation could be very expensive.

Newton's optimization can fail in some other cases. For instance the starting point x_0 lead to stop the iterative process if the objective function has $f'(x_0) = 0$ in (3.2) or $f''(x_0) = 0$ in (3.6) because a denominator equal zero appears.

³A function is differentiable if it has derivative for each points in its domain.

⁴A function is considered convex if a line segment between any two distinct points on the graph of the function lies above the graph between the two points.

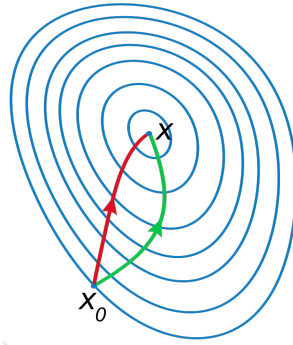


Figure 3.2: Green curve represents the gradient descent curve. Red curve represents Newton's method curve. The route of the Newton's curve is more direct because it uses the Hessian, so 2^{nd} derivative information, while the gradient descent exploits only the gradient, so 1^{st} derivative information.

Other reasons for failure can be that the objective function is discontinuous, and therefore not derivable in all points.

In general, the computational cost of iterative methods is high because the number of function evaluations is high. For instance, in each iteration the gradient and the Hessian should be evaluated. If there are N variables to optimize, the number of function evaluations increases as N^2 , for each iteration. If the algorithm takes k iterations to converge, the total number of function evaluations is $k \cdot N^2$.

In spite of all aforementioned drawbacks, the fact of evaluating both gradient and Hessian is a big advantage of these methods because it helps to improve the convergence rate.

In order to study non-linear constraints problems, Newton method is not sufficient because it is not suited for managing non-linear constraints. For this reason, other two algorithms will be analyzed:

- Sequential quadratic programming (SQP): it is a Newton based method for small-medium constrained problems
- Interior-point method (IPM): it is a large class of method for constrained optimization

In both these methods, there is not a direct evaluation of the Hessian.

3.4 Quadratic Programming (QP) [19]

QP is a method for solving optimization problems involving quadratic functions.

A QP problem, with n variables and m constraints is formulated as follow:

- a real-valued n -dimensional vector C
- a $n \times n$ dimensional real symmetric matrix Q
- $m \times n$ dimensional real matrix A
- m dimensional real vector b

the objective of QP is to find a n dimensional vector x that will minimize:

$$\min_{x \in \mathbb{R}^n} \frac{1}{2} x^T Q x + C^T x \quad (3.10)$$

subject to $Ax \leq b$

Note that $Ax \leq b$ is a system of linear inequalities, so QP is not fit for non-linear constraints. When minimizing a function f in the neighborhood of some reference point x_0 , Q is set to Hessian matrix $H(f(x_0))$ and C is set to gradient $\nabla f(x_0)$.

The main limitations of QP is the usage of linear constraints and having a quadratic objective function: this approach is not general. To overcome these restrictions, SQP method is introduced.

3.5 Sequential quadratic programming (SQP) [14]

SQP is an iterative method for constrained non-linear problems; it is also considered a *Quasi Newton Method*⁵. SQP is used if the objective function and the constraints are twice continuously differentiable, but not necessarily convex.

Considering a non-linear programming of the form (3.11), the Lagrangian for this problem is $\mathcal{L}(x, \lambda, \sigma) = f(x) - \lambda h(x) - \sigma g(x)$, where λ and σ are Lagrangian multiplier; $h(x)$ represents the inequality constraints while $g(x)$ the equality ones; both can be non linear.

$$\begin{aligned} & \min_x f(x) \\ & \text{subject to } h(x) \geq 0, \\ & \quad \quad \quad g(x) = 0 \end{aligned} \tag{3.11}$$

The advantage of using Lagrangian is that the whole problem is summarized in one equation.

If the standard Newton's method is applied now, the $\nabla \mathcal{L}(x, \lambda, \sigma) = 0$ is set and the problem is solved iterating $(x_0, \lambda_0, \sigma_0)$. It could happen that $H(\mathcal{L})$ is a singular matrix (and therefore non-invertible), so the Newton's step $d_k = [H(\mathcal{L})]^{-1} \cdot \nabla \mathcal{L}$ cannot be calculated. At this point the SQP method is applied.

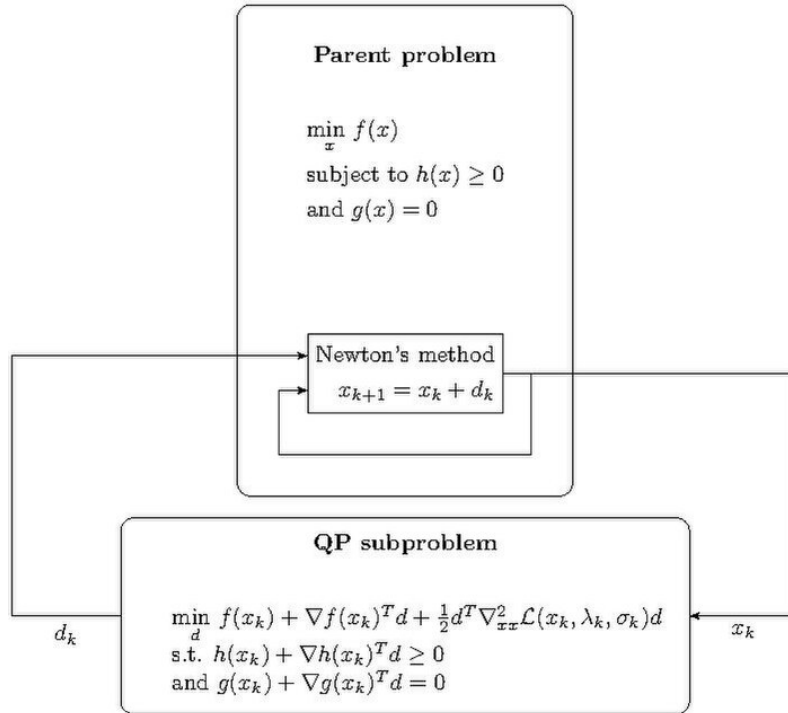


Figure 3.3: Explication of SQP algorithm, with parent problem and QP sub-problem.

Figure 3.3 depicts the procedure. SQP algorithm defines a search direction d_k at an iterate $(x_k, \lambda_k, \gamma_k)$ as a solution to the QP sub-problem (3.12).

$$\begin{aligned} & \min_d f(x_k) + \frac{1}{2} d^T H(\mathcal{L}(x_k, \lambda_k, \sigma_k)) d + \nabla f(x_k)^T d \\ & \text{subject to : } h(x_k) + \nabla h(x_k)^T d \geq 0, \\ & \quad \quad \quad g(x_k) + \nabla g(x_k)^T d = 0 \end{aligned} \tag{3.12}$$

Note that the term $f(x_k)$ can be eliminated because it is constant under the min operator.

⁵This word indicates the methods to find zeros or local maxima and minima function as an alternative to Newton's method. These procedures are used if the Jacobian or the Hessian are too expensive to compute at every iteration or are unavailable.

To sum up, the SQP algorithm starts by first choosing the initial iterate $(x_0, \lambda_0, \gamma_0)$, then calculating $H(\mathcal{L}(x_0, \lambda_0, \sigma_0))$ and $\nabla\mathcal{L}(x_0, \lambda_0, \gamma_0)$. Then the QP sub-problem is built and solved to find the Newton's step direction d_0 , which is used to update the parent problem iterate using $[x_{k+1}, \gamma_{k+1}, \sigma_{k+1}]^T$. The solving procedure of QP is easier: if QP has inequality constraints, (3.12) is equal to solving a sequence of systems. [22]

Moreover, SQP is not a feasible point method: it is not necessary that the initial point is feasible (viz. the initial point has not to satisfy all the constraints). A delicate step is the choice of the QP sub-problem. As said before, the QP deals with linear problems, while the SQP also solves non-linear problems. A good choice of QP sub-problem foresees a linearization of the search direction, about the current approximation x_k : the objective function appearing in (3.12) is a 2^{nd} order Taylor expansion of the search direction about the current iteration x_k ; also the constraints are linearized around x_k . [22]

3.6 Interior point method (IPM)

Interior point methods are used to solve various problems, from linear to non-linear, from convex to non-convex. [4]

First of all, it is relevant to define the *feasible region*. This region is defined by the constraints at which the optimization problem is subject to. Considering, at the beginning, only linear constraints, in 2-dimension the feasible region is a polygon while in 3-dimension is a polyhedron. The generalization of this concept in n -dimension is called *polytope*.

Before the introduction of IPM method (1984 [15]), the so-called 'simplex method' was adopted: it foresaw moving along the edges of the polytope, towards the vertex having the lowest value of cost function.

The innovation introduced by IPM regards the starting of the iterations inside the polytope, without passing through the edges: thus the optimum solution is reached with a low number of iterations and, as consequence, with a deducted computational time.

In the current section, there is a study of the method in linear programming (LP) and then its extension towards non-linear programming (NLP)

3.6.1 IPM with LP [18]

The function to minimize is

$$\begin{aligned} f(x) &= c^T x \\ \mathcal{K} &= \{x \mid Ax \geq b\} \end{aligned} \quad (3.13)$$

for $A \in \mathbb{R}^{n \times d}$, $c \in \mathbb{R}^d$ and $b \in \mathbb{R}^n$: x is the optimization variable, A is the constraint matrix, b is the constraint vector, and c is the objective function coefficient vector. $f(x)$ is a convex function and \mathcal{K} is a convex set. To find the starting point inside the convex set \mathcal{K} , another trivial IPM is exploited

$$\begin{aligned} \min t \\ \text{subject to } Ax &\geq (1-t)b \\ t &\geq 0 \end{aligned} \quad (3.14)$$

If $t^* = 0$, then x^* satisfies $Ax^* \geq b$, so it is a starting point inside the original polytope. The goal of IPM is to move towards the optimal solution, avoiding the immediate approach of the boundary of \mathcal{K} , denoted by $\partial\mathcal{K}$. To do so, the hard constraint $x \in \mathcal{K}$ is replaced by a smoother objective function that increases as x gets closer to $\partial\mathcal{K}$. The algorithm prevents getting closer to $\partial\mathcal{K}$ because it increases the objective function, not minimizes it.

The intermediate problem is enunciated as: for a scalar $w \geq 0$ and a convex function B , with $\lim_{x \rightarrow \partial\mathcal{K}} B(x) = \infty$

$$\min F_w(x) = wc^T x + B(x) \quad (3.15)$$

where $B(x)$ is called *barrier function*. A logarithmic barrier $B(x) = \sum_i^n -\log(a_i^T x - b_i)$ is chosen. The barrier function forces the iterations to remain in the interior of the feasible set. [11]

Let $x^*(w)$ be the optimal solution for F_w : $x^*(0)$ is called the 'analytical center' of polytope \mathcal{K} . As $w \rightarrow \infty$, $x^*(w)$ converges to the optimal solution. The curve traced by $x^*(w)$ for $w = [0, \infty]$ is called the 'central path'. A typical choice for w is a geometric sequence: w_1, \dots, w_T with $w_{i+1} = (1+q)w_i$, where q is the common ratio of the geometric sequence.

Eventually, $x^*(w_i)$ is found by means of Newton's method, using $x^*(w_{i-1})$ as the starting point. The figure

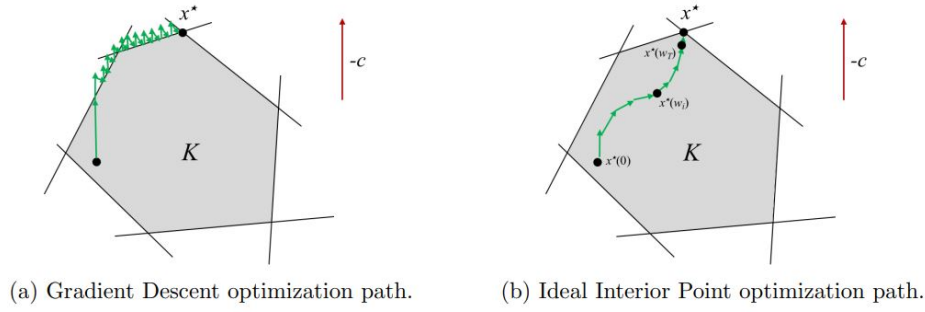


Figure 3.4: Comparison between gradient descent and IPM. $\nabla f = c$. [18]

3.4 illustrates the differences between the gradient descent and IPM. The latter starts from $x^*(0)$ and at the end it reaches $x^*(w_T)$ that is very close to the optimal solution x^* . In the gradient descent, the path is in the opposite direction of $\nabla f = c$, so the iterations move around the edge of the polytope. In IPM, the iterations do not move on $\partial\mathcal{K}$. In the end, IPM converges much faster than gradient descent because it uses 2^{nd} order derivative information, during Newton's iterations.

3.6.2 IPM with NLP [4]

After the description of LP, it is time to exhibit the solution of NLP using IPM. A function $f(x)$ has to be minimized⁶ subjected to equality and inequality constraints. The objective function and the constraints can be non-linear. The problem has the following standard form (it is slightly different from (3.11)):

$$\begin{aligned}
 & \min_x f(x) \\
 & \text{subject to } g(x) \geq b \\
 & \quad h(x) = 0 \\
 & \quad x \geq 0
 \end{aligned} \tag{3.16}$$

The problem has to be written without any inequalities: $g(x) \geq b$ is eliminated through the exploitation of *slack variables*⁷

$$g(x) \geq b \iff g(x) - b \geq 0 \iff g(x) - b - s = 0 \tag{3.17}$$

with $s \geq 0$.

Collecting all the equality of (3.16),

$$\begin{aligned}
 & \min_x f(x) \\
 & \text{subject to } c(x) = 0 \\
 & \quad x \geq 0
 \end{aligned} \tag{3.18}$$

Also the inequality $x \geq 0$ can be eliminated by introducing a logarithmic barrier function. The final form of the problem evolves in

$$\begin{aligned}
 & \min_x f(x) - \mu \sum_i^n \ln(x_i) \\
 & \text{subject to } c(x) = 0
 \end{aligned} \tag{3.19}$$

μ is known as *barrier parameter*: it is not a variable to optimize, but a parameter to decrease as much as possible; as a matter of fact, if x_μ is the solution of the barrier problem (3.19) and x^* is the solution of the original NLP, then

⁶the function can also be maximised simply taking into account the negative of the objective function.

⁷It is a variable added to an inequality constraint to turn it into an equality.

$$\lim_{\mu \rightarrow 0} x_\mu = x^*$$

It is not possible to simply put $\mu = 0$ because implementation problems can occur like singular or ill-conditioned matrices. [11]

In order to solve (3.19), the Lagrangian is calculated:

$$\mathcal{L}(x, \lambda) = f(x) - \mu \sum_i^n \ln(x_i) + \lambda c(x) \quad (3.20)$$

where λ is a lagrangian multiplier. Forcing $\nabla \mathcal{L} = 0$

$$\nabla f(x) - \mu \sum_i^n \frac{1}{x_i} + \lambda \nabla c(x) = 0 \quad (3.21)$$

In the end, defining $z_i = \frac{\mu}{x_i}$ and remembering the equality constraint $c(x) = 0$, the problem is written as

$$\begin{aligned} \nabla f(x) - z + \lambda \nabla c(x) &= 0 \\ c(x) &= 0 \\ XZe - \mu e &= 0 \end{aligned} \quad (3.22)$$

where $e = [1, 1, \dots, 1, 1_n]^T$.

The (3.22) is solved using Newton's method, with $[d_x^k, d_\lambda^k, d_z^k]^T$ as search direction. The iterations are

$$\begin{aligned} x_{k+1} &= x_k + \gamma d_x^k \\ \lambda_{k+1} &= \lambda_k + \gamma d_\lambda^k \\ z_{k+1} &= z_k + \gamma d_z^k \end{aligned} \quad (3.23)$$

where k is the iteration counter and γ is the step-size. γ is chosen in order to minimize the objective function and the constraint violations. A merit function $\Phi = f(x) + \sum |c(x)|$ is defined. The value of γ has to reduce this function at each iteration because a low merit function means a low value of cost function $f(x)$ and that the solution is zeroing the equality $c(x)$.

3.7 Gradient descent [9]

Gradient descent algorithms are used for optimizing neural networks and machine learning algorithms. [8]

The method of gradient descent is an iterative 1st order method that finds minima and maxima of a given function, that is the objective function. In the next the focus is on minimization, so gradient descent is used. To find maxima, gradient ascent has to be exploited.

The method works properly for convex and differentiable functions.

The basic idea is to take repeated steps in the opposite direction of the gradient of the function at a current point, because this is the direction of the steepest descent.

In the gradient descent algorithm, the next point is calculated using the gradient of the current point and subtracting this value to the current point. This is a step.

The subtracted quantity is multiplied by a scalar quantity $\gamma > 0$ called *step-size* or *learning rate*: a small learning rate implies a longer convergence or the function can reach the maximum number of iterations before reaching its minimum; vice versa, a large learning rate cannot converge because the algorithm could jump around the optimal point. It is possible to change the learning rate also at each iteration.

In a nutshell, the gradient finds the direction of the step while the learning rate finds the depth of the step.

Given a multivariable function $f(x)$ defined in $\mathfrak{R}^n \rightarrow \mathfrak{R}$, the value of the function at each iteration k is:

$$f(x_{k+1}) = f(x_k) - \gamma_k \nabla f(x_k) \quad (3.24)$$

The sign minus confirms the aim of minimization of the problem; if it were plus it would be a maximisation problem (gradient ascent). The algorithm can be stopped if the maximum number of iterations is reached or the

difference of two consecutive iterations is lower than a tolerance previously defined.

Choosing a starting point x_0 , a sequence x_0, x_1, x_2, \dots is such that $x_{k+1} = x_k - \gamma_k \nabla f(x_k)$ and the function $f(x)$ has a monotonic sequence like $f(x_0) > f(x_1) > f(x_2) > \dots$

An advantage of this algorithm is its simplicity of implementation and a low computational cost as only the gradient is evaluated, but not the Hessian.

Some disadvantages are clear if non convex functions are treated or during the optimization path some saddle points are found: in both cases the algorithm can stop because the $\nabla f(x_k) = 0$. In this case the 1st order algorithm is not enough, therefore 2nd order algorithms have to be investigated, but they require the evaluation of the Hessian. Moreover, gradient descent is a technique that cannot be used with constraints problems.

In the end, gradient descent is a method that relies on an objective function's gradient rather than an explicit exploration of the feasible region.

3.8 Conclusions about iterative methods

The main iterative method to solve non-linear constrained problems is Newton's method. Starting from this, others two methods are developed:

- Sequential quadratic programming (SQP)
- Interior point method (IPM)

Both evaluate the Hessian (or an approximation of it), so they are computationally expensive. The main difference is in the choice of the starting point: SQP is not a feasible point method, so the initial point (or any points of subsequent iterates) has not to satisfy the constraints. In contrast, IPM starts with a point that is inside the feasible region. A practical comparison of the two algorithms is given in table 6.11.

The gradient descent, instead, has the advantage of not evaluating the Hessian matrix, so if it converges it requires low computational cost but, perhaps, a high number of iterations if the learning rate is small. The main disadvantages of this technique are the use of 1st order derivative and the inability to be used with constraints. This drawback is shared with Newton-Raphson method. Moreover, gradient descent is not included in Matlab function `fmincon`, so it will not be discussed in the next.

4 Optimization of passive filters and APF

This chapter examines the variables that have to be optimized, so the unknowns of the problems. The known quantities have already been discussed in table 2.2. The aim of the optimization problem is to find the remaining unknowns. The table 4.1 lists the unknowns.

Then, the cost function and some parameters regarding its implementation in Matlab are introduced.

Physical quantity	Unit of measure	Description
C_{f1}	F	capacitance of passive filter #1
C_{f2}	F	capacitance of passive filter #2
L_{APF}	H	inductance of active power filter
I_{APF}^{-11}	A	current provided by APF at 11 th harmonic
I_{APF}^{-5}	A	current provided by APF at 5 th harmonic
I_{APF}^1 ⁸	A	imaginary current provided by APF at 1 st harmonic
I_{APF}^7	A	current provided by APF at 7 th harmonic
I_{APF}^{13}	A	current provided by APF at 13 th harmonic

Table 4.1: List of unknowns.

4.1 Absence of L_{f1} and L_{f2} in the list of unknowns

In the table 4.1 unknowns L_{f1} and L_{f2} are not quoted, even if they are two parameters of the passive filters that are not known;

A very important relationship between C_f and L_f is given by

$$f_h = \frac{1}{2\pi\sqrt{C_f L_f}} \quad (4.1)$$

f_h is called *cut-off frequency* or *resonance frequency*. As the frequencies of the harmonic content in the system are known, f_h can assume one of the following values: 250, 350, 550, 650 [Hz]. So once f_h is assigned, L_f is easily calculated as

$$L_f = \frac{1}{C_f(2\pi f_h)^2} \quad (4.2)$$

So now the main question regards the value of frequency to assign to f_h . It is reasonable to tune the passive filter on the frequency related to the highest harmonic magnitude in the grid. Usually the non-linear load injects the biggest harmonics at 250 and 350 [Hz], as confirmed by table 2.5. Nevertheless, this rule is not general, so much care has to be taken when choosing the tuning frequency for the passive filters. It can be demonstrated that an increase of the firing angle α makes higher the magnitude of the 11th than 7th one.

In the Matlab code used for the optimization, an automatic procedure detects the resonant frequency of the harmonics which have the highest magnitude among the harmonics of the non-linear load (see appendix B lines 11-36).

From a theoretical point of view, it would be possible to insert L_f into the class of variables to optimize and extract C_f by (4.1), once L_f is known. From a manufacturing point of view, it is more difficult to find the exact value of capacitance needed. Once acquired, the corresponding inductor is easier to trace because its value can be customized with higher accuracy than that of capacitance.

It is necessary to remember that once the passive filters are tuned, the physical system is built, that is, there is not any more chance to tune the passive filter for a different frequency.

⁸For I_{APF}^1 is only the imaginary part because it is not granted to compensate for the real part of the fundamental current: an APF can compensate for the magnitude of the harmonics and the imaginary part of the fundamental. In its simplest model, an APF is supplied by a capacitor which is not able to deliver a real net active power.

4.2 Optimization of active power filter

The APF has two main parts to optimize:

- L_{APF}
- total current of APF (I_{rated})

To prevent a significant voltage drop caused by the compensating current, it is desirable to have a low impedance. Therefore, the value of L_{APF} should be kept small.

However, if L_{APF} decreases too much, it leads to a negative effect: low impedance results in higher switching harmonics. In spite of this, in subsection 5.3 another criterion has been exploited to avoid that L_{APF} assumes scant values.

The sizing of the APF may be based on its nominal current. If the resistance of load decreases, in ceteris paribus, surely the current of the non-linear load will start to increase. Consequently, an APF with a higher I_{rated} may be required to accommodate the increased load current within its nominal rating; usually this device has to compensate for the reactive current of the fundamental and for two harmonics that are not caught by the passive filters. Furthermore, an increase of I_{rated} brings about an increase of the cost of the APF.

4.3 Formalization of the problem

This section describes what parameters are set in Matlab to use the solver `fmincon` (function minimization constrained). In the most general form, the problem of optimization aims to minimize a function, called *cost function* or *objective function* $f(x_i)$ where x_i is a vector of optimal solutions. The solution x_i has to comply with some constraints; there are two types of constraints:

- equality constraints $ceq(x_i) = 0$
- inequality constraints $c(x_i) < 0$

Also the lower (lb) and upper bound (ub) of the vector of solution has to be specified, therefore $lb_i < x_i < ub_i$. The Matlab solver used to face this problem is `fmincon`. `fmincon` has several algorithms: the one used to solve the problem is SQP which approximate the constraints with a second-order approximation. This algorithm is useful because the cost function has some quadratic elements, as said in section 4.8. Also the solver IPM is explored, but not used as the main solver because it has a larger running time.

Regardless of the solver used, the approach used is MultiStart, that runs uniformly distributed start points within bounds. The user can also select to run starting points outside the bound.

The user has to choose the k number of various starting points: The solver uses $k - 1$ starting points uniformly distributed in the bounds (if the option `bounds` is active, otherwise the starting points can be also outside the bounds) and one starting point is delivered by the user, i.e. the initial point requested by `fmincon`. The advantage of MultiStart is to run `fmincon` k times, each time from a different starting point. MultiStart stops if all the points has run or some stopping conditions are hit like:

- *FunctionTolerance*: $|f_{val}(k) - f_{val}(j)| < \text{FunctionTolerance}$
- *XTolerance*: $|x(k) - x(j)| < \text{XTolerance}$

The first conditions stop to search for a better solution if the difference of cost function between two consecutive iterates is lower than `FunctionTolerance`, that usually assumes small values like 10^{-6} , whereas the second condition stops the iteration if the difference between two consecutive iterates of optimal solutions is lower than `XTolerance` which is another small value like 10^{-6} . If the difference of two solutions is less than 10^{-6} , they are considered the same. [17]

Sometimes it could happen that the solver is not converging and a number of *MaxIterations* has to be defined to stop the iterative process.

If there are more than one solution, MultiStart will provide that with the lowest value of the cost function.

In order to understand if the solution found is complying with constraint, MultiStart produces a variable called *exitflag*: if its value is > 0 it means that the solution found is feasible, in particular if `exitflag=1` it means that all the constraints are satisfied, all solvers converged for all the starting points and solution found is close to the optimal one within a range called *OptimalityTolerance*, that could be 10^{-6} for example. The *OptimalityTolerance* is related

to the first-order optimality measure: this parameter indicates that the first derivative, close to a minimum, has to be as close as possible to zero or, better, assume values lower than 10^{-6} .

Instead, if the `exitflag=2`, it means that only a few solvers converged and the solution is complying with constraints within a range called *ConstraintTolerance*. Usually if the value of *ConstraintTolerance* is very low, i.e. 10^{-6} , the solver will not find any feasible solutions; if this happens, the value of *ConstraintTolerance* is increased until some solutions are found. The latter solutions could not be so precise because all the constraints are respected within a high margin, viz., *ConstraintTolerance*.

Conversely if the `exitflag` is < 0 it means that MultiStart stopped because it has not found a feasible solution. [6]

As stated before, all the variables to optimize have a lower and an upper bound; in the following sections these bounds for each variable are analyzed.

4.4 Lower bound *lb* and upper bound *ub* of C_f

To establish lower and upper bounds of capacitance, some considerations have to be made. First of all, considering all the possible values of f_h , plots in figure 4.1 of L_f vs. C_f have been traced.

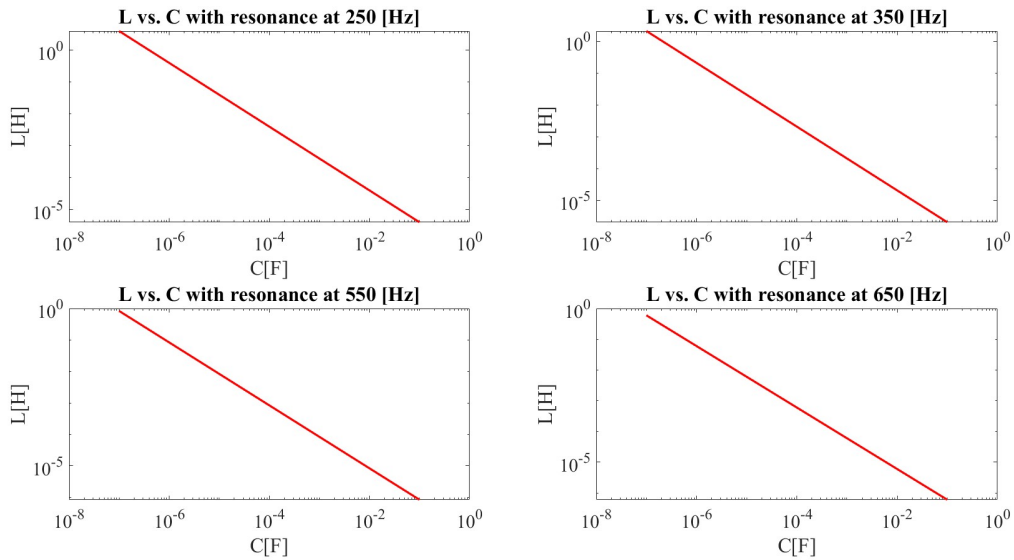


Figure 4.1: L_f vs. C_f for f_h equal 250, 350, 550 and 650 Hz. x and y axes are both logarithmic.

From figure 4.1 is clear that if capacitance increases, the inductance has to be reduced to maintain the cut-off frequency. The lower bound of capacitance can be set to 10^{-7} [F] because the corresponding lowest value of inductance is 0.5 [H] (at 650 [Hz]): the latter is already a big value, and, as a consequence, makes no sense to choose values of capacitance further lower because the corresponding values of inductance will be surely higher than 0.5 [H].

To find the upper bound, some considerations involving the Bode plot have to be taken into account. It has been noticed that if the magnitude of impedance of the filter at 50 [Hz] is too low, the passive filters are flowed by very huge values of current, in particular the reactive one.

To avoid this situation, it must be chosen a value of capacitance that let to have a high impedance of filter at 50 [Hz]. Arbitrarily, it has been decided to have a maximum magnitude of current in the filters at 50 [Hz] of $\frac{5}{100} I_L$, i.e. 16.4 [A], without load. This value of current, considering a circuit with no load, but only with grid voltage and passive filter, is reached if the magnitude of impedance is

$$|Z_{f,50 [Hz]}| = \frac{V_g}{\frac{5}{100} \cdot I_L} = \frac{230\sqrt{2}}{16.4} \approx 20 [\Omega] \quad (4.3)$$

Then, in the Bode plot the value to be searched is $20 \cdot \log_{10} 20 \approx 26$ [dB]. Considering s as Laplace variable, the

transfer function of impedance is

$$Z_f(s) = R_f + sL_f + \frac{1}{sC_f} \quad (4.4)$$

In figure 4.2 are shown Bode plots just for cut-off frequency of 250 [Hz]. Each curve is a spectral response of the impedance of the passive filter. The values of C_f are shown in the top right corner of figure 4.2. The corresponding values of L_f are derived by (4.2), fixing the cut-off frequency at 250 [Hz]. $R_f = 0.13$ [Ω] as mentioned in table 2.2. Figure 4.2 presents also the value of the impedance of filter at 50 [Hz], in [dB]. The value of $|Z_f|$ has to be greater than 20 [Ω] (or 26 [dB]). This condition is hit if, at least, the capacity takes on a value of 10^{-4} [F] because $|Z_{f,50 [Hz]}| = 30.55$ [Ω] as depicted in the table of figure 4.2.

In the end, it is possible to define the upper bound of capacitance at 10^{-4} [F].

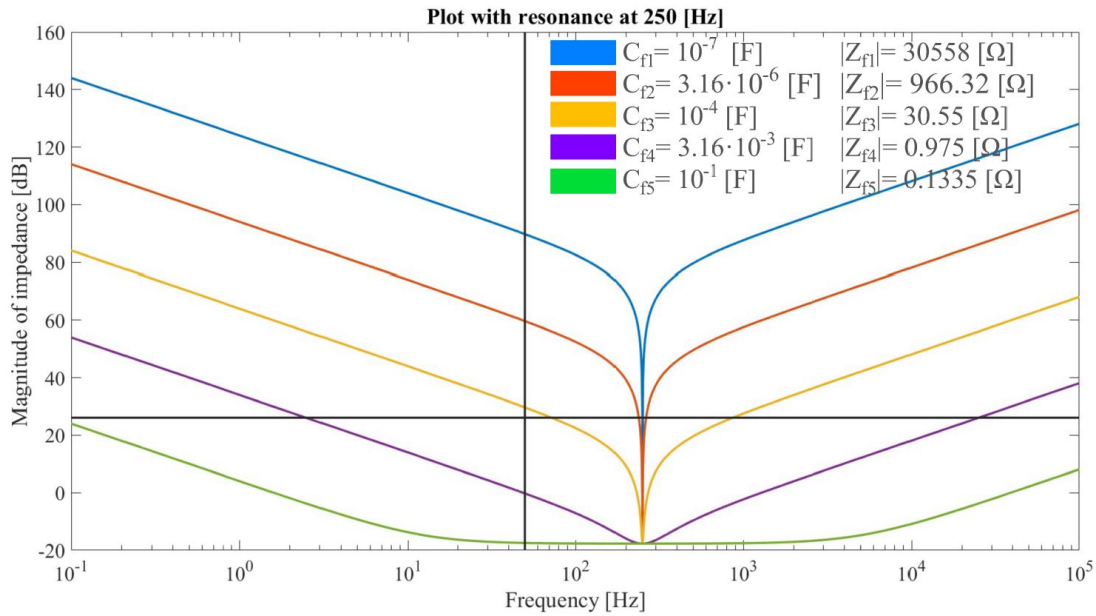


Figure 4.2: Bode plot for cut-off frequency of 250 [Hz] for various values of Z_f , and therefore capacitance. Focus on the values at 50 [Hz] (vertical line) and magnitude of 26 [dB] (horizontal line).

4.5 Selection of lower and upper bounds for L_{APF}

For the selection of L_{APF} two aspects must be considered:

- voltage drop on $Z_{APF} = R_{APF} + j\omega L_{APF}$ discussed in 5.3
- switching ripple of current due to the commutation of the power devices in the APF

The first phenomenon is not described in section 4.5 because it is a constraint while the second one is a bound. The difference between a constraint and a bound is related to the quantities involved: the numerical value of an upper or lower bound depends on variables that are not related to the optimization stages, while the constraint is related to some variables to be optimized.

To insert the bound of the ripple current in the optimization stage, it is necessary to find an analytical equation between the ripple of the current and the inductance of the APF. Moreover, the fundamental components of the voltage do not contribute to the ripple, so only the high-frequency voltage component has to be examined.

In [23], the analytical formulation (4.5) of the ripple current in an inductance is proposed.

$$\Delta i_{ripple} = \begin{cases} \frac{m_a V_{dc}}{2 \cdot L_{APF} \cdot f_s} \left(1 - \frac{3m_a}{2}\right) & m_a \in [0, m_a^*] \\ \frac{m_a V_{dc}}{2 \cdot \sqrt{3} L_{APF} \cdot f_s} & m_a \in [m_a^*, 1/\sqrt{3}] \end{cases} \quad (4.5)$$

where $m_a^* = \frac{2}{3} \left(1 - \frac{1}{\sqrt{3}}\right) \approx 0.28$.

Equation (4.5) is valid up to $m_a = \frac{1}{\sqrt{3}} \approx 0.57$, i.e. with the inverter operating in the linear region. So in the following, there will be assumed $m_a = 0.5$. The final value $m_a = \frac{1}{\sqrt{3}}$ is due to the fact that the inverter is working inside the circumference of radius $\frac{V_{dc}}{\sqrt{3}}$, inscribed in the hexagon with half-diagonal equal to $\frac{2}{3}V_{dc}$.

The APF, as with any inverter, has various operation modes and their modifications also change the modulation index, therefore the output voltage of the inverter. The figure 4.3 depicts three types of modulation:

- six-step
- triplen harmonic injection (SVM)
- sinusoidal (PWM)

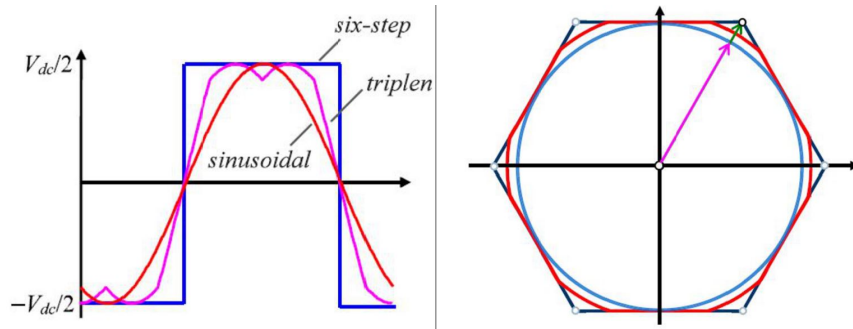


Figure 4.3: Three modes of operation of inverter. [2]

The six-step mode has the advantage of having the highest output voltage equal to $\frac{2}{\pi \cdot V_{dc}} \approx 0.64 \cdot V_{dc}$ and lowest switching frequency, but it produces a lot of harmonic content because the operations are on the edge of the hexagon: the inverter is in overmodulation.

The PWM mode has a lower harmonic content than six-step because it is not working on the edge of hexagon, but it is not exploiting at maximum the converter as the output voltage is $0.5 \cdot V_{dc}$. The vector voltage, seen on hexagon, is far from the edges.

The SVM, which corresponds to PWM with triplen harmonic injection, has an output voltage limit of $\frac{V_{dc}}{\sqrt{3}} \approx 0.57 \cdot V_{dc}$, that is higher than PWM. The inverter is operating on the inscribed circumference of the hexagon, so it is not touching the edge of the hexagon: the harmonic content is low because the inverter is not in overmodulation.

All the output voltages aforementioned are referred to a phase and the point O (see figure 2.6), so they are the peak values of the phase to line voltages.

The (4.5) is valid if the output voltage is lower than $\frac{V_{dc}}{\sqrt{3}}$, so for SVM and for PWM, not for six-step operating mode.

The (4.5) is very similar to that of the voltage at the ends of an inductance:

$$v_{L_{APF}} = L_{APF} \frac{di_{L_{APF}}}{dt} \quad (4.6)$$

that can be written with finite difference form as:

$$v_{L_{APF}} = L_{APF} \frac{\Delta i_{L_{APF}}}{T_s} \quad (4.7)$$

where

- $\Delta i_{L_{APF}}$ is the ripple of current
- T_s is the switching period of the APF

Equations (4.5) and (4.7) describe the decrease of the ripple of the current if the f_s or L_{APF} increase. Besides, (4.5) shows that the ripple of current is proportional to the modulation index. The value chosen for the DC-link voltage of the inverter is $V_{dc} = 600$ [V], which would be adequate if 1.2 kV power devices are used. A value of

$f_s = 10$ [kHz] is chosen. The ripple of current is decided to be $\Delta i_{ripple} = \frac{5}{100} I_L = 16.4$ [A], so a small fraction of the rated current I_L .

Therefore, by the second equation of (4.5)

$$L_{APF} = \frac{m_a V_{dc}}{2\sqrt{3} f_s \Delta i_{ripple}} = \frac{0.5 \cdot 600}{2 \cdot \sqrt{3} \cdot 10^4 \cdot 16.4} = 5.28 \cdot 10^{-4} \text{ [H]} \quad (4.8)$$

A minimum value of $L_{APF} = 0.528$ [mH] is found to provide an adequate current harmonic content. If the L_{APF} is lower than this value, it implies an increase of the harmonic content in the grid due to switchings of the inverter. At this point, one can think of taking the highest value of L_{APF} in order to have the lowest value of Δi_{ripple} . If this procedure is pursued, then the voltage drop along the impedance of APF will be extremely high. Until now, briefly, it is possible to say that the voltage drop along Z_{APF} is

$$\Delta V_{drop} = I_{APF,h} \cdot |Z_{APF,h}| \quad (4.9)$$

where, $Z_{APF,h} = R_{APF} + j \cdot \omega_h L_{APF}$. This topic is scrutinized in section 5.3 because it depends on $I_{APF,h}$, viz., a variable to optimize, so it is a constraint and not a bound. For the time being, a reasonable upper bound value of L_{APF} is 10^{-1} [H]. It is important to set an upper and lower value for each optimizing variable because, otherwise, the optimization algorithm will not start.

4.6 Lower bound and upper bound of I_{APF}

The extreme limit of the current of the APF are decided arbitrarily, adopting a maximum nominal current of $|I_{APF,h}| < \frac{I_L}{2}$, that means $-164.0 < I_{APF,h} < 164.0$. $I_{APF,h}$ is the current of the h -harmonic, but it also includes the reactive current at fundamental just for simplicity of notation. If the APF uses all its $\frac{I_L}{2}$ to compensate for one single harmonic or the reactive current, it will not be able to compensate for the remaining.

It is relevant to note that the currents appearing in I_{APF} are the magnitudes, and not only the real components of the harmonics. Just for the fundamental, the current provided by the APF is the reactive one; thus the sign of $I_{APF,h}$ has to be always the same as the component of the non-linear load that it is compensating for. This information is introduced in the Matlab code using some *if* structures (see appendix B lines 132-183).

4.7 Summarize of upper and lower bounds

The correct selection of ub and lb is very decisive to the success of the optimization procedure. Eventually the upper and lower bounds can be written in the table 4.2

Variable to optimize	Lower bound	Upper bound	Unit of measure
C_{f1}	10^{-7}	10^{-4}	[F]
C_{f2}	10^{-7}	10^{-4}	[F]
L_{APF}	$5.28 \cdot 10^{-4}$	10^{-1}	[H]
I_{APF}^{-11}	$-\frac{I_L}{2}$	$\frac{I_L}{2}$	[A]
I_{APF}^{-5}	$-\frac{I_L}{2}$	$\frac{I_L}{2}$	[A]
$I_{APF,react}^1$	$-\frac{I_L}{2}$	$\frac{I_L}{2}$	[A]
I_{APF}^7	$-\frac{I_L}{2}$	$\frac{I_L}{2}$	[A]
I_{APF}^{13}	$-\frac{I_L}{2}$	$\frac{I_L}{2}$	[A]

Table 4.2: List of upper and lower bounds of unknowns.

Remainder: I_L is the rated current and its value is 327.93 [A].

4.8 Cost Function

The cost function, often called objective function, is the function that has to be minimized. It has to contain all the variables to optimize. Consistently, one of the easiest choices for the cost function is a linear function consisting of the sum of all elements appearing in the variable x , i.e. the optimal solution.

$$f(x) = \sum_i^n x_i = x_1 + x_2 + \dots + x_n \quad (4.10)$$

where n is the number of variables to optimize. The major advantage of this kind of cost function is its simplicity and its linearity that helps the solver make calculations easier and faster.

A drawback of this solution is that if the variables can assume negative values, the solver tries to minimize $f(x)$ and, as a consequence, to maximize the variable with a negative sign. The target of the studied case is that also the variables with negative values assume the lowest value in magnitude.

In the study of variables of APF it is not possible to use linear cost function because the currents can assume negative values. In order to have all positive values, there are two solutions:

- use of absolute value
- use of quadratic coefficient

To help the solver with its computation is preferable the use of quadratic coefficient because the derivative of the quadratic coefficient is a continuous function; while for the absolute value the derivative has a discontinuity. As stated in section 3.3, Newton's method can be stopped not intentionally if discontinuous functions are used.

That said, the cost function is written as follow:

$$f(x) = \sum_i^n x_i^2 = x_1^2 + x_2^2 + \dots + x_n^2 \quad (4.11)$$

Finally, each element of the cost function is multiplied by a weighting factor. Introducing a weighting factor is vital when a cost function consists of variables whose nominal values can differ in several orders of magnitude, as is the case for capacitors, inductors and currents. With the appropriate selection of these factors, the final value of the cost function will give the same importance, same 'weight' to each variable. The final version of the cost function could be as:

$$f(x) = \sum_i^n w_i x_i^2 = w_1 x_1^2 + w_2 x_2^2 + \dots + w_n x_n^2 \quad (4.12)$$

In the case of passive filters and active one, the objective function contains quadratic elements: in fact another advantage is precisely that squared variables penalize larger values more than linear ones allowing, thus, to have small values of variables and therefore a reduction of the objective function. The form of the cost function is

$$f(x) = w_{C_{f1}} C_{f1}^2 + w_{C_{f2}} C_{f2}^2 + w_{L_{APF}} L_{APF}^2 + w_{I11} I_{APF,11}^2 + w_{I5} I_{APF,5}^2 + w_{I7} I_{APF,7}^2 + w_{I13} I_{APF,13}^2 + w_{APF,react} I_{APF,react}^2 \quad (4.13)$$

One of the most critical parts is the selection of the weighting coefficients: a reasonable criteria is to choose these coefficients so that the product $w_i x_i$ is equal to 1; with this method all the elements have the same significance. In most simulations, after the optimal results are obtained, it has to verify if the constraints are respected. If not, some weighting coefficient can be changed and the simulation is performed again.

In (4.14) are clarified the weights used in (4.13). This is an example of a cost function used in the optimization problem; it can be found in appendix B line 236.

$$w_{C_{f1}} = (4 \cdot 10^4)^2; w_{C_{f2}} = (4 \cdot 10^4)^2; w_{L_{APF}} = (3.8 \cdot 10^3)^2; w_{I11} = 10^{-2}; w_{I5} = 5 \cdot 10^{-1}; w_{I7} = 8 \cdot 10^{-1}; w_{I13} = 10^{-2}; w_{APF,react} = 10^{-2}; \quad (4.14)$$

By equation (4.14) can be seen that for variables with low values, high weighting factors are used and vice versa.

All the variables playing into the cost function have to be as low as possible:

- as for inductors and capacitors, lower is their value, then lower will be their economic cost and their bulk
- as for currents, they have to be small in order to not stress the APF and to reduce the ohmic losses that increase with the square of the current.

4.9 Initial value

Fmincon requires initial values to launch the solver. Using the MultiStart approach the initial points are uniformly distributed. These points should be evenly distributed within the upper and lower bounds in order to not 'waste' the initial guesses, i.e. choosing starting values that are not feasible.

Nevertheless, there is one initial point that has to be decided by the user. In fact, if MultiStart runs k number of points, the algorithm chooses only $k - 1$ points because the remaining is decided by the user. This procedure is mandatory in fmincon since it can be used also with other optimization approaches, like *GlobalSearch*, that does not exploit different initial points such as MultiStart, but uses only the starting point defined by the user.

If the optimization solver is not finding a feasible solution, a good relief could be the modification of initial values; the new initial point can be found, for instance, putting the cost function $f(x) = 0$, and using the solutions of the optimization stage as initial points. In this way only the points inside the bounds and those are complying with constraints will be considered. If that does not work either, the 'final solution' is to put equal to zero not only the cost function but also starting to reduce (or eliminate) the constraints; if all constraints are eliminated, the solution found is only contained inside the bound and can be used as initial value for a next optimization in which some constraints can be included again. Finally, the cost function can be restored to its original structure. More details are explored in [21].

The initial point is a vector containing all the initial values of the variables. If the solution of the optimization problem is known, then the initial point will coincide with the optimal solution.

Usually, the solution is not known but the user has to expect to find a certain reasonable solution. In the case of this problem, the non-linear load provides some useful information about the initial values: the two harmonics with the highest amplitude of the current have to be captured by the two passive filters, so the initial condition for these two harmonics is zero because the APF is not acting on them. The initial condition for the remaining harmonics has to be a value close to that of non-linear load. Same for the reactive current. The value of capacitance and inductance should be a value intermediate between their upper and lower bounds.

Fortunately, for the MultiStart approach the choice of the initial points is not as vital as in other approaches because a number of initial points are run. In other approaches, if the initial points are 'too far' from the optimal solution, the solver could not converge to a feasible solution.

Table 4.3 reports the initial condition used:

C_{f1} [F]	C_{f2} [F]	L_{APF} [H]	I_{APF}^{-11} [A]	I_{APF}^{-5} [A]	$I_{APF,react}^1$ [A]	I_{APF}^7 [A]	I_{APF}^{13} [A]
10^{-4}	10^{-4}	10^{-3}	-10^{-3}	-10^{-3}	-10^{-3}	-10^{-3}	-10^{-3}

Table 4.3: Table of initial solution.

The values used are not respecting the criteria aforementioned, just for practical reason: it has been avoided to change the initial conditions every time the non-linear load changes. However, for the MultiStart approach this is not so problematic.

5 Constraints of the optimization problem

This section presents all the constraints involved during optimization. In this problem of optimization, there are not equality constraints, but only inequality constraints. Reading documentation of `fmincon`, it is understood that all inequality has to be noted like $ceq(x) < 0$. If there is a constraint like $ceq(x) > 0$ it has to be converted in the form with < 0 .

5.1 IEEE 519-2022

The main equation used to comply with the constraints of IEEE 519-2022 is (2.3). This equation is simplified for the harmonics because the voltage source V_g at a frequency different of 50 [Hz] is zero.

$$I_{gh} = \frac{-V_{pcc,h}}{Z_{g,h}} = \frac{-I_{APF,h} + I_{nl,h}}{1 + \frac{Z_{g,h}}{Z_{f1,h}} + \frac{Z_{g,h}}{Z_{f2,h}}} \quad (5.1)$$

Equation (5.1) is used 4 times, once per each harmonic and it involves all the optimization variables, except L_{APF} . The absolute value of I_{gh} divided by I_L must be lower than the values taken from the table 2.3. $\frac{I_{gh}}{I_L}$ is called *individual harmonic distortion (IHD)*.

Similar considerations are valid for TDD (see equation (2.23)), that must be lower than 5% (by table 2.3).

5.2 Quality factor

The *quality factor* is defined as

$$Q_f = \frac{1}{R_f} \sqrt{\frac{L_f}{C_f}} \quad (5.2)$$

for a series⁹ of R, L and C.

It represents the ratio between the stored energy in L_f and C_f and the dissipated energy in R_f . It is a parameter regarding only the passive filters. By equation (5.2), it can be seen if Q_f is high, then R_f must be low; i.e. at the resonance frequency a lot of current flows through the passive filter. The disadvantage of having a high value of Q_f is that the filter is able to detect only the specific frequency for which it has been tuned. For instance, in reality, it could not exist a harmonic of exactly 250 [Hz], but maybe it would be at 248 [Hz]. If Q_f is high, this harmonic could be only partially captured by the passive filter.

On the other hand, having a low value of quality factor implies that the resistance of the filter is very high: the filter is able to capture harmonics on a wide range of frequencies, but the current flowing through the filter is limited by the resistance.

According to [5], a good range of value for Q_f is:

$$15 < Q_f < 80 \quad (5.3)$$

Figure 5.1 allows to understand more easily what happens if the resistance of the filter changes: with high value of resistance (f.i. $R_1 = 10$ [Ω]), the impedance at cut-off frequency is equal to resistance but the value of impedance changes slowly as frequency changes. So, also a harmonic with a frequency close to the resonance one is filtered. This kind of filter works well not only with the harmonics at cut-off frequency, but also with harmonics having a frequency close to that of resonance. The reverse deems are valid for the passive filter with low resistance (f.i. $R_2 = 0.01$ [Ω): it works very well at the cut-off frequency, but not for other harmonics having frequency different to that of the cut-off frequency. The change in impedance is very fast as frequency moves away from the resonance. In figure 5.1, the values of $L=6.62 \cdot 10^{-3}$ [H] and $C=6.12 \cdot 10^{-5}$ [F] are given, so the two values of quality factor are

$$\begin{aligned} Q_1 &= \frac{1}{R_1} \cdot \sqrt{\frac{L}{C}} = 1.038 \\ Q_2 &= \frac{1}{R_2} \cdot \sqrt{\frac{L}{C}} = 1038 \end{aligned} \quad (5.4)$$

⁹for a parallel configuration of R, L and C the quality factor $Q_f = R \cdot \sqrt{\frac{C}{L}}$.

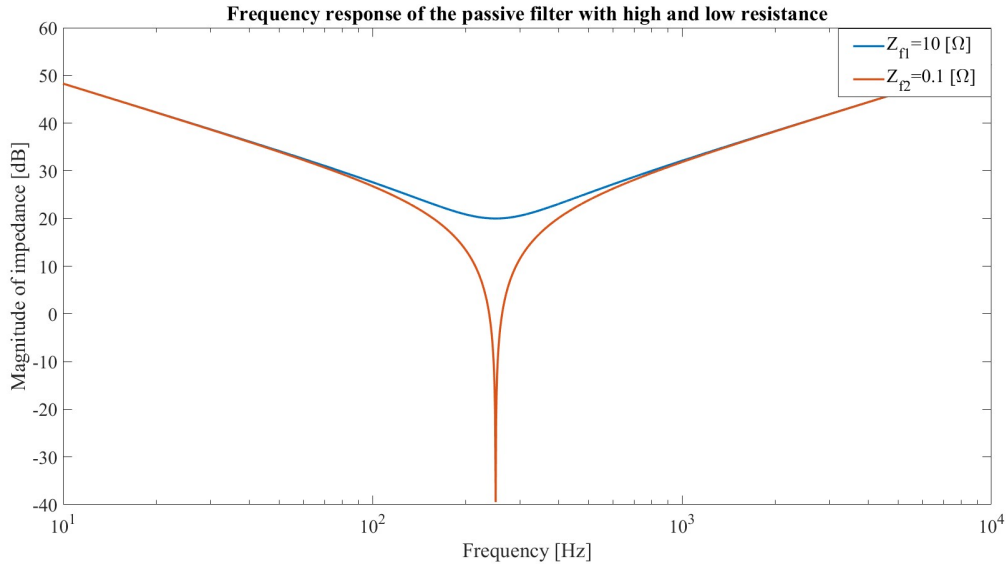


Figure 5.1: Response of RLC filter with $R=10$ [Ω] vs response of RLC filter with $R=0.01$ [Ω]. Both the filters have the same L and C . The resonance frequency is 250 [Hz].

As one can expect, if the difference in the resistance values spans three orders of magnitude, then the same is observed for the quality factors.

In addition, a higher R_f implies a higher damping effect, but also the response of the filter starts to be different from an ideal one.

5.2.1 Parallel resonance frequency

The passive filters do not operate isolated from the grid, so in the analysis of the response of the passive filters also the grid impedance has to be contemplated. To study this phenomenon, the simplified system of figure 5.2 is considered. There are three impedances in parallel and a harmonic current source; the APF is not included. The

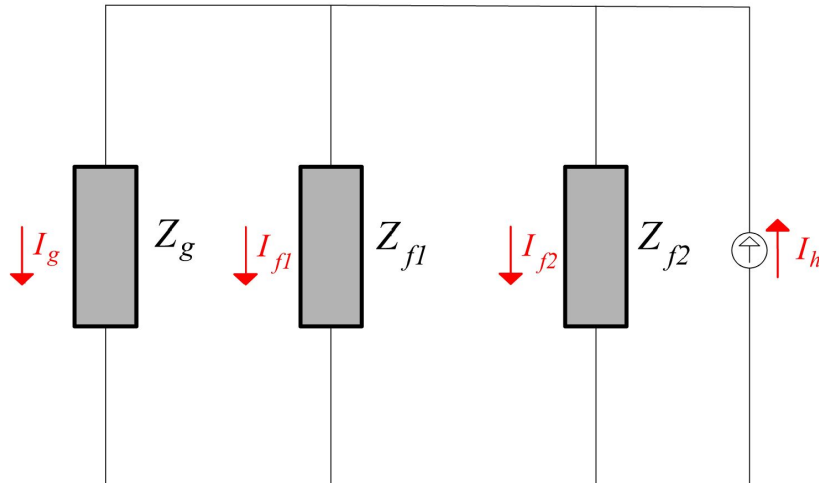


Figure 5.2: System of harmonic source I_h , Z_{f2} , Z_{f1} and Z_g . Voltage grid source V_g is a short-circuit at harmonic frequency $f_g \cdot h$.

transfer function of the grid and filters impedances in Laplace domain are:

$$\begin{aligned} Z_g(s) &= R_g + sL_g \\ Z_{f1}(s) &= R_{f1} + sL_{f1} + \frac{1}{sC_{f1}} \\ Z_{f2}(s) &= R_{f2} + sL_{f2} + \frac{1}{sC_{f2}} \end{aligned} \quad (5.5)$$

Looking upon the parallel of the two filters, it results

$$Z_{fp}(s) = \frac{Z_{f1} \cdot Z_{f2}}{Z_{f1} + Z_{f2}} \quad (5.6)$$

Z_{fp} is flowed by the current $I_{f1} + I_{f2}$, which can be written as $I_h - I_g$ according to *Kirchhoff current law (KCL)*. Then the voltage of the two remaining parallel branches is the same:

$$I_g \cdot Z_g = Z_{fp} \cdot (I_h - I_g) \quad (5.7)$$

Finally, the transfer function relating I_g and I_h is

$$\frac{I_g}{I_h} = \frac{Z_{fp}}{Z_g + Z_{fp}} \quad (5.8)$$

The frequency response of (5.8) is in figure 5.3. At low frequency, as 50 [Hz], the ratio I_g/I_h is 0 [dB], that is, the grid current is not affected by anti-resonance phenomenon. The disadvantage of having a passive filter is relevant at the peaks at 230 [Hz], due to the filter tuned at 250 [Hz] and 326 [Hz], due to the filter tuned at 350 [Hz] (the filters are tuned to these frequencies as explained in subsection 6.3). At these frequencies, the ratio I_g/I_h assumes high values, therefore, even just a small harmonic at frequency of 230 or 326 [Hz] will cause an enormous current into the grid. The risk of huge grid currents is avoided if there are no harmonics injected at the frequencies of the two peaks.

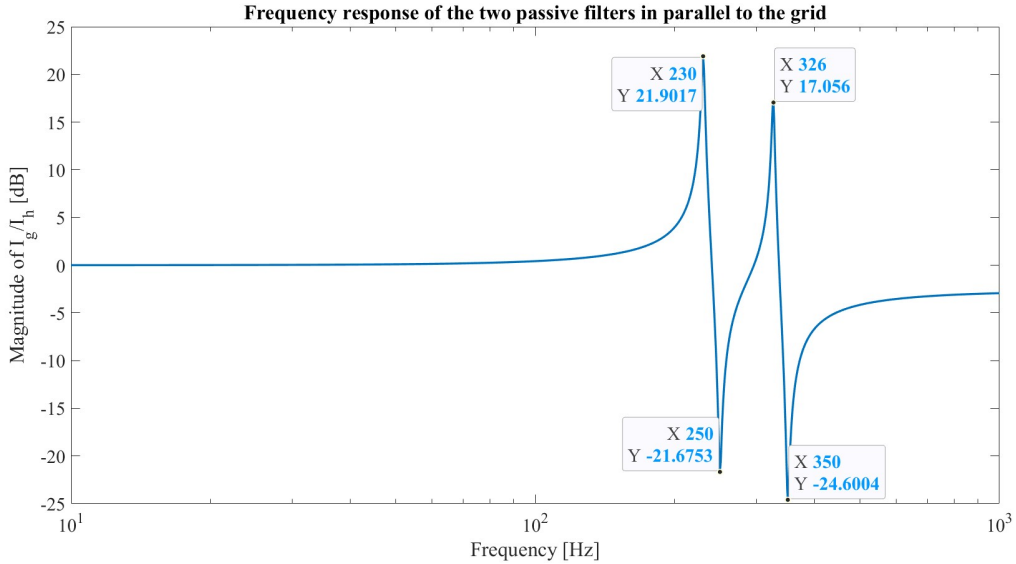


Figure 5.3: Frequency response of the two passive filters and the grid. The plot is obtained using following R, L and C values: $R_g = 22$ [m Ω]; $L_g = 1$ [mH]; $R_{f1} = R_{f2} = 0.13$ [Ω]; $L_{f1} = 6.6$ [mH]; $C_{f1} = 0.612$ [mF]; $L_{f2} = 4.7$ [mH]; $C_{f2} = 0.437$ [mF].

The peak frequencies are given by [20]:

$$f_p \approx \frac{1}{2\pi\sqrt{(L_g + L_f)C_f}} \quad (5.9)$$

The values of frequency obtained by Matlab bode diagram are very close to that derived by (5.9), hence using the value reported in caption of figure 5.3 it results

$$\begin{aligned} f_{p1} &= \frac{1}{2\pi\sqrt{(L_g + L_{f1})C_{f1}}} = 318 \text{ [Hz]} \\ f_{p2} &= \frac{1}{2\pi\sqrt{(L_g + L_{f2})C_{f2}}} = 233 \text{ [Hz]} \end{aligned} \quad (5.10)$$

The values of f_{p1} and f_{p2} are similar to that of figure 5.3. The values are not perfectly equal because (5.9) is valid for a single passive filter and it does not consider the parallel of the two passive filters: the values of (5.9) are obtained consider a system with only a passive filter and grid impedance.

The non-linear load of this thesis, i.e. I_h , injects harmonics at 250 [Hz] and 350 [Hz], where the magnitude of the ratio I_g/I_h is very low, preventing huge currents into the grid. The problem of the anti-resonance is relevant if the system undergoes sudden changes that alter the frequency of the injected harmonics: it is relevant during transient-state. As the problem studied is in steady-state, anti-resonance is neglected. In the optimization stages the problem of parallel resonance is not considered.

5.3 L_{APF} and voltage drop

The criterion decided for the L_{APF} is the voltage drop on the impedance of the APF. Theoretically, the ΔV_{drop} is due to the the sum of voltage drops provoked by each harmonic of current injected by APF. Therefore

$$\sum_h^{13} I_{APF,h} \cdot |Z_{APF,h}| = \sum_h^{13} I_{APF,h} \cdot |R_{APF} + j \cdot 2\pi f_h \cdot L_{APF}| = \Delta V_{drop,theoretical} \quad (5.11)$$

with $h = 1, 5, 7, 11, 13$.

For $h = 5, 7$, the voltage drops are equal to zero because the currents $I_{APF,5}$ and $I_{APF,7}$ are zero: these two harmonics are captured by the passive filter, so the APF does not provide them. For $h = 11, 13$, the magnitude of the currents $I_{APF,11}$ and $I_{APF,13}$ are usually zero or almost zero (see subsection 6.3). Finally, only the fundamental current contributes to the definition of voltage drop. These assumptions will be cleared up in subsection 6.3q.

Taking into account that the fundamental current of APF is only reactive, the practical formula of voltage drop becomes:

$$|I_{APF,1}| \cdot |Z_{APF,1}| = |I_{APF,1}| \cdot |R_{APF} + j \cdot 2\pi f_g L_{APF}| = \Delta V_{drop,practical} \quad (5.12)$$

The maximum voltage drop allowed has been established in 10% of the grid voltage, so the constraint related to L_{APF} and voltage drop is (5.13).

$$I_{APF,1} \cdot |Z_{APF,1}| < \frac{10}{100} V_g \quad (5.13)$$

So it had better to have a L_{APF} as low as possible to decrease the voltage drop: this constraint would to decrease the L_{APF} , in contrast to what discussed in section 4.5, where a higher value of L_{APF} was searched for reducing the harmonic content. The optimization solver, `fmincon`, will find a solution that complies with both the bound and the constraint.

5.4 Reactive current into the grid

The non-linear load generates a reactive current at the fundamental frequency, which has to be compensated by the APF.

The standards do not cite the limits of reactive current that can be injected into the PCC. These limits are established in the private contracts between user and supplier or are fixed by national grid codes. An in-depth analysis for wind turbines can be found in [13]. By and large, it can be supposed that the user is fined if a great amount of reactive current is injected into the grid. This is valid for the medium and low voltage grid system. In the high voltage grid, the management of the reactive power is completely different.

The reactive current into the grid is calculated using equation (2.3) at the fundamental, considering only its imaginary component.

Two criteria are been thought in order to fix the maximum reactive current into the grid:

- fix a limit of reactive current as a percentage of rated current
- fix the reactive current of the grid as a fraction of the active one at the fundamental frequency

The advantage of the first choice is the definition of an absolute threshold of reactive current allowed into the grid: this limit does not change even if the non-linear load changes. The numerical value can be, e.g.,

$$|\text{Im}(I_{g1})| < \frac{5}{100} I_L = 16.4 \text{ [A]} \quad (5.14)$$

Therefore, the APF will always try to produce a reactive current that according to (5.14) leads a maximum of 16.4 [A] into the grid. The disadvantage of the first option is clear when the non-linear load injects a restrained real current at the fundamental, e.g. smaller than 16.4 [A], whereas the reactive current injected into the grid is high: in these conditions, the grid will experience a low real current while the reactive one will be 16.4 [A] in the worst case. The power factor will be very modest.

The second choice has the advantage of having a reactive current into the grid that will be always lower than the real one, so the power factor could be higher. The disadvantage regards the amount of this reactive current that is unknown until the load is settled; e.g., the numerical value can be

$$|\text{Im}(I_{g1})| < 0.48 \cdot \text{Re}(I_{g1}) \quad (5.15)$$

where the value 0.48 comes out considering to maintain a minimum $\cos\phi = 0.9$, as stated in some national grid codes [13]. If the $\text{Re}(I_{g1})$ is very high, maybe due to a very high $\text{Re}(I_{nl1})$, the reactive current into the grid could be higher than the limit established in the first choice, i.e., 16.4 [A]. The disadvantage is of not having a fixed value of reactive current into the grid.

Both methods have been implemented in a Matlab code (appendix B reports only the first approach at lines 116-117, 329-335 and 371-372). Although both strategies are valid, the first has been chosen. An explication can be given by figure 5.4: only for very high values of α , the value of the $\text{Re}(I_{nl1})$, and thus $\text{Re}(I_{g1})$, starts to be similar to $\frac{5}{100} I_L$. Therefore the first approach fails in that few cases and the corresponding $\cos\phi$ begins to be very low. The second method has also the advantage of stressing less the APF because it delivers less reactive current, but always keeping $\cos\phi = 0.9$. With the first approach, excluding the cases in which α is high, the $\cos\phi$ can be also higher than 0.9.

The first choice is explicitly written in (5.16).

Acknowledging that the reactive current into the grid can be positive or negative, the upper and lower limit are defined as (5.16). The left inequality is used for $\text{Im}(I_{g1}) < 0$ and the right one for $\text{Im}(I_{g1}) > 0$.

$$-\frac{5}{100} I_L < \text{Im}(I_{g1}) < \frac{5}{100} I_L \quad (5.16)$$

5.5 Nominal current of active power filter

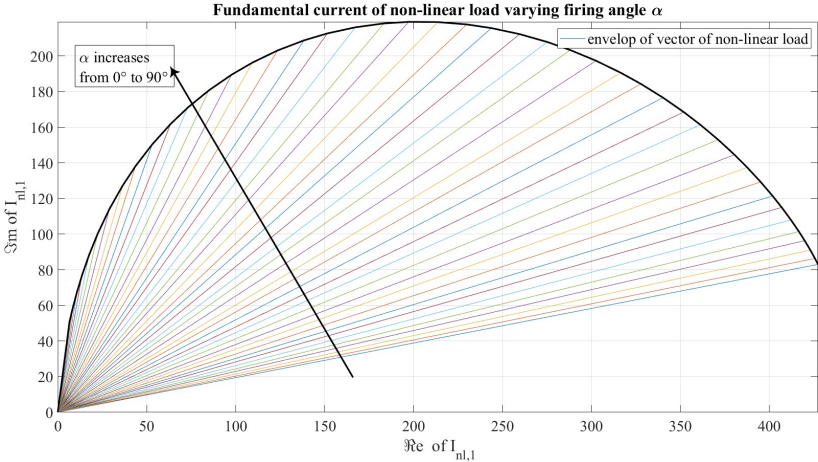
Even though the active power filter (APF) can supply a maximum of $\pm \frac{I_L}{2}$ for each harmonic component of the non-linear load, it cannot supply this amount of current for each harmonic and for the reactive current simultaneously. The rated value of the APF is decided to be equal to $\frac{I_L}{2}$. Thus, considering the absolute values, the constraint becomes:

$$|I_{APF,11}| + |I_{APF,5}| + |I_{APF,7}| + |I_{APF,13}| + |I_{APF,react}| < \frac{I_L}{2} \quad (5.17)$$

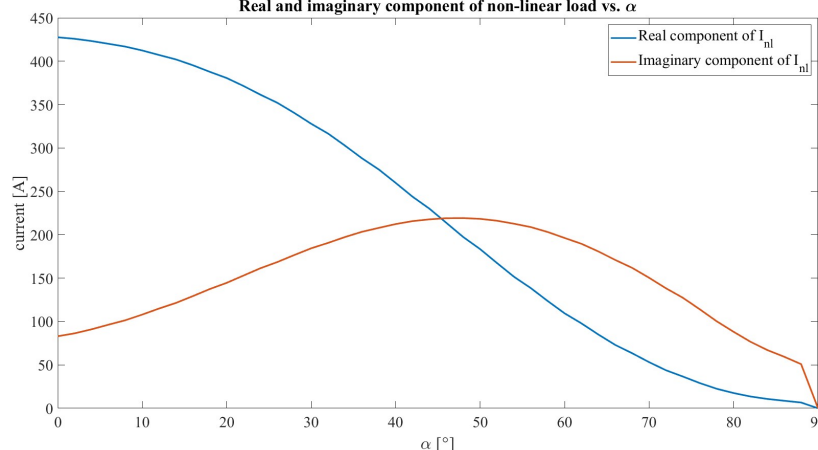
Frequently, two harmonics of equation (5.17) are null thanks to the passive filters.

5.6 Summarize of constraints

In the end, the table 5.1 sums up all the constraints.



(a) Fundamental current of non-linear load varying α .



(b) Real and imaginary component of non-linear load vs. α .

Figure 5.4: Real and imaginary current of fundamental of non-linear load vs α .

Quantity	Min Value	Max Value
Harmonic current into the grid $I_{g5,7}/I_L$ $I_{g11,13}/I_L$ TDD		$\frac{4}{100}$ $\frac{2}{100}$ $\frac{5}{100} I_L$
Quality factor Q_f	15	80
L_{APF} $\Delta V_{drop} = I_{APF,1} \cdot Z_{APF,1} $		$\frac{10}{100} V_g$
Reactive current into grid $\text{Im}(I_{g1})/I_L$	$-\frac{5}{100}$	$\frac{5}{100}$
Nominal current of APF $ I_{APF,11} + I_{APF,5} + I_{APF,7} + I_{APF,13} + I_{APF,react} $		$I_L/2$

Table 5.1: List of constraints.

6 Results of optimization

In this section, the optimization problem is presented: first a brief representation of the involved quantities is delivered, then two different algorithms (SQP and IPM) are studied and compared with each other.

6.1 Setting of optimization problem

The aim of the optimization problem is to find the minimum, that is the optimum solution, of the objective function, complying with some constraints. The objective function is (4.13), with weights of (4.14).

The variables to optimize appear in (4.13) and are also listed in table 4.1. These variables are the same as the models of figures 2.1 and 2.2. The quantities that are depicted in these two figures, but are not optimized, have been listed in table 2.2.

The variables to optimize are limited by the upper and lower bounds of table 4.2. The optimum values will be within the range of this table.

Eventually, the optimum solution has to comply with the constraints of table 5.1.

6.2 Introduction of analysis

In order to understand how the system changes, when α and R_L vary, it is worthwhile, first of all, an analysis of the system with some reference values. In the section 7, impedance Z_g of the grid and firing angle α are modified to see the robustness of the system.

The values chosen as base values are:

- $\alpha = 10^\circ$. If the non-linear load is the model of a diode rectifier, then $\alpha = 0$. So, usually, α does not space on a wide range of values.
- $R_L = 1 \Omega$. This is the rated value of resistance connected to the DC-link.

It has been decided to use a ConstraintTolerance of 10^{-4} . This value is quite high and it is akin to that of limits of table 4.2. For instance, the maximum harmonic content for the 11th and 13th harmonic is $\frac{2}{100}$, but since ConstraintTolerance is 10^{-4} , the maximum harmonic content becomes

$$\frac{2}{100} + 10^{-4} = \frac{2.01}{100} \quad (6.1)$$

So a solution that leads to a harmonic content lower than $\frac{2.01}{100}$ is considered acceptable, even if the solution is in conflict with the IEEE standards (see table 2.3).

The ConstraintTolerance can be furtherly increased when the exitflag=2, namely when not all the solvers are converging to a feasible point. If with exitflag=2, the ConstraintTolerance is lowered, then the exitflag can turn into < 0 , so the algorithm is not finding a feasible solution.

Usually, if the exitflag of the problem is 1, the ConstraintTolerance can be set to its default value, that is a very small value. The default value of ConstraintTolerance is set to 10^{-6} .

The values of ConstraintTolerance= 10^{-4} is a compromise that finds some solution even if they are not so accurate.

One of the possible reason of having exitflag=2, is that there are some constraints that are in conflict each other: e.g., if the value of $R_{f1} = R_{f2} = 0.001 [\Omega]$ is set to a very low value, then the constraint of Quality factor will not be ensured because $Q_f \propto \frac{1}{R_f}$, and so Q_f will assume a very huge value, not respecting the maximum and minimum limit of table 5.1. One option that has been considered to overcome the problem of having exitflag=2, is to split the optimization in two stages.

- The first stage is aimed to define the elements like inductance and capacitance of the passive filters, and the inductance of the APF. The optimal currents can be affected by some error if they are not complying with IEEE standards. Therefore, the currents of the APF will be optimized again.
- The second stage involves only the currents of the APF, therefore all the harmonics (except the two captured by the passive filters) and the reactive current.

To be meticulous, also the inductance of the APF has to be changed as the currents change because there is a variation in the voltage drop at its terminal, but for simplicity the same inductance of the 1st optimization is maintained. The entire flowchart is described in figure 6.1. The two-stages approach is exploited only if the $exitflag=2$.

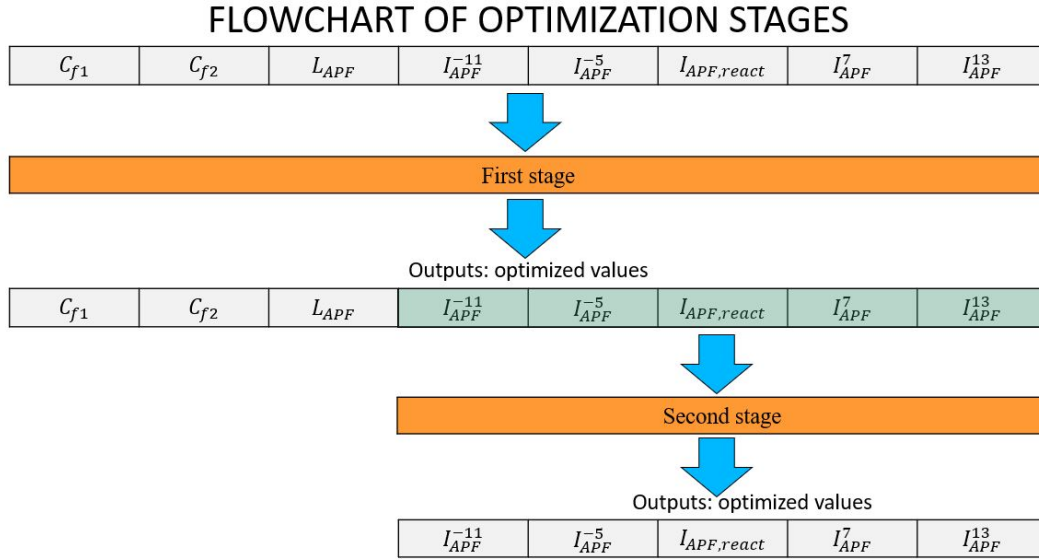


Figure 6.1: Flowchart of the two stages involved in optimization problem.

6.3 Optimization results using SQP

With the chosen values of α and R_L , the thyristor rectifier is modelled as a non-linear current source. The table 2.5 reports the peak values of the load. Below is the same table disclosed

-11 th harmonic	-5 th harmonic	1 st harmonic	7 th harmonic	13 th harmonic
9.2051	38.042	413.92+105.74i	21.306	6.3201

Table 6.1: Table of non-linear load.

The 1st optimization exploits 800 solvers: this number is chosen by the user and trades-off the time consumed by each solver to search a result and the possibility to find a feasible solution. Indeed, if the number of solvers increase, then the probability of finding an optimal solution increases, but also the time consumed by the solver escalates. The first simulation is obtained by setting *SQP* algorithm for the solution. The table 6.2 records the optimal solution:

C_{f1} [F]	C_{f2} [F]	L_{APF} [H]	I_{APF}^{-11} [A]
$6.12 \cdot 10^{-5}$	$4.37 \cdot 10^{-5}$	$5.28 \cdot 10^{-4}$	0
I_{APF}^{-5} [A]	$I_{APF,react}^1$ [A]	I_{APF}^7 [A]	I_{APF}^{13} [A]
0	100.28	0	0

Table 6.2: List of optimal solution with SQP algorithm.

From table 6.2, it is possible to figure out that 5th and 7th are captured by the passive filters because the APF is not acting at these frequencies and because the non-linear load has the 2nd and 3rd greatest current at 5th and 7th.

The capacitors of the passive filters are tuned for 250 [Hz] and 350 [Hz], since they are the harmonics with highest magnitude injected by the non-linear load. The inductances L_{f1} and L_{f2} derives from equation (4.2):

$$L_{f1} = \frac{1}{C_{f1}(2\pi \cdot 250)^2} = 0.00662085 \approx 6.62 \text{ [mH]} \quad (6.2)$$

$$L_{f2} = \frac{1}{C_{f2}(2\pi \cdot 350)^2} = 0.004729 \approx 4.72 \text{ [mH]} \quad (6.3)$$

The value of L_{APF} is hitting the lower bound: this can be explained because the value of $L_{APF} = 5.28 \cdot 10^{-4}$ [H], ensuring the adequate Δi_{ripple} , and a voltage drop $\Delta V_{drop} = 16.69 < 0.1 \cdot V_g = 32.25$ [V]. If an exactly voltage drop of $\Delta V_{drop} = |R_{APF} + j \cdot 2\pi \cdot f_g \cdot L_{APF}| \cdot I_{APF,1} = 32.25$ [V] is searched, then the inequality of (5.13) has to be turned into equality: this lead to an increase of L_{APF} that has the beneficial effect of reducing the Δi_{ripple} , but at the same time, increasing the ΔV_{drop} . In the next, the inequality is kept. The lower bound can change if switching frequency f_s , modulation index m_a , DC-link voltage V_{dc} or current ripple Δi_{ripple} change (see (4.5)).

The APF is not compensating for the 11th and 13th because their magnitude is so small that they comply with IEEE 519-2022 without exploitation of the APF.

The APF is providing $I_{APF,react}$ in order to respect the constraint of having low reactive current into the grid. Now, a verification of the main constraints can be made:

IHD11 [%]	IHD5 [%]	IHD7 [%]	IHD13 [%]
1.8	0.9	0.4	1.3
TDD [%]	$I_{grid,react}^1$ [A]	total current of APF [A]	
1.74	$16.4 = \frac{5}{100} I_L$	100.28	

Table 6.3: Table of constraints with SQP.

All the IHD and TDD are lower than the threshold of the IEEE 519-2022. The reactive current into the grid is exactly the maximum allowed, so the APF is working at its minimum. If there is a necessity to further decrease the reactive current into the grid, the APF has to inject much current. It is noted that the total current of APF is only reactive.

The quality factors can be verified using (5.2). It results that Q_{f1} and Q_{f2} of both passive filters are 80: the constraint is not violated.

As well the ΔV_{drop} on Z_{APF} is 16.69 [V]: it is within the range preset.

Another quantity that deserves to be scrutinized is the $I_{grid,active}^1$, that is obtained considering the real part of (2.3): its value is $I_{grid,active}^1 = 418.42$ [A]; the power factor into the grid is given by (6.4).

$$\cos \left(\operatorname{atan} \left(\frac{I_{grid,react}^1}{I_{grid,active}^1} \right) \right) = \cos \left(\operatorname{atan} \left(\frac{16.4}{418.42} \right) \right) = 0.99 \quad (6.4)$$

Power factor is higher than 0.9; the latter value would be obtained if (5.15) were used.

The result reported by the SQP algorithm achieves an optimal and feasible solution that respects all the constraints. The exitflag is equal to 1.

6.4 Optimization results using IPM

Using the same operating conditions as the SQP algorithm, the optimization procedure is run a second time, using the IPM algorithm. Also the optimization parameters, like ConstraintTolerance, OptimalityTolerance etc..., are kept the same. The table 6.4 reports the results obtained.

The values of capacitors are similar to the previous method. Similarly for the inductors of the passive filters. They are tuned on the 5th and 7th.

The APF is compensating for the reactive component, as in the previous case; the main difference is that the APF is also compensating for the 11th. In table 6.5, a verification of the main constraints is presented.

¹⁰Value of the reactive current into the grid calculated as the imaginary part of equation 2.3

C_{f1} [F]	C_{f2} [F]	L_{APF} [H]	I_{APF}^{-11} [A]
$6.12 \cdot 10^{-5}$	$4.37 \cdot 10^{-5}$	$5.28 \cdot 10^{-4}$	0.002
I_{APF}^{-5} [A]	$I_{APF,react}^1$ [A]	I_{APF}^7 [A]	I_{APF}^{13} [A]
0	100.28	0	0

Table 6.4: List of optimal solution with IPM algorithm.

IHD11 [%]	IHD5 [%]	IHD7 [%]	IHD13 [%]
1.8	0.9	0.4	1.3
TDD [%]	$I_{grid,react}^1$ [A]	total current of APF [A]	
1.74	$16.4 = \frac{5}{100} I_L$	100.28	

Table 6.5: Table of constraints with IPM.

Although all the IHD values comply with the constraints, the APF is injecting a slightly unnecessary 11th harmonic of current to meet the goal. The reactive current into the grid is equal to the constraint because the APF is injecting the same reactive current than the previous method. As a consequence, also the $\cos\Phi$ is the same.

A drawback of this solution is that APF is using a little bit of more current than before, although all the constraints are respected. This, however, is not the crucial aspect to prefer the SQP to IPM; the vital aspect is the exitflag: IPM has an exitflag=2, while in SQP is 1, so the algorithm SQP is better than IPM: the cons of IPM is having exitflag=2.

This method is able to obtain an optimal solution with exitflag=1 if a second stage of optimization is exploited as seen in figure 6.1.

6.4.1 Second stage of optimization with IPM

The 1st optimization stage enables the definition of $C_{f1}, C_{f2}, L_{f1}, L_{f2}, L_{APF}$. The nominal current of the APF is decided a priori, so it is not the result of the optimization problem. Nevertheless, the current provided to compensate for the harmonics has to be optimized. Thus, the second optimization problem involves a minor number of variables.

The cost function is the following:

$$f(x) = 8 \cdot 10^{-4} I_{APF,11}^2 + 5 \cdot 10^{-1} I_{APF,5}^2 + 8 \cdot 10^{-1} I_{APF,7}^2 + 10^{-4} I_{APF,13}^2 + 10^{-5} I_{APF,react}^2 \quad (6.5)$$

The choice of weight of equation (6.5) is derived after some runs to appreciate the most appropriate values: the useful terms ($I_{APF,11}, I_{APF,13}$ and $I_{APF,react}$) have a low weighting factor, hence they are more susceptible to be used. All the elements of the cost function are squared because they can assume positive or negative values.

Regarding the initial values, it is advantageous to utilize the values obtained from the 1st optimization, even if the system is not complying with constraints. Picking the initial solution near to the optimal one, increases the chance to get a converging optimal solution.

The table 6.6 represents the initial solution:

I_{APF}^{-11} [A]	I_{APF}^{-5} [A]	$I_{APF,react}^1$ [A]	I_{APF}^7 [A]	I_{APF}^{13} [A]
0.002	0	100.28	0	0

Table 6.6: Table of initial solution of 2nd stage optimization. These values come from 1st optimization stage.

The table 6.7, instead refers to the upper and lower bounds. Upper and lower bounds are exactly the same as the 1st optimization.

In the end, the table 6.8 fixes the constraints of the 2nd optimization stage.

The maximum and minimum values are not changed from the 1st optimization: the constraints regarding the quality factor and the voltage drop on the impedance of the APF are eliminated.

	I_{APF}^{-11} [A]	I_{APF}^{-5} [A]	$I_{APF,react}^1$ [A]	I_{APF}^7 [A]	I_{APF}^{13} [A]
Upper bound	$\frac{I_L}{2}$	$\frac{I_L}{2}$	$\frac{I_L}{2}$	$\frac{I_L}{2}$	$\frac{I_L}{2}$
Lower bound	$-\frac{I_L}{2}$	$-\frac{I_L}{2}$	$-\frac{I_L}{2}$	$-\frac{I_L}{2}$	$-\frac{I_L}{2}$

Table 6.7: List of upper and lower bounds of unknowns with 2^{nd} optimization.

Quantity	Min Value	Max Value
Harmonic current into grid		
$I_{g5,7}/I_L$		$\frac{4}{100} I_L$
$I_{g11,13}/I_L$		$\frac{2}{100} I_L$
TDD		$\frac{5}{100} I_L$
Reactive current into grid		
$\text{Im}(I_{g1})/I_L$	$-\frac{5}{100} I_L$	$\frac{5}{100} I_L$
Nominal current of APF		
$ I_{APF,11} + I_{APF,5} + I_{APF,7} + I_{APF,13} + I_{APF,react} $		$I_L/2$

Table 6.8: List of constraints of 2^{nd} optimization.

This time 400 solvers are used, and all of them converge to a feasible point: this means that the exitflag is equal 1. The table 6.9 reports the optimal solution

I_{APF}^{-11} [A]	I_{APF}^{-5} [A]	$I_{APF,react}^1$ [A]	I_{APF}^7 [A]	I_{APF}^{13} [A]
0.01	0	100.28	0	0

Table 6.9: Table of optimal solution with exitflag 1.

By table 6.9, it is underlined that the APF is supplying less current where is not needed, i.e. 11th and more current where needed, i.e. the reactive one. Furthermore, the current at 13th is not compensated because its presence into the grid is low. 5th and 7th current harmonics are managed by the passive filters. So, the hitting of constraints is explained in the table 6.10.

Once can behold that the table 6.10 and table 6.3 are equal. This suggests that the solution found by applying twice the optimization is optimal.

6.5 Comparison between SQP vs. IPM

The SQP algorithm reaches the optimal solution immediately, so it is better than IPM. The table 6.11 explains some computational aspects of the two algorithms.

The table 6.11 presents a comparative analysis between the SQP and IPM methods: the total computational effort of IPM is given by the sum of the two stages; it is clear that SQP is not only faster than IPM, but also reaches exitflag 1 in less time; the higher speed of SQP can be attributed to the lower number of *Func*count occurrences. The *Func*count is the total number of evaluations of the objective function: this number increases if the iterations increase. The evaluation of the objective function is necessary in order to calculate each step of Newton-Raphson method. A high *Func*count implies also a high computational time.

If only SQP and IPM 2^{nd} stage are compared, SQP shows a slightly higher number of *Func*count, but it is working with the double of solvers.

The SQP approach shows better results because the Matlab MultiStart optimization tool works considering uniformly distributed points; as remembering that SQP is an infeasible point method, the choice of the number of uniformly distributed points is not relevant. For these reasons, in the following analyses SQP algorithm will be preferred than IPM. In IPM, that is a feasible point method, if a point is chosen outside the polytope it will not converge to a solution, so this approach does not fit well with MultiStart.

IHD11 [%] 1.8	IHD5 [%] 0.9	IHD7 [%] 0.4	IHD13 [%] 1.3
TDD [%] 1.74	$I_{grid,react}^1$ [A] $16.4 = \frac{5}{100} I_L$	total current of APF [A] 100.28	

Table 6.10: Table of constraints with exitflag 1.

	SQP	IPM 1 st stage	IPM 2 nd stage
Funccount	104691	208080	64274
exitflag	1	2	1
time [s]	19.45	39.43	12.28
Number of solvers	800	800	400

Table 6.11: Comparative analysis between single stage SQP and two stages of IPM.

Another important conclusion is that a solution with exitflag=2 can be turned into a solution with exitflag=1 through the exploitation of the double optimization stage: f.i., the table 6.4 is turned into table 6.9.

7 Sensitivity analysis to grid impedance and firing angle

Once the results for the base value $\alpha = 10^\circ$ and $R_L = 1 \text{ } [\Omega]$ are defined, the next step is to verify what happens to the whole system if some parameters are changed.

In the next, an analysis of the system as changing grid impedance Z_g and firing angle α is provided. For both cases, there is the verification of standard IEEE 519-2022 for harmonics and of the constraint of reactive current into the grid. The aim of sensitivity analysis is finding critical values of Z_g and α that violate the constraints.

The passive filters and the APF parameters remain invariant for sensitivity analyses.

7.1 Sensitivity to Z_g variations

The base value of the grid impedance is $Z_{gb} = R_{gb} + j2\pi \cdot 50 \cdot L_{gb}$, with $R_{gb} = 22 \cdot 10^{-3} \text{ } [\Omega]$ and $L_{gb} = 10^{-3} \text{ } [\text{H}]$.

To catch the variations of system, only Z_g has been modified, while the physic system (C_{f1} , C_{f2} and L_{APF}) and the currents supplied by APF have to be maintained fixed at their optimal value found for base grid impedance.

To verify if the system is still capable of agreeing to IEEE standards in the event of deviations of the grid impedance from its base value, R_g and L_g are changed as shown in table 7.1. The maximum values are augments of 100% while the minimum ones are reductions of 50%. The reductions are not of 100% because the grid impedance would be nil. Figure 7.1 exhibits this behaviour.

	Base value	Min value	Max value
$R_g \text{ } [\Omega]$	$22 \cdot 10^{-3}$	$0.5 \cdot 22 \cdot 10^{-3}$	$2 \cdot 22 \cdot 10^{-3}$
$L_g \text{ } [\text{H}]$	10^{-3}	$0.5 \cdot 10^{-3}$	$2 \cdot 10^{-3}$

Table 7.1: Table of base, maximum and minimum values of R_g and L_g .

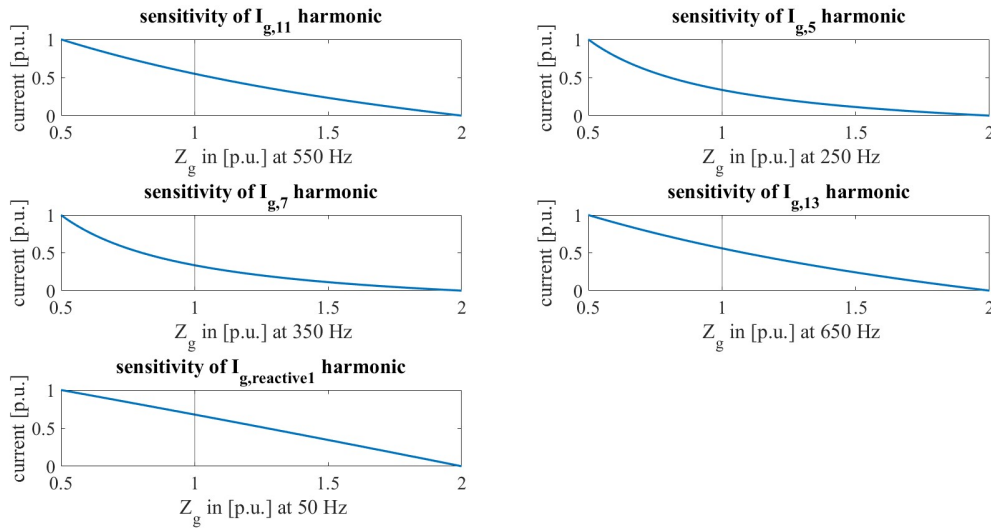


Figure 7.1: Behaviour of harmonics and reactive current at fundamental if Z_g changes of +100% and -50%. The vertical line points out the base value of grid impedance, namely always in 1 [p.u.].

In order to define the per unit values of x and y axis of figure 7.1, the following assumptions are established:

- for x -axis: a generic impedance on x -axis is written as

$$z_{gpu} = \frac{Z_g}{Z_{bh}} \quad (7.1)$$

where Z_g is the generic value of an impedance varying within the values of table 7.1 and Z_{bh} is the base value of impedance for each different harmonic: this base value is not fixed, but changes as the frequency: e.g., for the 13th,

$$|Z_{b13}| = |R_{gb} + 2 \cdot \pi \cdot 650 \cdot L_{gb}| = 22 \cdot 10^{-3} + 2 \cdot \pi \cdot 650 \cdot 10^{-3} = 4.106 \text{ } [\Omega] \quad (7.2)$$

and considering, f.i., the minimum value:

$$|Z_{g,13,min}| = \left| \frac{R_{gb}}{2} + 2 \cdot \pi \cdot 650 \cdot \frac{L_{gb}}{2} \right| = \left| \frac{22 \cdot 10^{-3}}{2} + 2 \cdot \pi \cdot 650 \cdot \frac{10^{-3}}{2} \right| = 2.053 \text{ } [\Omega] \quad (7.3)$$

and finally the minimum value of the x -axis found on the plots of figure 7.1 is

$$\frac{|Z_{g,13,min}|}{|Z_{b13}|} = \frac{2.053}{4.106} = 0.5 \text{ } [p.u.] \quad (7.4)$$

When the x -axis is equal to 1, it means that the base value is reached. When it is equal to 2, the maximum value is reached. Eventually, as demonstrated in (7.4), the minimum value is reached for x -axis equal to 0.5.

- for y -axis, a generic h harmonic current assumes value

$$i_{gh,pu} = \frac{I_{gh} - I_{gh,min}}{I_{gh,max} - I_{gh,min}} \quad (7.5)$$

where I_{gh} can assume values within the range $[I_{gh,min} \ I_{gh,max}]$. The values of $I_{gh,min}$ and $I_{gh,max}$ are different for each harmonic.

The vertical axes of figure 7.1 have different values since the grid impedance $Z_g = R_g + j\omega_h L_g$ changes with the frequency: the largest value impedance is displayed for the 13th harmonic, conversely the lowest value belong to the reactive current operating only at 50 [Hz]. Due to the variable frequency, also the vertical line, representing the base value of impedance, takes on different values, larger as the order of harmonic raises.

The general trend for the harmonics is the increase of magnitude when the impedance of the grid starts to become smaller and smaller: the harmonic content is inversely proportional to Z_g . This trend can be easily understood if the denominator of (2.3) is considered. The behaviour of 5th and 7th harmonics is slightly different from 11th and 13th at small grid impedance. A possible explanation is due to the fact that 5th and 7th are captured by passive filters, so their value of current is very small: this decreases the denominator of (7.5) having more steep behaviour at low grid impedance. Whereas 11th and 13th have a more smooth behaviour at low grid impedance because they are not trapped by the passive filters. Despite these alterations, the system is robust to confront the variations of grid impedance. Hence almost all constraints are respected as portrayed in figure 7.2.

By figure 7.2, it is noticed that nearly all constraints are respected even if Z_g changes, as all the green lines are quite below the red lines. The only exceptions are IHD11 and the reactive current into the grid. In order to use less current as possible from APF, at base value of Z_{gb} , the reactive current of the grid was already hitting the constraints and it was $\frac{5}{100} I_L = 16.4$ [A]. So a slight decrease of Z_g , that causes a slight increase of $I_{grid,react}$, makes sure that the constraint is not respected anymore. However, the increase is very small: at the lowest grid impedance, $I_{grid,react,max} = 16.46$ [A]: the increase is only 0.36%, so negligible.

As regards IHD11, it hits the standard until $z_{g,pu} = 0.73$, that is for $Z_{g,11} = 0.0163 + j \cdot 2\pi \cdot 550 \cdot 7.4 \cdot 10^{-4}$, while the worst case happens for the minimum of Z_g , where the IHD11=0.022; the sense of grid sensitivity is of not changing the optimized variables, but it is clear that if APF provides current at 11th, the IEEE 519-2022 will be complied with. In the next, the optimal results are reported for the minimum of the grid impedance $Z_g = 0.5 \cdot 22 \cdot 10^{-3} + j \cdot \omega_h \cdot 0.5 \cdot 10^{-3}$. When the grid impedance Z_g reaches its minimum value, also the non-linear load changes. The table 7.2 delineates the non linear load.

-11 th harmonic	-5 th harmonic	1 st harmonic	7 th harmonic	13 th harmonic
8.6275	81.819	467.64+145.96i	33.028	5.867

Table 7.2: Table of non-linear load with minimum of grid impedance, $\alpha = 10^\circ$ and $R_L = 1$ [Ω].

The table 7.3 reports the optimal solution with minimum of grid impedance. The solution is obtained after two

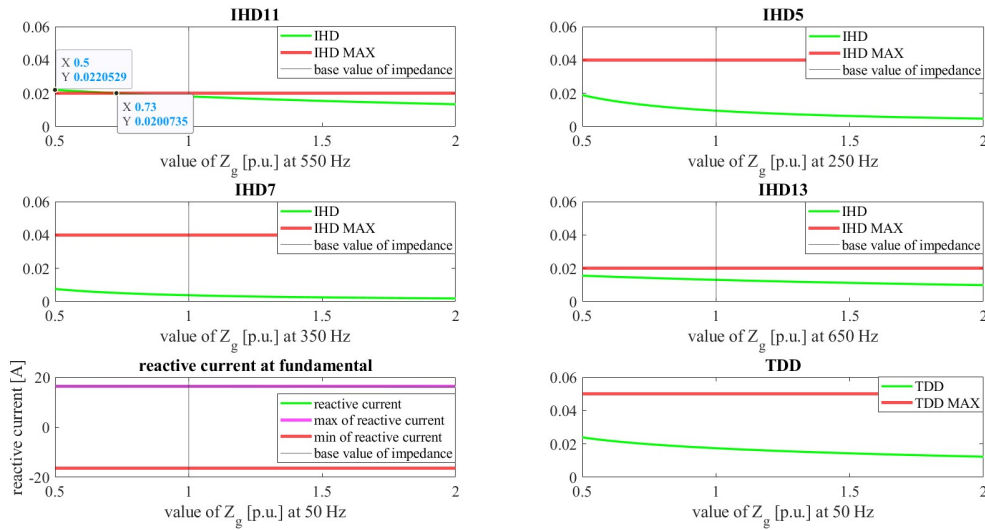


Figure 7.2: The green curve is the quantity changing with Z_g . The red horizontal lines are the limits. The black vertical lines are the base values of $|Z_g|$. The plot of reactive current into the grid has the green and red curve almost overlapped.

optimization stages using SQP; IPM was requiring too much time to reach a solution.

C_{f1} [F]	C_{f2} [F]	L_{APF} [H]	I_{APF}^{-11} [A]
$6.12 \cdot 10^{-5}$	$4.37 \cdot 10^{-5}$	$5.28 \cdot 10^{-4}$	0.28
I_{APF}^{-5} [A]	$I_{APF,react}^1$ [A]	I_{APF}^7 [A]	I_{APF}^{13} [A]
0	140.54	0	0

Table 7.3: List of optimal solution with minimum of grid impedance.

The table 7.4 displays the constraints.

IHD11 [%]	IHD5 [%]	IHD7 [%]	IHD13 [%]
2	4	1.1	1.4
TDD [%]	$I_{grid,react}^1$ [A]	total current of APF [A]	
3.4	$16.4 = \frac{5}{100} I_L$	140.82	

Table 7.4: Table of constraints with minimum of grid impedance.

It is seen that $I_{APF}^{-11} = 0.28$ [A], so the APF is providing exactly the optimal current that leads to having IHD11=2%.

The $I_{APF,react}^1$ is injected in order to have into the grid the exact amount of $\frac{5 \cdot I_L}{100} = 16.4$ [A]. The total current provided by the APF is increased respect to the case of having base value of grid impedance, but it is far away to hit the limit $\frac{I_L}{2} = 164.0$

7.2 Sensitivity to α variations

This section analyzes the effect of changes of the firing angle of the controlled rectifier. The starting value is the base one, i.e. $\alpha_0 = 10^\circ$. Unlike the grid impedance, the firing angle can change within a specified range $\alpha \in [0^\circ, 90^\circ]$. In addition, the figure 5.4 reports how the fundamental of non-linear load changes as varying α . The

most challenging condition for the APF happens when the imaginary component of the fundamental of non-linear load reaches its maximum, that is for $\alpha = 48^\circ$. Figure 7.3 reports the behaviour of the other harmonics of the non-linear load as varying α .

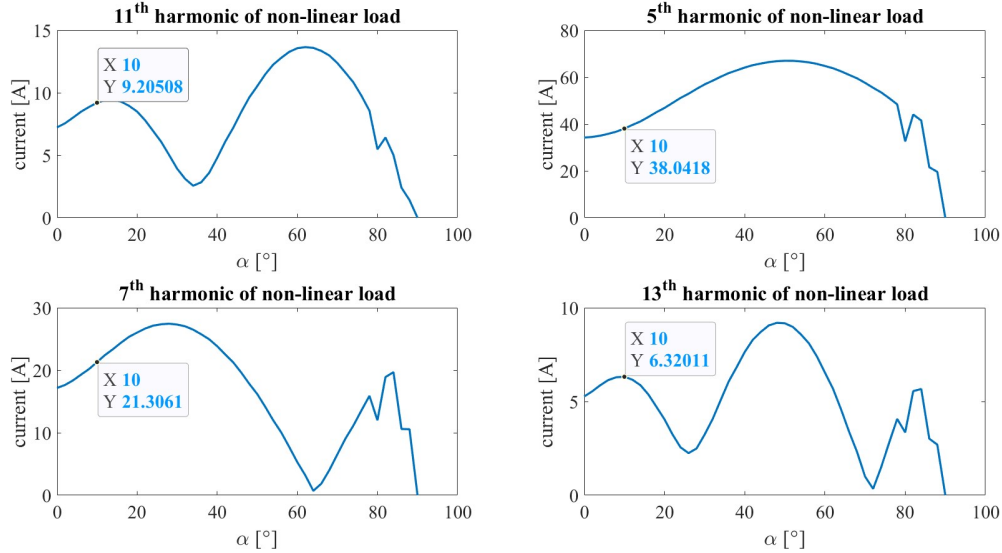


Figure 7.3: Amplitude of harmonics vs. firing angle. The labels indicate the base non-linear load, with $\alpha_0 = 10^\circ$: they are the values of table 6.1. The spikes are due to the capacitance C_{dc} .

By figure 7.3 it is clear that the two highest harmonics are in general the 5^{th} and 7^{th} , so their variation will not affect the grid because they will be captured by the passive filters. The 11^{th} and 13^{th} vary more than 100% from the base value, but their absolute value is small, so their variation will not induce the APF to work at its maximum current of $\frac{I_L}{2}$. The 11^{th} reaches its maximum for $\alpha = 63^\circ$, while the 13^{th} for $\alpha = 50^\circ$. Nevertheless, the study of IHD and reactive current into the grid is done keeping all the system optimized at its base value. In figure 7.3 the harmonics have some peaks and the passage from one value of α to another is not smooth, but abrupt. This is due to the capacitor connected to the load resistance R_L , upstream the thyristor rectifier (i.e. C_{dc} in figure 2.1). In a diode rectifier, the capacitor C_{dc} has the target of reducing the ripple of the output voltage: as higher is the value of capacitance, as lower is the voltage ripple. In thyristor rectifier, however, the capacitor has the negative effect of producing sub-harmonics (harmonics at a frequency lower than those of the grid) that explain why the currents in figure 7.3 are not so smooth. Those currents are obtained with $C_{dc} = 10^{-3}$ [F]. If the value of this capacitance is decreased up to $C_{dc} = 10^{-6}$ [F], the figure 7.4 is obtained. In the following calculation the value of $C_{dc} = 10^{-3}$ is kept.

The figure 7.5 reports the variation of grid current when α changes. The plots of figure 7.5 have the same shape of those of figure 7.3. The grid currents and the non-linear load are linked by (2.3). It make sense that the two shapes are perfectly the same because in (2.3) only I_{nl} changes, as a consequence of changing α , while all the other quantities appearing in that equation are the ones find after optimization using all base values or are assumptions: in both cases they are constant. The x -axis in per unit of figure 7.5 is obtained by

$$\alpha_{pu} = \frac{\alpha}{\alpha_0} = \frac{\alpha}{10} \quad (7.6)$$

This time the x -axis is the same for all the harmonics as firing angle does not depend on frequency.

The y -axis is obtained using the same equation of (7.5).

Now it is interesting to know if the constraints of IEEE 519-2022 and reactive current are observed. The figure 7.6 meets this necessity. As concerning the harmonics, 5^{th} and 7^{th} are far away from the limits as one can expect because they are ensnared by the passive filters. Also the 13^{th} is almost touching the limit for $\alpha = 50^\circ$. The 11^{th} is exceeding the limit for $\alpha \in [50^\circ, 76^\circ]$. The latter result can be foreseen because the absolute value of 11^{th} of non-linear load has the maximum at $\alpha = 63^\circ$, as portrayed in figure 7.3.

Thanks to low values of IHD, also the TDD does not assume critical values.

Finally, the $I_{grid,react}$ is not complying with the constraints for a certain range of $\alpha \in [10^\circ, 78^\circ]$ as shows the

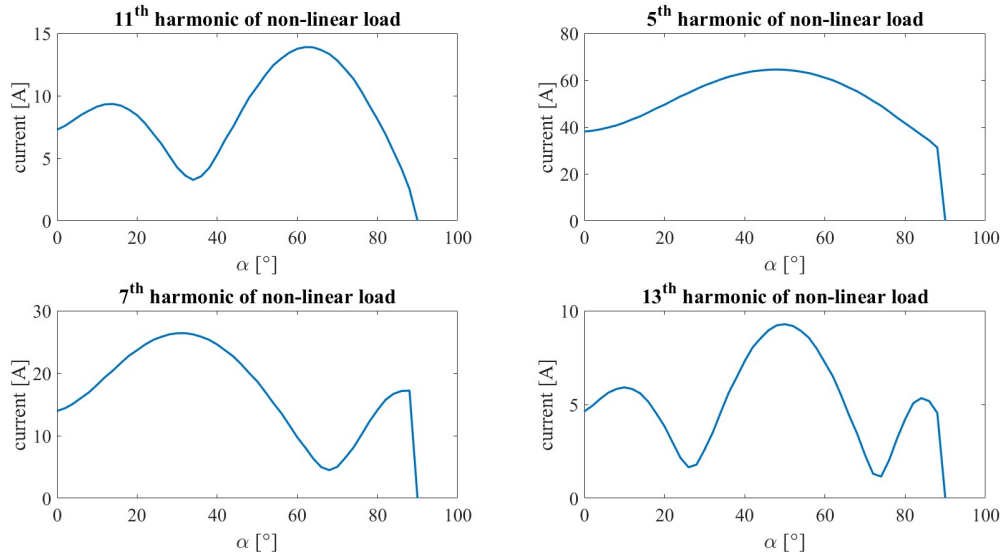


Figure 7.4: Amplitude of harmonics vs. firing angle. The smooth behaviour is reached neglecting the capacitance C_{dc} .

label in figure 7.6. This implies that the presence of higher reactive current into the grid reduces the $\cos\Phi$ of the grid itself. This situation is due to the fact that the APF works at the optimum point just for a single value of firing angle, that is $\alpha = 10^\circ$. The fact that the system is able to comply with constraint also for $\alpha > 78^\circ$ is not a merit of the optimization problem, but it is simply caused by the non-linear load that becomes less dangerous for the grid because, being α so big, the IGBT of thyristor are maintained close for a long time, decreasing I_{nl} .

In order to make APF able to comply with higher reactive current, its base value has to be changed: it is possible to change the operating point of APF acting on control system, in particular changing the reference of q-current I_q^* (see figure 2.9). The next subsection describes an optimization problem for $\alpha = 48^\circ$, i.e. the point in which there is the highest reactive current into the grid (see labels of figure 7.6).

7.2.1 Case with highest reactive current of non-linear load: $\alpha = 48^\circ$.

The scenario with the highest reactive current in the non-linear load can be regarded as the worst-case scenario for the APF, as it must deliver significantly more current than the base case ($\alpha = 10^\circ$). The load resistance R_L keeps the same value of $1 [\Omega]$.

The non-linear load is presented in table 7.5.

-11 th harmonic	-5 th harmonic	1 st harmonic	7 th harmonic	13 th harmonic
9.62	66.80	196.31+219.76i	17.83	9.20

Table 7.5: Table of non-linear load with $\alpha = 48^\circ$.

As expected, the reactive current absorbed by non-linear load is very high. Keeping the same optimization parameters used in section 6.3, the optimal solution is shown in table 7.6.

C_{f1} [F]	C_{f2} [F]	L_{APF} [H]	I_{APF}^{-11} [A]
$6.12 \cdot 10^{-5}$	$4.37 \cdot 10^{-5}$	$5.28 \cdot 10^{-4}$	0
I_{APF}^{-5} [A]	$I_{APF,react}^1$ [A]	I_{APF}^7 [A]	I_{APF}^{13} [A]
0	$163.4 = \frac{I_L}{2}$	0	0

Table 7.6: List of optimal solution with $\alpha = 48^\circ$.

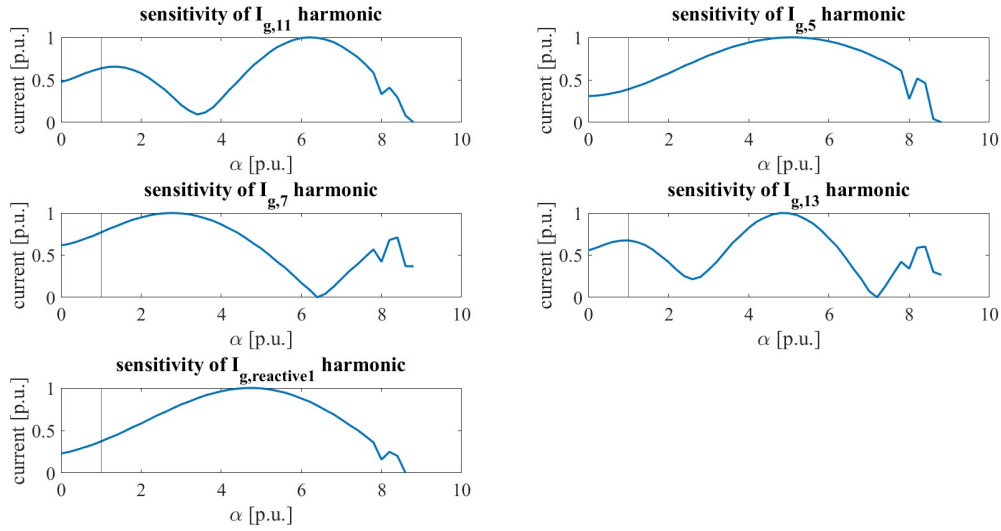


Figure 7.5: Behaviour of harmonics and reactive current into grid when $\alpha \in [0^\circ, 90^\circ]$. The vertical line indicates the base value of α , that is $\alpha_0 = 10^\circ$.

The optimal solution has all quantities equal to solution with $\alpha = 10^\circ$, except the reactive current of APF: now it is injecting the maximum reactive current, i.e., $163.4 = \frac{I_L}{2}$ [A] to compensate for the 219.76 [A] of the non-linear load. The APF is not compensating for harmonics. As the APF is working at its maximum, the `exitflag=2` is obtained, although SQP is used.

In the end, the constraints table 7.7 is created: all the constraints regarding IEEE 519-2022 are observed even if

IHD11 [%]	IHD5 [%]	IHD7 [%]	IHD13 [%]
1.89	1.68	0.3	1.9
TDD [%]	$I_{grid,react}^1$ [A]	total current of APF [A]	
2.22	$67.4 > \frac{5}{100} I_L = 16.4$	$164.4 = \frac{I_L}{2}$	

Table 7.7: Table of constraints with $\alpha = 48^\circ$.

the values of IHD and TDD are higher than the case of $\alpha = 10^\circ$. This demonstrates that this case is more stressing for the grid than the previous one.

The $I_{grid,react}^1$ is above the limit, so this constraint is not observed. If the value of $I_{grid,active}^1$ is considered, the corresponding power factor is, however, quite high as illustrated in (7.7):

$$\cos \left(\text{atan} \left(\frac{I_{grid,react}^1}{I_{grid,active}^1} \right) \right) = \cos \left(\text{atan} \left(\frac{67.4}{198.5} \right) \right) = 0.94 \quad (7.7)$$

Obviously, if the $I_{grid,react}^1$ were 16.4 [A] and the constraint were respected, the power factor would be higher.

Other strategies to comply with the reactive current into the grid could involve the increasing of the upper bound of $I_{APF,react}^1$ (see subsection 4.6) or also the increase of the constraint of the nominal current of APF (see subsection 5.5).

Furthermore, in subsection 5.4, the criteria that always keep the $\cos(\Phi) = 0.9$ was depicted: now it can be used. Therefore the constraint of (5.14) is turned into (5.15). In the latter case, keeping the same non-linear load of table 7.5, the optimal solution is depicted in table 7.8. The table 7.9, instead, reports the constraints.

The constraints of IEEE 519-2022 are unchanged; while the $I_{grid,react}^1 = 95.34$ [A]: even if this values is higher than $\frac{5}{100} I_L$, that is not a problem because the reactive current into the grid has not upper bounded. The

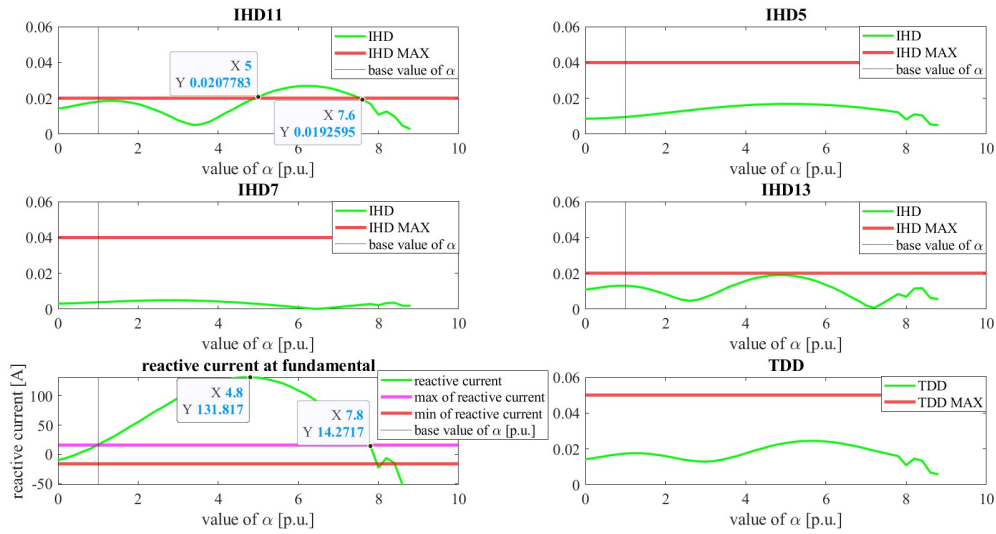


Figure 7.6: The green curve is the quantity changing with α . The red horizontal lines are the limits. The black vertical lines are the base values of α . The plot of reactive current into the grid has two labels marking the reactive current for $\alpha = 48^\circ$ and $\alpha = 78^\circ$.

C_{f1} [F]	C_{f2} [F]	L_{APF} [H]	I_{APF}^{-11} [A]
$6.12 \cdot 10^{-5}$	$4.37 \cdot 10^{-5}$	$5.28 \cdot 10^{-4}$	0
I_{APF}^{-5} [A]	$I_{APF,react}^1$ [A]	I_{APF}^7 [A]	I_{APF}^{13} [A]
0	$136.35 < \frac{I_L}{2}$	0	0

Table 7.8: List of optimal solution with $\alpha = 48^\circ$ and $\cos(\Phi) = 0.9$.

verification of $\cos(\Phi)$ is given in (7.8).

$$\cos \left(\operatorname{atan} \left(\frac{I_{grid,react}^1}{I_{grid,active}^1} \right) \right) = \cos \left(\operatorname{atan} \left(\frac{95.34}{198.5} \right) \right) = 0.90 \quad (7.8)$$

The advantage of using the constraint of (5.15) is that the APF is not working at its maximum capacity ($136.35 < \frac{5}{100} I_L = 166.4$ [A]), so, if there is any necessity, it could compensate for the 11th (not for the 13th because as seen in figure 7.6 it has a IHD13 always $< 2\%$).

In conclusion, also the worst case can be managed by the APF, always remembering to change the reference I_q^* in the control system, if there is necessity, to work with variable firing angle α .

7.3 Conclusion of sensitivity

The system is robust to the variation of Z_g : if the latter changes, the system works well, without impressive alterations of the currents. The APF can supply roughly the same currents at least and the system is within the constraints, except for IHD11 as proved by figure 7.2.

The system tolerates quite well the variation of firing angle α : all the constraints are respected, except for reactive current and for IHD11. In order to be compliant with the standards, the APF has to change the reactive current supplied.

The variation of firing angle α has a larger effect than the variation of grid impedance Z_g .

Figure 7.7 illustrates the grid impedance sensitivity, also considering the variation of α : it tries to consider what could happen if both grid impedance Z_g and firing angle α change. Only the load resistance R_L remains constant.

The x -axis is the same as the figure 7.1. All the colorful lines represent different values of α . As the behaviour of firing angle sensitivity is not monotonic, also the colorful lines are not increasing or decreasing when α increases

IHD11 [%]	IHD5 [%]	IHD7 [%]	IHD13 [%]
1.89	1.68	0.3	1.9
TDD [%]	$I_{grid,react}^1$ [A]	total current of APF [A]	
2.225	95.34	136.35	

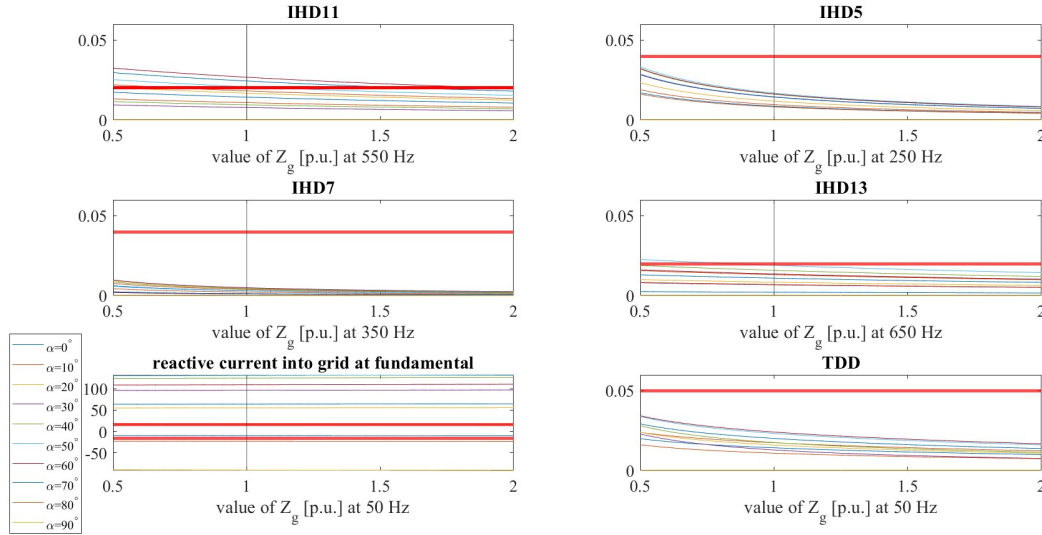
Table 7.9: Table of constraints with $\alpha = 48^\circ$.

Figure 7.7: Figure showing IHD, TDD and reactive current into the grid: the thick red lines represent the limits; the light colorful lines represent the quantity for various values of α . To avoid a mass figure, just for the reactive current the legend is given.

or decreases (see figure 7.6 and 7.5).

However, IHD5 and IHD7 are always kept under the limits, because of the tuning of the passive filters to 5th and 7th. IHD13 does not comply for small value of grid impedance Z_g and for values of α in which the I_{nl}^{13} assumes the maximum value, so for values of α around 50° as stated in subsection 7.2. Likewise, IHD11 is not complying for small values of grid impedance Z_g and for a wide range of α around 63° (see subsection 7.2).

The plot of reactive current into the grid confirms the discussion held separately regarding α and Z_g : all the lines have a very low change in slope when changing Z_g , therefore this current is not much sensitive to the variation of grid impedance. For values of α close to 50° , the maximum reactive current into the grid is reached. In this case, the APF has to provide more current.

Finally, the TDD remains always under the limit established by IEEE 519-2022.

Perhaps a satisfactory, though not optimal, operating point can be achieved by utilizing the optimal solution presented in table 7.6.: the APF is providing $I_{APF,react}^1 = 136.35$ [A] keeping a $\cos(\Phi) = 0.9$, and the difference $\frac{I_L}{2} - I_{APF,react}^1 = 166.4 - 136.35 = 30.0$ [A]; so a 'safe margin' of 30 [A] can be used to compensate for 11th and 13th. Achieving this target requires a control system capable of finding the optimal solution in real-time.

The plots of figure 7.7 are obtained using the optimal solution valid for $\alpha = 10^\circ$, $R_L = 1$ [Ω] and grid impedance Z_g with base values of $R_g = 22 \cdot 10^{-3}$ [Ω] and $L_g = 10^{-3}$ [H]. Then, the values of α and Z_g are changed.

Eventually, another parameter that can be changed is R_L but its variations are not studied in detail as that of Z_g and α . Partly in the subsection 2.4.2 and in figure 2.14 it is explained that as R_L increases the harmonics current of the non-linear load decreases, resulting in a low stress situation for the system. Three brief considerations can be taken into account:

- if R_L increases, then the amplitude of the harmonics into the grid decrease and therefore the APF is more 'relaxed' since it has to supply lower currents (see figure 2.14)

- if R_L decreases, then the amplitude of the harmonics is higher
- If R_L assumes very small values, the APF reaches its limited current $\frac{I_L}{2}$, given by the sum of all harmonics current and the reactive one: the APF is not able anymore to compensate and a new APF, tolerating larger current, has to be searched.

Eventually, the optimal solution loses its significance if some parameters are modified; to solve this issue a real-time optimal solution has to be calculated.

8 Conclusions and future works

At the end a fast and brief summary is illustrated for each chapter, then the conclusions are listed and finally the possible future works are presented.

8.1 Summary of each chapter

The 1st chapter introduces the problem of harmonics into the grid and explains what is the structure of the thesis.

The 2nd chapter starts with a description of the three-phase and of the single-phase system. The analytical equations are validated by the numerical solutions. The APF is introduced as being supplied by capacitors. The control scheme is not studied extensively because the main focus of the thesis is on the optimization problem rather than the control technique.

After that the standard IEEE 519-2022 is displayed: it is not shown together with the others constraints because it is necessary to introduce the rated current I_L .

Therefore the values of resistance of the two passive filters and of APF are established.

Finally, the non-linear load is obtained, and also the active and reactive power vs. load resistance vs. firing angle are explored.

The 3rd chapter reviews four iterative methods: Newton-Raphson method, Sequential quadratic programming, Interior point method and Gradient descent. The Newton-Raphson method is used in both SQP and IPM. These two algorithms are used by fmincon solver in Matlab; also the gradient descent is studied as a method in which only the gradient is evaluated and not the Hessian, but it is not exploited by the solver fmincon.

The 4th chapter starts to detail the optimization problem: at first all the variables to optimize are listed, then the absence of L_f is explained, after that the upper and lower bounds of each variable to optimize are defined. Some bounds are chosen as reasonable limits, others are derived after some analytical considerations. Lastly, the cost function is introduced with a little description of the initial point selection.

In the 5th chapter all the constraints are listed: IEEE 519-2022, quality factor, anti-resonance, voltage drop on L_{APF} , reactive current into the grid and the nominal current of the APF; they are all inequalities.

In the 6th chapter, the optimization problem is run: at first with SQP algorithm and then with IPM algorithm: in both analyses, all the parameters have been kept equal in order to compare the two methods. The optimal solution emerged by SQP has exitflag=1, while with IPM has exitflag=2. By means of 2nd optimization stage, also IPM can reach exitflag=1, even if spending more time. For this reason, all the next optimizations are sustained by SQP.

In the 7th chapter the sensitivity analyses are conducted. Mainly:

- sensitivity of grid impedance
- sensitivity of firing angle

The system is quite robust to tolerate the variation of Z_g , while it is more difficult to follow the variations of firing angle α . Moreover, the worst case has been discovered to happen at firing angle $\alpha = 48^\circ$. The APF can also manage this case if it works at its optimum point.

8.2 Conclusions

The problem of harmonics into the grid and their mitigation turn out to be a complex problem in which many variables and cases are involved. In this thesis only the part of optimization has been studied, without caring of the practical feasibility of the results obtained: a part regarding the measurements in a real system is missing. Anyway the results are corroborated by the numerical simulation.

The figure 8.1 portrays the current of a phase with the presence of the filters: the shape of the current seems to be similar to a sinusoidal wave. It is not a perfect sine wave because the IEEE 519-2022 standard allows a certain amount of harmonic content into the grid; moreover, the harmonics of order greater than 13th have been neglected, therefore they are polluting the grid current. The waveform of figure 8.1 is more similar to a sinusoidal wave than figure 2.3 because the latter does not have filters. In both cases, the current of the same phase (phase b) has been considered.

Another vast topic regards the optimization strategies: here only SQP and IPM has been exploited, but surely other techniques can be explored like the heuristic ones.

In the end, the main conclusion can be listed:

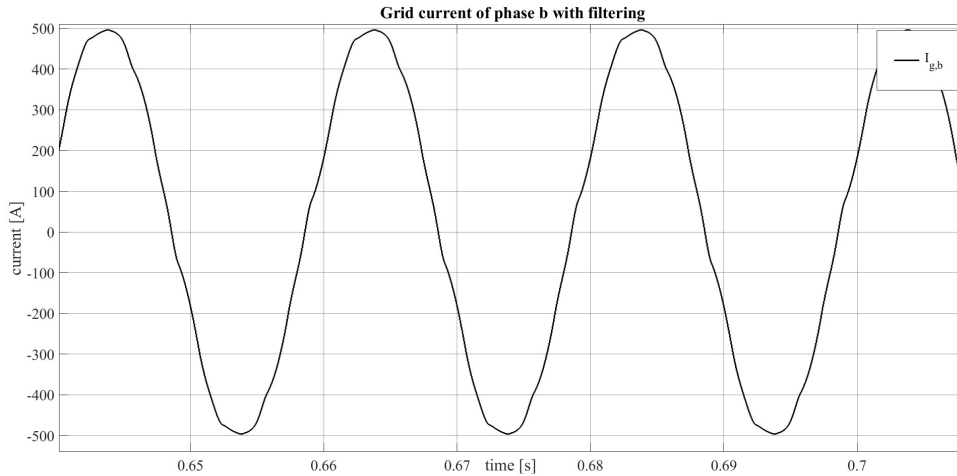


Figure 8.1: Grid current of phase b with passive and active filters. It has to be compared with figure 2.3. $\alpha = 10^\circ$ and $R_L = 1 [\Omega]$.

- the resistance of the passive filter is a quantity that cannot be optimized because it is strongly related to the parasitic resistance of the capacitor and of the inductor: therefore no efforts have to be spent in this parameter optimization (see subsection 2.4.1);
- in the optimization of passive filters, not only the cut-off frequency has a vital role, but also the fundamental frequency: a low impedance has to be prevented because it allows a huge flow of current into the passive filters at 50 [Hz];
- the APF can be used to control the quantity of reactive current into the grid, and, if necessary, also for compensating the harmonics;
- the passive filters are tuned on the harmonics that have the highest magnitude: they are usually the 5th and 7th;
- the IEEE 519-2022 are often observed; the constraint of reactive current is complied with for certain values of firing angle α ;
- the optimization tool used in Matlab is MultiStart: SQP algorithm of Matlab function fmincon works better than IPM algorithm because MultiStart is used;
- with the two stages optimization a problem with exitflag 2 can be treated;
- by means of sensitivity analysis it has been known that the system tolerates better the variation of grid impedance than that of firing angle;
- if the current provided by the APF starts to become close to its nominal value, it has to be taken into consideration the possibility of changing the constraint of the reactive power into the grid, using that one that allow a fixed $\cos(\Phi) = 0.9$.

8.3 Future works

As this thesis is born as a continuation of a previous work, [20], others topics can be explored, starting from the ideas developed here:

- optimization of parameters of APF like switching frequency f_s , modulation index m_a , voltage of DC-link V_{dc} , ripple of current Δi_{ripple} etc...this procedure increase the size of the vector of optimal solution, increasing, as a consequence, the complexity of overall the problem;
- implementation of the control system of the APF into the optimization problem such that the APF can work at optimum point for each value of firing angle α and grid impedance Z_g . In this way the joule losses of the APF will be minimized for each working conditions because the current provided will be minimum;

- creation of a user-friendly interface that calculates the optimal solution and verifies it in a single time. In this way, it is not necessary to change the working file and, therefore, also the running time decreases. Starting from input data as R_L and α , the output will tell the user if all the constraints are observed. Perhaps this procedure will also help the creation of a control system;
- replacement of L_{APF} by more complicated circuits like LC or LCL in order to verify and reduce the switching harmonics; thanks to this procedure, also APF working at frequency < 10 [kHz] can be exploited;
- in this work all the constraints are analytical expressions. It would be useful to also include some constraints containing numerical data from Simulink: this can extend the types of constraints that can be used;
- searching for other optimization techniques, exploiting heuristic criterion like *particle swarm optimization (PSO)*.

9 Riassunto esteso in italiano / Extended summary in Italian

9.1 Descrizione del sistema

Questa tesi è la continuazione di un precedente lavoro di tesi magistrale ([20]) e tratta un problema di ottimizzazione: la rete studiata è visualizzata in figura 2.1, mentre la sua rappresentazione monofase si trova in figura 2.2.

La rete ha un carico non lineare, ovvero un raddrizzatore a tiristori trifase che assorbe una corrente; le armoniche considerate sono la 5^a, 7^a, 11^a e la 13^a: il modello di questo carico è un parallelo di generatori di corrente sinusoidali alle varie frequenze. Il carico non-lineare dipende dall'angolo di accensione $\alpha = 10^\circ$ e dalla resistenza del carico $R_L = 1 [\Omega]$. La rete contiene anche un filtro attivo, cioè un inverter trifase (APF), modellizzato come un parallelo di generatori di corrente e un'impedenza $Z_{APF} = R_{APF} + j\omega_h \cdot L_{APF}$ in serie.

Lo scopo dell'ottimizzazione è trovare i valori dei filtri passivi (C_{f1} , C_{f2} , L_{f1} ed L_{f2}) e del filtro attivo (L_{APF} ed I_{APF}) che permettano il rispetto dei vincoli stabiliti dalla IEEE 519-2022 (si veda tabella 2.3) e di ulteriori vincoli riassunti nella tabella 5.1. Si è deciso di non ottimizzare le resistenze dei filtri perché dipendono dalle componenti parassite di capacità e induttanze. In generale, tutte le quantità di cui si assume il valore sono descritte nella tabella 2.2.

Le equazioni usate provengono dalla risoluzione del circuito monofase di figura 2.2 e sono (2.2) ed (2.3). La validità di queste equazioni è dimostrata dall'analisi numerica di figura 2.5.

9.2 Metodi iterativi per l'ottimizzazione

La formulazione del problema è descritta in (3.11): si deve minimizzare una funzione a più variabili $f(x)$ rispettando alcune equazioni/disequazioni dette vincoli. La funzione e i vincoli non sono lineari.

Due differenti algoritmi sono stati sfruttati nel seguito per la risoluzione del problema: *sequential quadratic programming (SQP)* e *interior point method (IPM)*. Entrambi i metodi si basano sul metodo iterativo di Newton-Raphson.

Nel metodo SQP si risolve prima un sottoproblema quadratico, cioè un'espansione di Taylor al secondo ordine della lagrangiana della funzione $f(x)$. Anche i vincoli sono linearizzati nel sottoproblema. Dunque si calcola la direzione di ricerca d_k da inserire nel problema principale. Si veda figura 3.3.

Nel metodo IPM si cerca di trovare la soluzione partendo da un punto interno al politopo descritto dai vincoli. Il problema viene riscritto eliminando le disequazioni dai vincoli mediante l'uso di *slack variables*. Anche la funzione $f(x)$ cambia perché viene introdotta una *funzione barriera* di tipo logaritmico (si veda (3.19)); se la soluzione x -esima è vicino al bordo del politopo, allora la funzione da minimizzare aumenta, grazie alla presenza del logaritmo. Così l'algoritmo può allontanarsi dal bordo per trovare la direzione di ricerca. Si veda (3.23).

In conclusione, entrambi i metodi sono dispendiosi computazionalmente perché richiedono il calcolo della Hessiana. Nel metodo SQP il punto iniziale da cui parte l'iterazione può essere esterno al politopo dei vincoli.

9.3 Variabili da ottimizzare e funzione costo

Le variabili da ottimizzare sono le incognite del problema e sono elencate nella tabella 4.1: mancano le induttanze L_{f1} ed L_{f2} perché si ricavano da (4.1), una volta saputo il valore di C_{f1} e C_{f2} e la frequenza di risonanza. Le variabili da ottimizzare non variano in un range che va da $-\infty$ a $+\infty$, ma sono limitate. È necessario definire i limiti di variazione per avviare il problema di ottimizzazione. La tabella 4.2 mostra questi limiti.

I limiti inferiori (lb) delle capacità dipendono dai valori delle induttanze (si veda figura 4.1). Il limite superiore (ub) permette di avere filtri passivi attraversati da basse correnti a 50 [Hz], cioè ad una frequenza diversa da quella di lavoro.

Il lb di L_{APF} dipende dalle armoniche di corrente prodotte dal APF. Se il valore di L_{APF} è troppo basso allora il ripple di corrente aumenta. Non si può, comunque, scegliere un valore troppo alto di L_{APF} perché aumenta la caduta di tensione su Z_{APF} . La caduta di tensione è analizzata nella sezione riguardante i vincoli.

Infine, sono stati scelti arbitrariamente i limiti superiori ed inferiori delle correnti iniettate dal APF per le varie armoniche e per la corrente reattiva. Il valore numerico che limita il APF è $\pm I_L/2$. Il valore di I_L è la massima corrente richiesta dal carico: questo valore è citato nello standard IEEE 519-2022.

Si noti che i limiti sono tutti valori numerici e non dipendono dalle variabili di ottimizzazione.

Tutte le variabili da ottimizzare sono legate tra loro tramite la funzione costo (4.13). Ogni termine è pesato con (4.14). Questa è la funzione che appare nel problema di ottimizzazione e deve essere minimizzata. Le variabili

che compongono questa funzione devono assumere i valori più bassi possibili: condensatori con capacità basse risultano poco ingombranti ed economici. Lo stesso per L_{APF} . Anche le correnti del APF devono essere limitate per ridurre le perdite per effetto joule; dunque si vogliono rispettare i vincoli iniettando la minima corrente.

9.4 Vincoli del problema di ottimizzazione

Il vettore della soluzione ottimale, oltre ad essere limitato superiormente ed inferiormente, deve anche rispettare i vincoli di tabella 5.1. I vincoli sulle armoniche di corrente in rete sono decisi dallo standard IEEE 519-2022, mentre i rimanenti sono scelti arbitrariamente.

Le armoniche di corrente in rete devono essere inferiori ai limiti della tabella 2.3: si considera la prima riga della tabella nel caso di questa tesi. L'equazione di riferimento è (2.1).

Il secondo vincolo considera il fattore di qualità Q_f definito in (5.2). È valutato solo per i filtri passivi. Se Q_f assume valori infimi, il filtro ha il vantaggio di essere poco selettivo e quindi di lavorare intorno alla frequenza di risonanza per un ampio range di frequenze. Lo svantaggio è dovuto ad una R_f molto alta che, quindi, dissipa molta energia. Viceversa per un Q_f elevato. I valori ottimizzati devono permettere di mantenere Q_f entro il range di (5.3).

Un fenomeno negativo che si verifica a seguito dell'inserimento dei filtri passivi nella rete è l'antirisonanza, cioè la circolazione di elevate correnti nella rete a seguito di armoniche di corrente, anche di bassa ampiezza, alla frequenza di antirisonanza, ovvero ad una frequenza inferiore a quella di risonanza dei filtri passivi; il diagramma di Bode di figura 5.3 mostra che le antirisonanze, per due filtri passivi in parallelo, avvengono a frequenze in cui non ci sono armoniche a regime. Tuttavia esse potrebbero verificarsi durante i transitori.

Un ulteriore vincolo riguarda la caduta di tensione sull'impedenza Z_{APF} causata dalla corrente iniettata dal APF. Per i calcoli pratici, la corrente che causa la caduta di tensione è principalmente reattiva, quindi l'equazione (5.12) può essere sfruttata con il vincolo imposto da (5.13).

Il penultimo vincolo è riferito alla corrente reattiva presente in rete. In questo caso due condizioni sono state individuate, ma non sono applicabili contemporaneamente: la prima fissa la quantità di corrente reattiva in rete ad un valore arbitrariamente scelto, cioè $\frac{5}{100} \cdot I_L$. Si vedano (5.14) e (5.16). La seconda condizione, invece, non fissa la quantità di corrente reattiva in rete ad un valore arbitrario, ma impone al APF di agire in modo da garantire che il fattore di potenza della rete sia sempre 0.9 ($\cos(\Phi) = 0.9$). Si veda (5.15). Nel proseguimento si utilizzerà la prima condizione. Si specificherà quando sarà necessario ricorrere alla seconda.

L'ultimo vincolo riguarda la corrente per cui è dimensionato il APF; si è deciso arbitrariamente che la massima corrente sia pari a $\frac{I_L}{2}$, come delineato in (5.17).

Si noti che tutti i vincoli descritti sono disuguaglianze.

9.5 Risultati dell'ottimizzazione

In sintesi, il problema dell'ottimizzazione prevede di trovare il valore delle incognite di tabella 4.1 che minimizzano la funzione (4.13) con i pesi di (4.14). Il vettore soluzione ottimale deve rispettare i limiti della tabella 4.2 e i vincoli della tabella 5.1. Il risolutore usato è la funzione *fmincon* in Matlab, con il tool di ottimizzazione *MultiStart*. Tra i vari parametri da impostare, si deve scegliere anche l'algoritmo di risoluzione.

Se si seleziona l'algoritmo SQP, si trova la soluzione ottimale di tabella 6.2 con i valori di L_{f1} ed L_{f2} , usando (6.2) ed (6.3). La tabella 6.3 mostra che i principali vincoli di corrente sono rispettati. Anche il fattore di potenza della rete risulta quasi unitario. Si noti che il APF riesce a far rispettare i vincoli iniettando solo corrente reattiva, ma nessuna corrente alle armoniche perché la 5^a e la 7^a sono intrappolate dai filtri passivi, mentre l'11^a e la 13^a non hanno bisogno dell'intervento del APF perché hanno un'ampiezza ridotta.

La situazione si complica se l'algoritmo IPM viene implementato. La soluzione ottimale, in tabella 6.4, è identica alla precedente se non per il fatto che APF inietta corrente anche alla 11^a armonica. Dunque questa soluzione non è ottimale perché il APF non sta lavorando al minimo, sebbene i vincoli siano rispettati.

Per procedere comunque alla risoluzione, si è pensato di adottare un secondo stadio di ottimizzazione in cui le variabili da ottimizzare sono solo le correnti del APF. L'algoritmo adottato è sempre IPM. La nuova ottima soluzione, riportata in tabella 6.9, è equivalente a quella ottenuta con l'algoritmo SQP.

L'algoritmo IPM risulta peggiore del SQP perché richiede due stadi di ottimizzazione, oltre ad un maggiore tempo di esecuzione come riporta la tabella 6.11. Di seguito, dunque, si sfrutterà l'algoritmo SQP.

9.6 Sensitività dell'impedenza di rete e dell'angolo di accensione

Fissata la soluzione ottimale, si è deciso di verificare il rispetto dei vincoli variando l'impedenza di rete e l'angolo di accensione. Le due quantità sono dapprima variate singolarmente, mantenendo l'altra costante e, di seguito, simultaneamente.

Il range di variazione dell'impedenza di rete è indicato nella tabella 7.1. La condizione peggiore si verifica per il valore minimo dell'impedenza di rete perché le correnti risultano più elevate. In particolare l'11^a armonica non rispetta più il vincolo indicato dalla IEEE 519-2022 come indicato in figura 7.2. Per osservare i vincoli si deve cambiare la soluzione ottimale, sfruttando quella della tabella 7.3.

Il range di variazione dell'angolo di accensione $\alpha \in [0^\circ, 90^\circ]$. Dalla figura 7.6 si nota che i vincoli sull'11^a armonica e sulla corrente reattiva in rete non sono rispettati per svariati valori di α . Si noti che il caso peggiore, ovvero il caso in cui il APF è maggiormente stressato avviene per $\alpha = 48^\circ$; si riesce ad ottenere una soluzione che rispetta i vincoli solamente variando quello sulla corrente reattiva in rete, dunque utilizzando il vincolo che permette di avere un fattore di potenza pari a 0.9 ($\cos(\Phi) = 0.9$). Si veda, in proposito, la soluzione ottimale di tabella 7.8.

Infine, se entrambi i parametri sono variati, si ottiene la soluzione di figura 7.7: ai vincoli precedentemente non rispettati, cioè l'11^a armonica e la corrente reattiva in rete, si aggiunge anche la 13^a per valori d'impedenza di rete bassi e per valori di α intorno ai 50° .

In conclusione, si può dedurre che le variazioni dell'angolo di accensione impattano maggiormente sul rispetto dei vincoli rispetto alle variazioni dell'impedenza di rete.

9.7 Conclusioni e progetti futuri

La figura 8.1 mostra come l'azione dei filtri renda la corrente in rete, ad esempio nella fase b, più sinusoidale che in loro assenza (figura 2.3). Le principali conclusioni di questa tesi riguardano il problema di ottimizzazione: si può concludere che l'algoritmo SQP sia migliore rispetto all'algoritmo IPM con la funzione fmincon e il tool di ottimizzazione MultiStart.

Inoltre, si può ritenere che le resistenze dei filtri non si possano ottimizzare perché dipendono dalle resistenze parassite delle capacità e delle induttanze.

Per i filtri passivi è importante considerare non solo le correnti alla frequenza di risonanza, ma anche il loro comportamento alla fondamentale.

Infine, la sensitività dell'angolo di accensione è più influente rispetto a quella dell'impedenza di rete.

Un progetto futuro può prevedere la realizzazione di un sistema di controllo che vari le correnti iniettate dal APF autonomamente al variare delle condizioni di carico quali l'angolo di accensione α oppure la resistenza di carico R_L . Le correnti iniettate devono sempre essere quelle che permettono un utilizzo ottimale del APF, cioè le minime correnti che rispettano i vincoli.

List of Figures

2.1	Three-phase model of the system.	5
2.2	Single-phase equivalent circuit.	6
2.3	Current of phase b of non-linear load without compensation; $\alpha = 10^\circ$ and $R_L = 1 [\Omega]$	7
2.4	Phasors' diagram before and after compensation.	8
2.5	Red bars: numerical solution; green dots: analytical solution. Both solutions are in all plots very similar. For instance the grid currents are very similar (Analytical solution $I_{ganalytical}$ vs numerical solution $I_{gnumerical}$).	9
2.6	Active power filter: From left, there is a capacitance, six IGBT with diode, impedance of the APF and the grid.	10
2.7	Voltage references with and without homopolar injection.	11
2.8	From top left to bottom right: V_{pcc} , V_{inv} , V_{ref} , V_g , I_{inv} , $V_{h,ref}$	12
2.9	Close loop control scheme of APF.	13
2.10	ESR of capacitance vs frequency and temperature. [3]	15
2.11	Inductance selection based on the current flowing through itself and the losses. [12]	16
2.12	Active and reactive power vs. firing angle α with fixed load.	17
2.13	Active and reactive power vs. firing angle vs load resistance.	18
2.14	Absolute value of current upstream the rectifier, with firing angle $\alpha = 10^\circ$ and null capacitance of DC-link.	19
2.15	Magnitude of current. The colorbar illustrates the magnitude of the current in ampere [A]. The isocurves help to read the plot, without the exploitation of the colorbar.	19
2.16	Magnitude of voltage at PCC. The colorbar displays the magnitude of V_{pcc} in volt [V].	20
2.17	Displacement between V_t and I . The colorbar indicates the displacement in degree $[\circ]$. The isocurves help to read the plot, without the exploitation of the colorbar.	20
2.18	Active power vs. α vs. R_L	21
2.19	Reactive power vs. α vs. R_L	21
3.1	Graphical representation of Newton-Raphson method.	22
3.2	Green curve represents the gradient descent curve. Red curve represents Newton's method curve. The route of the Newton's curve is more direct because it uses the Hessian, so 2^{nd} derivative information, while the gradient descent exploits only the gradient, so 1^{st} derivative information.	24
3.3	Explication of SQP algorithm, with parent problem and QP sub-problem.	25
3.4	Comparison between gradient descent and IPM. $\nabla f = c$. [18]	27
4.1	L_f vs. C_f for f_h equal 250, 350, 550 and 650 Hz. x and y axes are both logarithmic.	32
4.2	Bode plot for cut-off frequency of 250 [Hz] for various values of Z_f , and therefore capacitance. Focus on the values at 50 [Hz] (vertical line) and magnitude of 26 [dB] (horizontal line).	33
4.3	Three modes of operation of inverter. [2]	34
5.1	Response of RLC filter with $R=10 [\Omega]$ vs response of RLC filter with $R=0.01 [\Omega]$. Both the filters have the same L and C. The resonance frequency is 250 [Hz].	39
5.2	System of harmonic source I_h , Z_{f2} , Z_{f1} and Z_g . Voltage grid source V_g is a short-circuit at harmonic frequency $f_g \cdot h$	39
5.3	Frequency response of the two passive filters and the grid. The plot is obtained using following R, L and C values: $R_g = 22 [m\Omega]$; $L_g = 1 [mH]$; $R_{f1} = R_{f2} = 0.13 [\Omega]$; $L_{f1} = 6.6 [mH]$; $C_{f1} = 0.612 [mF]$; $L_{f2} = 4.7 [mH]$; $C_{f2} = 0.437 [mF]$	40
5.4	Real and imaginary current of fundamental of non-linear load vs α	43
6.1	Flowchart of the two stages involved in optimization problem.	46
7.1	Behaviour of harmonics and reactive current at fundamental if Z_g changes of +100% and -50%. The vertical line points out the base value of grid impedance, namely always in 1 [p.u.].	51
7.2	The green curve is the quantity changing with Z_g . The red horizontal lines are the limits. The black vertical lines are the base values of $ Z_g $. The plot of reactive current into the grid has the green and red curve almost overlapped.	53
7.3	Amplitude of harmonics vs. firing angle. The labels indicate the base non-linear load, with $\alpha_0 = 10^\circ$: they are the values of table 6.1. The spikes are due to the capacitance C_{dc}	54
7.4	Amplitude of harmonics vs. firing angle. The smooth behaviour is reached neglecting the capacitance C_{dc}	55

7.5	Behaviour of harmonics and reactive current into grid when $\alpha \in [0^\circ, 90^\circ]$. The vertical line indicates the base value of α , that is $\alpha_0 = 10^\circ$	56
7.6	The green curve is the quantity changing with α . The red horizontal lines are the limits. The black vertical lines are the base values of α . The plot of reactive current into the grid has two labels marking the reactive current for $\alpha = 48^\circ$ and $\alpha = 78^\circ$	57
7.7	Figure showing IHD, TDD and reactive current into the grid: the thick red lines represent the limits; the light colorful lines represent the quantity for various values of α . To avoid a mass figure, just for the reactive current the legend is given.	58
8.1	Grid current of phase b with passive and active filters. It has to be compared with figure 2.3. $\alpha = 10^\circ$ and $R_L = 1 [\Omega]$	61
A.1	Model used inside the code	70

List of Tables

2.1	Current distortion limits admitted. [10]	14
2.2	Table of assumptions.	18
2.3	Table of non-linear load with $\alpha = 10^\circ$ and $R_L = 1 [\Omega]$.	18
4.1	List of unknowns.	30
4.2	List of upper and lower bounds of unknowns.	35
4.3	Table of initial solution.	37
5.1	List of constraints.	44
6.1	Table of non-linear load.	46
6.2	List of optimal solution with SQP algorithm.	46
6.3	Table of constraints with SQP.	47
6.4	List of optimal solution with IPM algorithm.	48
6.5	Table of constraints with IPM.	48
6.6	Table of initial solution of 2 nd stage optimization. These values come from 1 st optimization stage.	48
6.7	List of upper and lower bounds of unknowns with 2 nd optimization.	49
6.8	List of constraints of 2 nd optimization.	49
6.9	Table of optimal solution with exitflag 1.	49
6.10	Table of constraints with exitflag 1.	50
6.11	Comparative analysis between single stage SQP and two stages of IPM.	50
7.1	Table of base, maximum and minimum values of R_g and L_g .	51
7.2	Table of non-linear load with minimum of grid impedance, $\alpha = 10^\circ$ and $R_L = 1 [\Omega]$.	52
7.3	List of optimal solution with minimum of grid impedance.	53
7.4	Table of constraints with minimum of grid impedance.	53
7.5	Table of non-linear load with $\alpha = 48^\circ$.	55
7.6	List of optimal solution with $\alpha = 48^\circ$.	55
7.7	Table of constraints with $\alpha = 48^\circ$.	56
7.8	List of optimal solution with $\alpha = 48^\circ$ and $\cos(\Phi) = 0.9$.	57
7.9	Table of constraints with $\alpha = 48^\circ$.	58

References

- [1] Bertolozzo. Sistemi per l'automazione. *lecture notes*, 2022.
- [2] Briz. Power converters for ac drives. *lecture notes*, 2023.
- [3] Type unidirectional link and filter capacitors [Manufacturer website link](#), december 2023, [Link to pdf datasheet](#).
- [4] [https://optimization.cbe.cornell.edu/index.php?title=Interior-point method for NLP](https://optimization.cbe.cornell.edu/index.php?title=Interior-point%20method%20for%20NLP), december, 2023.
- [5] F.C. De La Rosa. *Harmonics and Power Systems (1st ed.)*. Boca Raton, 2006.
- [6] <https://it.mathworks.com/help/optim/ug/fmincon.html#busog7r-exitflag>, december, 2023.
- [7] S.J. Garrett. Chapter 13 - introductory numerical methods. In S.J. Garrett, editor, *Introduction to Actuarial and Financial Mathematical Methods*, pages 411–463. Academic Press, San Diego, 2015.
- [8] <https://www.ruder.io/optimizing-gradient-descent/>, december, 2023.
- [9] <https://towardsdatascience.com/gradient-descent-algorithm-a-deep-dive-cf04e8115f21>, december, 2023.
- [10] IEEE. Ieee standard for harmonic control in electric power systems. *IEEE*, 2022.
- [11] https://www.tu-ilmenau.de/fileadmin/Bereiche/IA/prozessoptimierung/vorlesungsskripte/abebe_geletu/IPM_Slides.pdf, december, 2023.
- [12] Filtro pasivo de armónicos para vfd series spfs [Manufacturer website link](#), december 2023 [Link to pdf datasheet](#).
- [13] Willi Christiansen & David T. Johnsen. Analysis of requirements in selected grid codes. *Ørsted•DTU, Section of Electric power Engineering, Technical University of Denmark (DTU)*, 2006.
- [14] Stephen J. Wright Jorge Nocedal. *Sequential Quadratic Programming*, pages 529–562. Springer New York, New York, NY, 2006.
- [15] N Karmarkar, A new Polynomial - Time algorithm for linear programming, *Combinatorica*, VOL. 4, No. 8, 1984, pp. 373-395.
- [16] Arash Khoshkbar-Sadigh, Vahid Dargahi, Ketan Lakhera, and Keith Corzine. Analytical design of Lc filter inductance for two-level inverters based on maximum ripple current. In *IECON 2019 - 45th Annual Conference of the IEEE Industrial Electronics Society*, volume 1, pages 1621–1626, 2019.
- [17] <https://it.mathworks.com/help/gads/how-globalsearch-and-multistart-work.html>, december, 2023.
- [18] <https://www.cs.princeton.edu/courses/archive/fall18/cos521/Lectures/lec17.pdf>, Princeton University, *Advanced Algorithm Design, Lecture 17: Interior point methods*, Professor Cristopher Musco, december, 2023.
- [19] <https://it.mathworks.com/discovery/quadratic-programming.html>, december, 2023.
- [20] Reem Mohamed Rezk Sobh. Design and optimization of filters for power quality improvement of high power rectifiers, page 45, july 2023.
- [21] <https://it.mathworks.com/help/optim/ug/when-the-solver-fails.html#br53c03-1>, december, 2023.
- [22] <https://web.cse.ohio-state.edu/~parent.1/classes/788/Au10/OptimizationPapers/SQP/actaSq.pdf>, december, 2023.
- [23] Saurabh Tewari, Kaushik Basu, and Apurva Somani. Analytical evaluation of the peak-to-peak ripple current in the filter inductor for a space vector modulated grid-tied vsi. In *2014 IEEE International Conference on Power Electronics, Drives and Energy Systems (PEDES)*, pages 1–6, 2014.

A Code defining non-linear load

This code generates the vector of non-linear load. It works with a Simulink model reported in figure A.1.

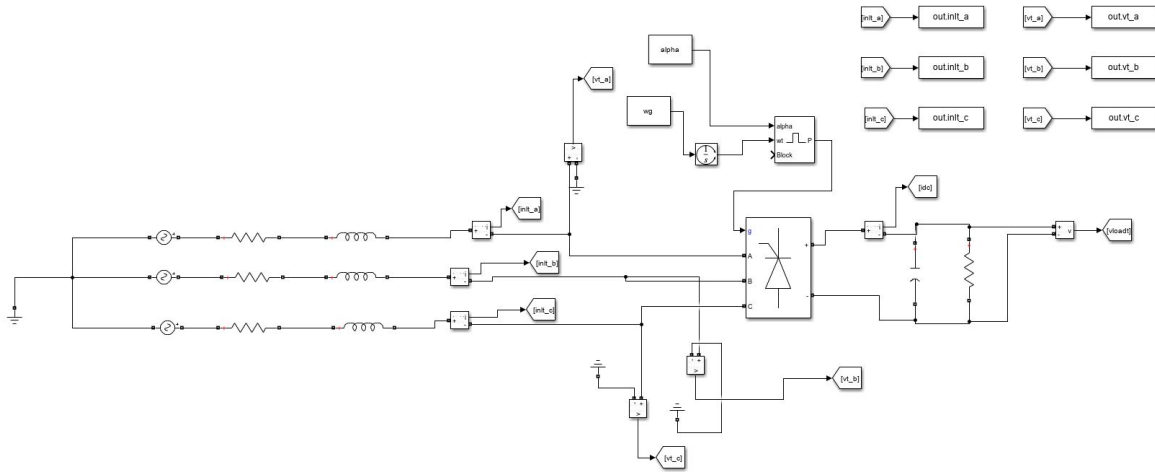


Figure A.1: Model used inside the code

```

1  function [vec_inl]=model(rload, fire_angle)
2
3  vg=230*sqrt(2);
4  fg=50;
5  rg=22e-3;
6  lg=1e-3;
7  cdc=1e-3;
8  rl_min=0.8;
9
10 rl_max=1.4;
11 vec_rl=rl_min:0.2:rl_max; %this is the range of variation of load
    resistance rl
12 wg=2*pi*fg;
13
14 zg=rg+j*wg*lg;
15 %Now I compute SCCR (short circuit current ratio)
16 rload_rated=1; % I decide to have a minimum resistance of 1 ohm
17 vload=400; % it comes from a previous solution. It's the voltage of DC-Link
18 iload=vload/rload_rated; %These three parameters are all in DC
19 vg_rms=230;
20 i_sc_3ph_max=vg_rms*sqrt(2)/abs(zg); %3-phase short circuit current RMS
21
22 il_rated=(vload*iload*sqrt(2))/(3*vg_rms);
23
24 sccr=i_sc_3ph_max/il_rated;
25
26 vec_alpha=40:2:50; %this is the range of variation of firing angle alpha
27
28 N=2000; %total number of samples
29 T=50e-6; % sampling time
30 t=(0:1:N-1)*T; t=t';
31
32 complex_vecfreq=(-N/2:1:N/2-1)/(N*T);

```

```

33 index50Hz=find(complex_vecfreq==50);
34 index_minus250Hz=find(complex_vecfreq==--250);
35 index350Hz=find(complex_vecfreq==350);
36 index_minus550Hz=find(complex_vecfreq==--550);
37 index650Hz=find(complex_vecfreq==650);
38 % Start allocation of data
39 vec_inlt1_abs=zeros(length(vec_rl),length(vec_alpha));
40 vec_inlt_minus_5_abs=zeros(length(vec_rl),length(vec_alpha));
41 vec_inlt7_abs=zeros(length(vec_rl),length(vec_alpha));
42 vec_inlt_minus_11_abs=zeros(length(vec_rl),length(vec_alpha));
43 vec_inlt13_abs=zeros(length(vec_rl),length(vec_alpha));
44 vec_inlt1_real=zeros(length(vec_rl),length(vec_alpha));
45 vec_inlt1_imag=zeros(length(vec_rl),length(vec_alpha));
46 % End allocation
47 %%
48 for cc=1:length(vec_rl)
49
50     rl=vec_rl(cc);
51     for jj=1:length(vec_alpha)
52         alpha=vec_alpha(jj);
53
54     output=sim('thyristor_with_variable_load_and_firing_angle01.slx','
55         SrcWorkspace', 'current');
56     % srcWorkspace, current: these two word let working of a simulink model
57     % inside a function;
58
59 inlt_a=output.inlt_a;
60 inlt_a=inlt_a(end-N+1:end); % this is used to eliminate the transient
61
62 inlt_b=output.inlt_b;
63 inlt_b=inlt_b(end-N+1:end);
64
65 inlt_c=output.inlt_c;
66 inlt_c=inlt_c(end-N+1:end);
67
68 inlt_dq=(2/3)*(inlt_a+inlt_b*exp(j*2*pi/3)+inlt_c*exp(j*4*pi/3)); %from abc
69     to alfabeta
70
71 vt_a=output.vt_a;
72 vt_a=vt_a(end-N+1:end);
73
74 vt_b=output.vt_b;
75 vt_b=vt_b(end-N+1:end);
76
77 vt_c=output.vt_c;
78 vt_c=vt_c(end-N+1:end);
79
80 vt_dq=(2/3)*(vt_a+vt_b*exp(j*2*pi/3)+vt_c*exp(j*4*pi/3));
81
82 fftinlt_dq=fftshift(fft(inlt_dq))/N;
83 fftvt_dq=fftshift(fft(vt_dq))/N;
84
85 vec_inlt1_abs(cc, jj)=abs(fftinlt_dq(index50Hz));
86 vec_inlt_minus_5_abs(cc, jj)=abs(fftinlt_dq(index_minus250Hz));
87 vec_inlt7_abs(cc, jj)=abs(fftinlt_dq(index350Hz));
88 vec_inlt_minus_11_abs(cc, jj)=abs(fftinlt_dq(index_minus550Hz));

```



```

86 vec_inlt13_abs(cc, jj)=abs(fftinlt_dq(index650Hz));
87
88 phase_between_vt_and_inlt=angle(fftvt_dq(index50Hz))-angle(fftinlt_dq(
      index50Hz));
89 % vec_inlt1_real(cc, jj)=real(fftinlt_dq(index50Hz));
90 vec_inlt1_real(cc, jj)=vec_inlt1_abs(cc, jj)*cos(phase_between_vt_and_inlt);
91
92 % vec_inlt1_imag(cc, jj)=imag(fftinlt_dq(index50Hz));
93 vec_inlt1_imag(cc, jj)=vec_inlt1_abs(cc, jj)*sin(phase_between_vt_and_inlt);
94
95
96     end
97 end
98 %% new definition of vec_inlt1_real
99 % I am trying to write the nonlinear load in a sort of table
100 vec_inlt1_real=[vec_rl' vec_inlt1_real];
101 new_vec_alpha=[NaN vec_alpha];
102 new_vec_rl=[NaN vec_rl]';
103 vec_inlt1_real=[new_vec_alpha;
104     vec_inlt1_real];
105 %% new definition of vec_inlt1_imag
106 vec_inlt1_imag=[vec_rl' vec_inlt1_imag];
107
108 vec_inlt1_imag=[new_vec_alpha;
109     vec_inlt1_imag];
110 %% new definiton of vec_inlt11_abs
111 vec_inlt_minus_11_abs=[vec_rl' vec_inlt_minus_11_abs];
112 vec_inlt_minus_11_abs=[new_vec_alpha;
113     vec_inlt_minus_11_abs];
114 %% new definiton of vec_inlt_minus_5_abs
115 vec_inlt_minus_5_abs=[vec_rl' vec_inlt_minus_5_abs];
116 vec_inlt_minus_5_abs=[new_vec_alpha;
117     vec_inlt_minus_5_abs];
118 %% new definiton of vec_inlt7_abs
119 vec_inlt7_abs=[vec_rl' vec_inlt7_abs];
120 vec_inlt7_abs=[new_vec_alpha;
121     vec_inlt7_abs];
122 %% new definitio of vec_inlt13_abs
123 vec_inlt13_abs=[vec_rl' vec_inlt13_abs];
124 vec_inlt13_abs=[new_vec_alpha;
125     vec_inlt13_abs];
126
127 position_fire_angle=find(abs(new_vec_alpha-fire_angle)<0.01);
128 position_rload=find(abs(new_vec_rl-rload)<0.01); % sometimes the function
      find does not work with ==, so < is used
129 vec_inl=zeros(1, 5);
130 vec_inl(1)=abs(vec_inlt_minus_11_abs(position_rload, position_fire_angle));
131 vec_inl(2)=abs(vec_inlt_minus_5_abs(position_rload, position_fire_angle));
132 vec_inl(3)=vec_inlt1_real(position_rload, position_fire_angle)+j*
      vec_inlt1_imag(position_rload, position_fire_angle);
133 vec_inl(4)=abs(vec_inlt7_abs(position_rload, position_fire_angle));
134 vec_inl(5)=abs(vec_inlt13_abs(position_rload, position_fire_angle));
135
136 thyristor_with_variable_load_and_firing_angle01
137 end

```

B Code defining optimization problem

This code finds the optimal solution. This code works with the non-linear load defined in appendix A.

```

1  function optimization
2
3  clc,clear all,close all
4
5  s=tf('s');
6  j=sqrt(-1);
7
8  %here the non linear load is copied as[-11th, -5th, 1st, 7th, 13th]
9  %vec_inl with RL=1 ohmm and alpha=10
10 vec_inl=[9.20508230282813      38.0418145606741
11          413.921906509934+105.745934892630i      21.3061325132367
12          6.32011427410371i];
13
14 %% Automatic procedure to choose the cut of frequency of the two passive
15 filters
16 %The two passive filters are tuned on the two highest harmonics of vec_inl
17 fg=50;
18
19 vec_inl_ord=zeros(1,5); % I sort the vector of non-linear load as 50Hz 250
20 Hz
21 %350 550 650, instead of -550 -250 50 350 650
22
23 vec_inl_ord(1)=vec_inl(3);
24 vec_inl_ord(2)=vec_inl(2);
25 vec_inl_ord(3)=vec_inl(4);
26 vec_inl_ord(4)=vec_inl(1);
27 vec_inl_ord(5)=vec_inl(5);
28
29 vec_freq_ord=[50 250 350 550 650];
30 real_vec_inl_ord=real(vec_inl_ord);
31 abs_real_vec_inl_ord=abs(real_vec_inl_ord); %Elimination of the imaginary
32 part of vec_inl(3)
33
34 [maximum1, first_index]=max(abs_real_vec_inl_ord(2:end));% '2:end' exclude
35 the 1st harmonic
36 first_index=first_index+1;
37 fc1=vec_freq_ord(first_index);
38
39 [maximum2, second_index]=max(abs_real_vec_inl_ord(2:end));
40 abs_real_vec_inl_ord(second_index+1)= NaN; % This is a trick to found the
41 2nd greates element of a vector(the first one
42 %has already been found above)
43 [max_2, index2]=max(abs_real_vec_inl_ord(2:end));
44 index2=index2+1;
45 fc2=vec_freq_ord(index2);
46
47 %In the first run I Have to define the initial values of the variables to
48 %optimize
49 % active filter
50 L_apf_init=1e-3;
51 Rapf=0.013 ;
52 %passive filters
53 Rf1=0.13;
54
55 Cf1_init=1e-4;

```

```

47 Lf1_init=1/(Cf1_init*(2*pi*fc1)^2);
48
49 Rf2=0.13;
50
51 Cf2_init=1e-4;
52 Lf2_init=1/(Cf2_init*(2*pi*fc2)^2);
53 vec_h=[-11,-5,1,7,13];
54
55 %grid parameter
56 Lg=1e-3;
57 Rg=22e-3;
58 wg=fg*2*pi;
59 vg=230*sqrt(2);
60 xg= j* wg*Lg;
61 zg=Rg+xg;
62
63 rload_rated=1; % I decide to have a minimum resistance of 1 ohm
64 vload=400; % it comes from a previous solution. It's the voltage of DC-Link
65 iload=vload/rload_rated; %These three parameters are all in DC
66 vg_rms=230;
67 i_sc_3ph_max=vg_rms*sqrt(2)/abs(zg); %3-phase short circuit current RMS
68
69 il_rated=(vload*iload*sqrt(2))/(3*vg_rms);
70
71 sccr=i_sc_3ph_max/il_rated;
72
73 vec_fh=abs(vec_h*fg);
74
75 iapf_reactive_init=-1e-3;
76 vec_iapf_init=[-1e-3 -1e-3 0+j*iapf_reactive_init -1e-3 -1e-3];
77
78 vec_vg=[0 0 vg 0 0];
79
80 for cc=1:length(vec_h)
81     s=j*wg*vec_h(cc);
82
83
84
85     Zg=Lg*s+Rg;
86
87     Zapf_init=L_apf_init*s+Rapf;
88
89     Zf1_init=Rf1+ s*Lf1_init+ 1/(s*Cf1_init);
90     Zf2_init=Rf2+ s*Lf2_init+ 1/(s*Cf2_init);
91
92     vec_Zg_init(:,cc)=Zg;
93     vec_Zf1_init(:,cc)=Zf1_init;
94     vec_Zf2_init(:,cc)=Zf2_init;
95 end
96 %% constraints of active current filter
97 TDD_max=5/100; % This value comes from IEEE519
98
99 %individual_harmonic_distortion---> IHD
100 IHD_max_5=4/100; %This value comes from IEEE519
101
102 IHD_max_7=4/100; %This value comes from IEEE519

```

```

103
104 IHD_max_11=2/100;           % This value comes from IEEE519
105
106 IHD_max_13=2/100;           % This value comes from IEEE519
107
108
109 %% constraints of passive filter
110 %quality factor
111 Q_min=15;
112 Q_max=80;
113
114 %% constraint of Lapf. The voltage drop is due to the highest harmonic of
      the active power filter
115 max_volatge_drop_Lapf=0.1*vg;
116 %% constraint of reactive current at fundamental in the grid
117 max_reactive_current_into_grid=5/100;
118
119
120 %% constraint to define the lower bound of inductance of apf
121 vdc=600; %voltage that supply the active power filter
122 fs=10e3; %frequency switching of active power filter
123 ripple_of_current=(5/100)*il_rated; %5 percent of rated current I_L
124 maximum2=0.5; %index of modulation of inverter
125 %% maximum and minimum values: ub and lb
126 L_min=(vdc*maximum2)/(2*sqrt(3)*fs*ripple_of_current);
127 L_max=1e-1;
128 C_min=1e-7;
129 C_max=1e-4;
130
131
132 % Below the upper and lower bound of I_APF are written, depending on
      vec_inl
133 iapf_min=zeros(1,length(vec_inl));
134 iapf_max=zeros(1,length(vec_inl));
135 index1_to_eliminate_from_iapf=find(vec_fh==fc1);
136 index2_to_eliminate_from_iapf=find(vec_fh==fc2);
137
138 if(vec_inl(1)<0)
139     iapf_min(1)=-il_rated/2;
140     iapf_max(1)=0;
141 else
142     iapf_min(1)=0;
143     iapf_max(1)=il_rated/2;
144 end
145
146 if(vec_inl(2)<0)
147     iapf_min(1)=-il_rated/2;
148     iapf_max(1)=0;
149 else
150     iapf_min(1)=0;
151     iapf_max(1)=il_rated/2;
152 end
153
154 if(vec_inl(4)<0)
155     iapf_min(1)=-il_rated/2;
156     iapf_max(1)=0;

```

```

157 else
158     iapf_min(1)=0;
159     iapf_max(1)=il_rated/2;
160 end
161
162 if(vec_inl(5)<0)
163     iapf_min(1)=-il_rated/2;
164     iapf_max(1)=0;
165 else
166     iapf_min(1)=0;
167     iapf_max(1)=il_rated/2;
168 end
169
170 if(imag(vec_inl(3))<0)
171     iapf_react_min=-il_rated/2;
172     iapf_react_max=0;
173 else
174     iapf_react_min=0;
175     iapf_react_max=il_rated/2;
176 end
177
178 % The upper and lower bound for harmonics captured by the two
179 % passive filters are not defiend
180 iapf_min([index1_to_eliminate_from_iapf index2_to_eliminate_from_iapf])=[0
181     0];
182 iapf_max([index1_to_eliminate_from_iapf index2_to_eliminate_from_iapf])=[0
183     0];
184 %% variables initialization = x variables
185
186 %Initial values used by the optimization problem(before they
187 %were used by a for cycle)
188
189 iapf_react=-1e-3;
190 vec_iapf=[-1e-3 -1e-3 0 -1e-3 -1e-3]; %here you cannot write imaginary
191     value
192 Cf1=1e-4;
193 Cf2=1e-4;
194 Lapf=1e-3;
195
196 %% defining x variables
197 X=[ Cf1 Cf2 Lapf vec_iapf iapf_react ];
198 %% fmincon constraints
199 lb=[ C_min C_min L_min iapf_min iapf_react_min ];
200 ub=[ C_max C_max L_max iapf_max iapf_react_max ];
201
202 %% Set options for FMINCON
203 rng default % For reproducibility
204 opts = optimoptions(@fmincon,'Algorithm','sqp','Disp','iter');
205 %% Create problem for Multistart
206 problem = createOptimProblem('fmincon','objective',@filtersize,'x0',X,...
207     'lb',lb,'ub',ub,'nonlcon',@mycon,'options',
208     opts);

```

```

209 problem.options.MaxIterations=2000;
210 problem.options.ConstraintTolerance =1e-4;
211 problem.options.MaxFunctionEvaluations=1e7;
212 problem.options.StepTolerance=1e-6;
213 problem.options.OptimalityTolerance=1e-6;
214 %% make a multistart object
215
216 ms=MultiStart( 'Display','iter','StartPointsToRun','bounds');
217 %% run the optimization
218 [xopt, fval,eflag,output,allmins]= run(ms,problem,800);
219 xopt
220 fval
221 eflag
222 output
223 allmins
224 %% cost function
225 function F=filtersize(X)
226 Cf1=X(1);
227 Cf2=X(2);
228 Lapf=X(3);
229 vec_iapf(1)=X(4);
230 vec_iapf(2)=X(5);
231 vec_iapf(3)=X(6);
232 vec_iapf(4)=X(7);
233 vec_iapf(5)=X(8);
234 iapf_react=X(9);
235
236 F= (4.0*1e4)^2*Cf1^2 + (4.0*1e4)^2*Cf2^2 + (3.8*1e3)^2*Lapf^2+ 1*1e-2*(
    vec_iapf(1))^2 + 5*1e-1*(vec_iapf(2))^2 + 0*(vec_iapf(3))^2 ...
237     + 8*1e-1*(vec_iapf(4))^2 + 1*1e-2*(vec_iapf(5))^2 + 1e-2*(iapf_react
    ^2);
238
239 end
240
241 %% constraints function
242 function [c,ceq]=mycon(X)
243
244 Cf1=X(1);
245 Cf2=X(2);
246 Lapf=X(3);
247 vec_iapf(1)=X(4);
248 vec_iapf(2)=X(5);
249 vec_iapf(3)=X(6);
250 vec_iapf(4)=X(7);
251 vec_iapf(5)=X(8);
252 iapf_react=X(9);
253
254 Lf1=1/(Cf1*(2*pi*fc1)^2);
255
256 Lf2=1/(Cf2*(2*pi*fc2)^2);
257 %Now I start to write igh. This end with line of TDD
258 Zpf1_13arm=Rf1+ j*wg*vec_h(5)*Lf1 + 1/(j*wg*vec_h(5)*Cf1);
259 Zpf2_13arm=Rf2+ j*wg*vec_h(5)*Lf2 + 1/(j*wg*vec_h(5)*Cf2);
260
261 Zpf1_11arm=Rf1+ j*wg*vec_h(1)*Lf1 + 1/(j*wg*vec_h(1)*Cf1);
262 Zpf2_11arm=Rf2+ j*wg*vec_h(1)*Lf2 + 1/(j*wg*vec_h(1)*Cf2);

```

```

263
264 Zpf1_7arm=Rf1+ j*wg*vec_h(4)*Lf1 + 1/(j*wg*vec_h(4)*Cf1);
265 Zpf2_7arm=Rf2+ j*wg*vec_h(4)*Lf2 + 1/(j*wg*vec_h(4)*Cf2);
266
267
268 Zpf1_5arm=Rf1+ j*wg*vec_h(2)*Lf1 + 1/(j*wg*vec_h(2)*Cf1);
269 Zpf2_5arm=Rf2+ j*wg*vec_h(2)*Lf2 + 1/(j*wg*vec_h(2)*Cf2);
270
271 num_13=vec_vg(5)+vec_Zg_init(5)*vec_iapf(5)-vec_Zg_init(5)*vec_inl(5);
272 den_13=1+ vec_Zg_init(5)/Zpf1_13arm + vec_Zg_init(5)/Zpf2_13arm ;
273 igh13=abs((vec_vg(5)-(num_13/den_13))/vec_Zg_init(5));
274 IHD13=igh13/il_rated;
275
276 num_11=vec_vg(1)+vec_Zg_init(1)*vec_iapf(1)- vec_Zg_init(1)*vec_inl(1);
277 den_11=1+ vec_Zg_init(1)/Zpf1_11arm+ vec_Zg_init(1)/Zpf2_11arm;
278 igh11=abs((vec_vg(1)-(num_11/den_11))/vec_Zg_init(1));
279 IHD11=igh11/il_rated;
280
281 num_7=vec_vg(4)+ vec_Zg_init(4)*vec_iapf(4)-vec_Zg_init(4)*vec_inl(4);
282 den_7=1+ vec_Zg_init(4)/Zpf1_7arm + vec_Zg_init(4)/Zpf2_7arm;
283 igh7=abs((vec_vg(4)-(num_7/den_7))/vec_Zg_init(4));
284 IHD7=igh7/il_rated;
285
286 num_5=vec_vg(2)+ vec_Zg_init(2)*vec_iapf(2)- vec_Zg_init(2)*vec_inl(2);
287 den_5=1+ vec_Zg_init(2)/Zpf1_5arm+ vec_Zg_init(2)/Zpf2_5arm;
288 igh5=abs((vec_vg(2)-(num_5/den_5))/vec_Zg_init(2));
289 IHD5=igh5/il_rated;
290
291 TDD=sqrt((igh11/sqrt(2))^2 + (igh13/sqrt(2))^2 + (igh7/sqrt(2))^2 +(igh5/
sqrt(2))^2)/il_rated;
292
293
294
295 % voltage drop on Lapf: if cycle is used because could happen than one of
the
296 % harmonic has a greater magnitude than the fundamental
297 [i_apf_max, index_of_max]=max(abs((vec_iapf)));
298 if (abs(iapf_react)>max(abs((vec_iapf))))
299
300     Zapf=abs(Rapf + j*wg*Lapf);
301 else
302
303     if (index_of_max==1)
304         order_of_harmonic=11;
305     end
306
307
308     if (index_of_max==2)
309         order_of_harmonic=5;
310     end
311
312     if (index_of_max==3)
313         order_of_harmonic=1;
314     end
315
316

```

```

317     if (index_of_max==4)
318         order_of_harmonic=7;
319     end
320
321     if (index_of_max==5)
322         order_of_harmonic=13;
323     end
324
325     Zapf=abs(Rapf + j*wg*order_of_harmonic*Lapf);
326
327 end %end of first if cycle end of voltage drop
328
329 %reactive current in the grid
330 Zpf1_larm=Rf1+ j*wg*vec_h(3)*Lf1 + 1/(j*wg*vec_h(3)*Cf1);
331 Zpf2_larm=Rf2+ j*wg*vec_h(3)*Lf2 + 1/(j*wg*vec_h(3)*Cf2);
332
333 num_1=vec_vg(3)+vec_Zg_init(3)*(j*iapf_react)- vec_Zg_init(3)*vec_inl(3);
334 den_1=1+ vec_Zg_init(3)/Zpf1_larm+ vec_Zg_init(3)/Zpf2_larm;
335 react_igh1=(imag((vec_vg(3)-(num_1/den_1))/vec_Zg_init(3)))/il_rated;
336
337
338 tot_current_of_apf=abs(vec_iapf(1))+abs(vec_iapf(2))+abs(vec_iapf(4))+...
339     abs(vec_iapf(5)) + abs(iapf_react);
340 %Quality factor
341 Qf1=(1/Rf1)*sqrt(Lf1/Cf1);
342
343 Qf2=(1/Rf2)*sqrt(Lf2/Cf2);
344
345
346
347 p=1;
348
349 c(p)=IHD13-IHD_max_13;           p=p+1;
350
351 c(p)=IHD11-IHD_max_11;           p=p+1;
352
353 c(p)=IHD7-IHD_max_7;             p=p+1;
354
355 c(p)=IHD5-IHD_max_5;             p=p+1;
356
357
358 c(p)=TDD-TDD_max;                p=p+1;
359
360 c(p)=Qf1-Q_max;                   p=p+1;
361 c(p)=-Qf1 +Q_min;                 p=p+1;
362
363 c(p)=Qf2-Q_max;                   p=p+1;
364 c(p)=-Qf2 +Q_min;                 p=p+1;
365
366 imax_harm_plus_react_of_apf=max([abs(iapf_react), abs(vec_iapf)]);
367
368
369 c(p)=imax_harm_plus_react_of_apf*Zapf-max_volatge_drop_Lapf;           p=p+1;
370
371 c(p)=react_igh1-max_reactive_current_into_grid;                         p=p+1;
372 c(p)=-react_igh1-max_reactive_current_into_grid;                         p=p+1;

```



```

373 % Note that react_igh should be within +/- 5/100 of il rated
374
375 c(p)=tot_current_of_apf-il_rated/2;                                p=p+1;
376
377
378 e=1;
379
380 ceq=[];
381 end
382
383 %below lines are used to print and save the results
384 format long
385 fprintf('Optimal filter parameters:\n');
386 fprintf('Cf1 = %g F\n', xopt(1));
387 fprintf('Lf1 = %g H\n', 1/(xopt(1)*(2*pi*fc1)^2));
388
389 fprintf('Cf2 = %g F\n', xopt(2));
390 fprintf('Lf2 = %g H\n', 1/(xopt(2)*(2*pi*fc2)^2));
391 fprintf('Lapf = %g H\n', xopt(3));
392 fprintf('vec_iapf11 = %g A\n', xopt(4));
393 fprintf('vec_iapf5 = %g A\n', xopt(5));
394 fprintf('vec_iapf1 = %g A\n', xopt(6));
395 fprintf('vec_iapf7 = %g A\n', xopt(7));
396 fprintf('vec_iapf13 = %g A\n', xopt(8));
397 fprintf('iapf_react = %g A\n', xopt(9));
398
399 v_Cf1=xopt(1);
400 v_Cf2=xopt(2);
401 v_Lapf=xopt(3);
402 vec_iapf11=xopt(4);
403 vec_iapf5=xopt(5);
404 vec_iapf1=xopt(6);
405 vec_iapf7=xopt(7);
406 vec_iapf13=xopt(8);
407 v_iapf_react=xopt(9);
408 v_fval=fval;
409 v_Lf1=1/(v_Cf1*(2*pi*fc1)^2);
410 v_Lf2=1/(v_Cf2*(2*pi*fc2)^2);
411 optresults_double=[ v_Cf1 v_Lf1 v_Cf2 v_Lf2 v_Lapf vec_iapf11 vec_iapf5
    vec_iapf1 vec_iapf7 vec_iapf13 v_iapf_react v_fval lb ub ];
412 dirname='C:\Users\Gurjot\Tesi Oviedo\sum up of simulations\';% in this line
    the working directory path is written
413
414 filename = [dirname '\' datestr(now,'yyyy_mmmm_dd_HH_MM_SS') '.mat']; %
    Filename
415 save(filename,'optresults_double');
416
417 end

```

C Code verifying the constraints

This code verify if the optimal solution find in appendix B complies with constraints.

```

1 clear all,close all,clc
2 load('2024_January_18_17_37_53.mat') %here the optimal solution is loaded
3
4 vec_iapf=zeros(1,5);
5 vec_iapf(1)=optresults_double(6);
6 vec_iapf(2)=optresults_double(7);
7 vec_iapf(3)=optresults_double(8)+j*optresults_double(11);
8 vec_iapf(4)=optresults_double(9);
9 vec_iapf(5)=optresults_double(10);
10 Cf1=optresults_double(1);
11 Lf1=optresults_double(2);
12 Cf2=optresults_double(3);
13 Lf2=optresults_double(4);
14 Lapf=optresults_double(5);
15 iapf_react=optresults_double(11);
16 fval=optresults_double(12);
17
18 j=sqrt(-1);
19
20 lb=optresults_double(12:19);
21 ub=optresults_double(20:end);
22
23 Rapf=0.013;
24
25 %passive filter resistance: not optimized
26 Rf1=0.13;
27 Rf2=0.13;
28
29 vec_h=[-11,-5,1,7,13];
30
31 vec_inl=[9.20508230282813      38.0418145606741
          413.921906509934+105.745934892630i      21.3061325132367
          6.32011427410371i];
32 Lg=1e-3;
33 Rg=22e-3;
34 fg=50;
35 wg=fg*2*pi;
36 vg=230*sqrt(2);
37 xg= j* wg*Lg;
38 zg=Rg+xg;
39
40 rload_rated=1; % I decide to have a minimum resistance of 1 ohm
41 vload=400; % it comes from a previous solution. It's the voltage of DC-Link
42 iload=vload/rload_rated; %These three parameters are all in DC
43 vg_rms=230;
44 i_sc_3ph_max=vg_rms*sqrt(2)/abs(zg); %3-phase short circuit current RMS
45
46 il_rated=(vload*iload*sqrt(2))/(3*vg_rms);
47
48 sccr=i_sc_3ph_max/il_rated;
49
50 vec_fh=vec_h*fg;
51

```

```

52 vec_vg=[0 0 vg 0 0];
53
54 vec_vpcc=zeros(1,length(vec_h));
55 vec_ig=zeros(1,length(vec_h));
56 vec_vapf=zeros(1,length(vec_h));
57 vec_ipf1=zeros(1,length(vec_h));
58 vec_ipf2=zeros(1,length(vec_h));
59 vec_Zg_init=zeros(1,length(vec_h));
60 vec_Zf1=zeros(1,length(vec_h));
61 vec_Zf2=zeros(1,length(vec_h));
62
63 for cc=1:length(vec_h)
64
65     s=j*wg*vec_h(cc);
66
67     Zg=Lg*s+Rg;
68
69     Zapf=Lapf*s+Rapf;
70
71     Zpf1=Rf1+ s*Lf1+ 1/(s*Cf1);
72     Zpf2=Rf2+ s*Lf2+ 1/(s*Cf2);
73
74     vec_vpcc(cc)=(vec_vg(cc)+Zg*vec_iapf(cc)-Zg*vec_inl(cc))/(1+Zg/Zpf1+Zg/
        Zpf2);
75
76     vec_ig(cc)= (vec_vg(cc)-vec_vpcc(cc))/Zg;
77
78
79     vec_vapf(cc)= vec_vpcc(cc) + Zapf*vec_iapf(cc);
80
81     vec_ipf1(cc)= vec_vpcc(cc)/Zpf1;
82
83     vec_ipf2(cc)= vec_vpcc(cc)/Zpf2;
84
85     vec_Zg_init(:,cc)=Zg;
86     vec_Zf1(:,cc)=Zpf1;
87     vec_Zf2(:,cc)=Zpf2;
88
89 end
90
91
92 igh11=abs(vec_ig(1));
93 IHD11=igh11/il_rated
94
95 igh13=abs(vec_ig(5));
96 IHD13=igh13/il_rated
97
98 igh7=abs(vec_ig(4));
99 IHD7=igh7/il_rated
100
101 igh5=abs(vec_ig(2));
102 IHD5=igh5/il_rated
103
104 TDD=sqrt((igh11/sqrt(2))^2 + (igh13/sqrt(2))^2 + (igh7/sqrt(2))^2 +(igh5/
        sqrt(2))^2)/il_rated
105

```

```

106 cut_of_frequency_of_filter_1=1/(2*pi*sqrt(Lf1*Cf1))
107 cut_of_frequency_of_filter_2=1/(2*pi*sqrt(Lf2*Cf2))
108 tot_current_of_apf=abs(vec_iapf(1))+abs(vec_iapf(2))+abs(vec_iapf(4))+...
109     abs(vec_iapf(5)) + abs(iapf_react)
110 Qf1=1/Rf1*(sqrt(Lf1/Cf1))
111 Qf2=1/Rf2*(sqrt(Lf2/Cf2))
112 voltage_drop=imag(vec_iapf(3))*(abs(Rapf+j*2*pi*fg*Lapf))
113
114 %Plot of optimal result to see, in particular, imag(Ig1)
115 x_axis_of_harmonics=vec_h;
116
117 y_axis_of_ipf1=abs(vec_ipf1);
118 y_axis_of_ipf2=abs(vec_ipf2);
119 y_axis_of_ig=abs(vec_ig);
120 y_axis_of_iapf=abs(vec_iapf);
121 y_axis_of_inl=abs(vec_inl);
122
123 real_y_axis_of_ipf1=real(vec_ipf1);
124 imag_y_axis_of_ipf1=imag(vec_ipf1);
125
126 real_y_axis_of_ipf2=real(vec_ipf2);
127 imag_y_axis_of_ipf2=imag(vec_ipf2);
128
129 real_y_axis_of_ig=real(vec_ig);
130 imag_y_axis_of_ig=imag(vec_ig);
131
132 real_y_axis_of_iapf=real(vec_iapf);
133 imag_y_axis_of_iapf=imag(vec_iapf);
134
135 real_y_axis_of_inl=real(vec_inl);
136 imag_y_axis_of_inl=imag(vec_inl);
137
138 figure(32)% for all harmonics, except the first one, only the absolute
     value can be considered.
139 subplot(421)
140 aa=plot(x_axis_of_harmonics, real_y_axis_of_ipf1, 'or');
141 hold on
142 a1=plot(x_axis_of_harmonics, imag_y_axis_of_ipf1, 'ob');
143 legend('ipf1 real','ipf1 imag'), title('ipf1')
144 subplot(422)
145 bb=plot(x_axis_of_harmonics, real_y_axis_of_ipf2, 'or');
146 hold on
147 b1=plot(x_axis_of_harmonics, imag_y_axis_of_ipf2, 'ob');
148 legend('ipf2 real','ipf2 imag'), title('ipf2')
149 subplot(423)
150 cc=plot(x_axis_of_harmonics, real_y_axis_of_ig, 'or');
151 hold on
152 c1=plot(x_axis_of_harmonics, imag_y_axis_of_ig, 'ob');
153 legend('ig real','ig imag'), title('ig')
154 subplot(424)
155 dd=plot(x_axis_of_harmonics, real_y_axis_of_iapf, 'or');
156 hold on
157 d1=plot(x_axis_of_harmonics, imag_y_axis_of_iapf, 'ob');
158 legend('iapf real','iapf imag'), title('iapf')
159 subplot(425)
160 ee=plot(x_axis_of_harmonics, real_y_axis_of_inl, 'or');

```

```

161 hold on
162 e1=plot(x_axis_of_harmonics, imag_y_axis_of_inl,'ob');
163 legend('inl real','inl imag'), title('inl')
164 subplot(426)
165 plot(vec_h,real(vec_vpcc), 'or')
166 hold on
167 plot(vec_h,imag(vec_vpcc),'ob')
168 legend('vpcc real','vpcc imag'), title('vpcc')
169 subplot(427)
170 plot(vec_h,real(vec_vapf), 'or')
171 hold on
172 plot(vec_h,imag(vec_vapf),'ob')
173 legend('vapf real','vapf imag'), title('vapf')
174
175 %% Plot of IHD and TDD
176 figure(22)
177 subplot(311)
178 x_axis_of_IHD_11_and_13=[-11 13];
179 y_axis_of_IHD_11_and_13=[IHD11 IHD13];
180 plot(x_axis_of_IHD_11_and_13,y_axis_of_IHD_11_and_13,'+')
181 hold on
182 up_of_11_and_13=[2/100 2/100];
183 plot(x_axis_of_IHD_11_and_13,up_of_11_and_13,'g-')
184 legend('values of IHD','ub'), legend('Location','southoutside'), title('
    IHD of 11 and 13')
185 subplot(312)
186 x_axis_of_IHD_5_and_7=[-5 7];
187 y_axis_of_IHD_5_and_7=[IHD5 IHD7];
188 plot(x_axis_of_IHD_5_and_7,y_axis_of_IHD_5_and_7,'+')
189 hold on
190 up_of_5_and_7=[4/100 4/100];
191 plot(x_axis_of_IHD_5_and_7,up_of_5_and_7,'g-')
192 legend('values of IHD','ub'), legend('Location','southoutside'), title('
    IHD of 5 and 7')
193 subplot(313)
194 plot(1,TDD,'+')
195 hold on
196 up_of_TDD=[5/100 5/100];
197 plot(0.5:1.5,up_of_TDD,'g-')
198 legend('values of TDD','ub'), legend('Location','southoutside'), title('
    TDD')
199 %% Bode plot of the two passive filters
200 s=tf('s');
201 opzioni=bodeoptions;
202 opzioni.FreqUnits='Hz';
203 Zpf1=Rf1+Lf1*s+ 1/(Cf1*s);
204 figure(8)
205 bode(Zpf1, opzioni), title('module and phase of Zpf1')
206 figure(9)
207 Zpf2=Rf2+ Lf2*s + 1/(Cf2*s);
208 bode(Zpf2, opzioni), title('module and phase of Zpf2')

```